UNIVERSITÀ DEGLI STUDI DI TRIESTE

UNIVERSITÀ DEGLI STUDI DI TRIESTE

XXXVIII CICLO DEL DOTTORATO DI RICERCA IN

BIOMEDICINA MOLECOLARE

ICGEB

ROLE OF TICK-BORNE ENCEPHALITIS VIRUS NON-STRUCTURAL PROTEINS IN MODULATING THE CELLULAR RESPONSE TO INFECTION

Settore scientifico-disciplinare: BIO/11

DOTTORANDA
CHIARA KALEBIĆ

COORDINATORE
PROF. ALESSANDRO TOSSI

SUPERVISORE DI TESI
PROF. ALESSANDRO MARCELLO

CO-SUPERVISORE DI TESI
DR. TEA CARLETTI

ANNO ACCADEMICO 2024/2025

To my mimi, papi and Debi

SYNOPSIS

The Tick-Borne Encephalitis virus is a member of the Orthoflaviviruses endemic in Europe and Asia. The role of the non-structural NS viral proteins in modulating the intracellular environment to facilitate virus infection and, conversely, the cell response to virus infection are still poorly understood. In this thesis I focused on two TBEV NS proteins: NS2B and NS4B. During my PhD studies I found that: (i) IKKε recognizes TBEV NS2B to induce an antiviral response and reduce viral replication, and (ii) TBEV NS4B protein inhibits PKR-induced SGs formation, a proviral mechanism to facilitate TBEV infection.

IKKε recognizes TBEV NS2B to induce an IRF3 mediated antiviral response

TBEV induces an early unfolded protein response (UPR) of the endoplasmic reticulum (ER) aimed at restoring proteostasis. Recent findings have shown that the same pathway also induces a cell-intrinsic antiviral response with induction of specific Interferon Stimulated Genes (ISGs) through the inositol-requiring enzyme IRE1α axis. We observed that five out of the eleven TBEV proteins could induce IRE1-dependent activation of ISGs. Interestingly, only NS2B could induce the upregulation of the innate immune response independently of IRE1. We thus wanted to understand at which molecular level was NS2B having an effect, or, even better, which cellular component was recognizing NS2B to induce an antiviral response. To address this question, I performed a dissection of the RIG-I pathway, known to be involved during TBEV infection, leading to IRF3 nuclear translocation and IFN/ISG activation. I observed that NS2B functionally interacted with IKKε, the kinase that phosphorylates IRF3. This finding was further confirmed by a co-immunoprecipitation assay showing specific IKKε interaction with NS2B and by a co-localization assay. Next, I wanted to explore the role of overexpression prior to TBEV infection. Interestingly, and in line with what just described, TBEV infection in cells overexpressing NS2B, resulted in a reduced viral replication as visible at the plaque levels, as well as mRNA levels and visually by immunofluorescence. However, NS2B is principally known to be the cofactor of the NS3 viral protease. When the fully active NS2B3 protease was transfected, the antiviral effect was much stronger, something we need to explore in more detail, but the phenotype was maintained also by transfecting the enzymatically inactive protease NS2B3 S135A, which had the same effect as NS2B alone. In this part of the work, I defined a novel function of TBEV NS2B, which may have implications for viral pathogenesis. A suggestive hypothesis is also that IKKε could act as a sort of pattern-recognition receptor recognizing NS2B as a viral factor.

TBEV NS4B inhibits dsRNA mediated PKR activation to inhibit stress granules formation

Several Orthoflaviviruses, such as DENV, ZIKV, WNV and others have been shown to exploit viral components such as the viral genome or viral proteins, to inhibit the activation of the integrated stress response (ISR). The ISR is triggered by various stresses, including viral infection, and leads to translation arrest and formation of stress granules SG in the cytoplasm. Two cellular kinases are involved: PKR, which is activated by dsRNA viral intermediates, and PERK, which is an effector of the UPR. Both kinases are induced following infection by +ssRNA viruses, which culminates in the phosphorylation of eIF2α and transient formation of stress granules (SGs) to inhibit protein translation and restore homeostasis. With our work we discovered that upon TBEV infection less than 10% of cells form SGs, suggesting that TBEV exploits some mechanisms to inhibit this cell-induced antiviral strategy. We further determined that TBEV NS4B is strongly inhibiting the induction of SG by PolyI:C (a synthetic dsRNA that mimics viral intermediates of replication) by a direct interaction of the cytoplasmic loop (C-loop) of NS4B with PKR. Of note, NS4B is a protein which spans the ER membrane three times thus the C-loop is the only region available for the interaction with cytoplasmic proteins such as PKR. Indeed, this interaction inhibits phosphorylation of PKR thus inhibiting the downstream phosphorylation of eIF2α and SGs formation. I further observed that in the context of stable PKR overexpression, a rescue of the formation of SGs can be observed. Interestingly, we observed that by inserting deletions in the C-loop, hence altering its original sequence and conformation, the strength of inhibition of SGs formation is decreased, therefore being more permissive for the formation of SGs. I then inserted the same NS4B deletions in the TBEV genome and observed that in response to infection with the mutant viruses a higher percentage of cells contained SGs. In this work I could show that NS4B targets PKR to block the formation of virus induced SGs, a mechanism exploited by the virus to avoid the activation of the integrated stress response.

ACKNOWLEGMENTS

Fist and foremost I want to thank **Dr. Alessandro Marcello**, my thesis supervisor. Thank you, Alessandro, for taking me to your laboratory in the middle of a pandemics when I was just a curious student wondering how viruses work and every now and then decide to completely lock Earth down. From you I learnt in these four years how to think critically like a real scientist to finally become a virologist. But, apart from the purely scientific point of view, the patience and kindness which distinguish you as a boss always capable of managing a big group of people will always be imprinted in my mind. Thank you for believing in me.

Dear **Dr. Tea Carletti**, my co-supervisor, thank you so much for always being present for me during this journey. You are both the heart and head of our laboratory capable of homogenising a heterogeneous group of people. Our scientific discussions are one of the memories I will mostly cherish from this PhD both in the moments in which we agreed, and the ones when we did not. I learned really a lot from you. Thank you.

Then I need to thank all my present and past colleagues from the Molecular Virology lab. Mostly, I want to thank **Fede** and **Orsini** who were fundamental pilasters during these years and with whom I have shared many beautiful (sometimes also less beautiful) memories – your presence was fundamental. Next, thank you **Pamela** for the discussions and laughs, **Ying** just for being your-fantastic-self, **Bea** in the last year your presence, kindness and our long talks were of main importance as well, **Denis** for always making me laugh, **Urša** for our confessional-runs, **Bilal** for our philosophical talks, **Mariana** for your kindness and **Giudy** for your suggestions and ideas. A special thanks for **Gloria** for the experimental help in the last months – it is a pleasure working with you.

I need to thank also **Prof. Daniel Ruzek** for welcoming me to his laboratory for a training.

I must also extend my gratitude to **Dr. Lara Manganaro** and **Dr. Cinzia Borgogna** for accepting to review my thesis.

Then, from the bottom of my heart thanks to my biggest supporters, my family – **mimi**, **papi**, **Debi** – to whom I dedicate this thesis. Thanks also to **Luka** and to all my friends who listened to me complaining about failed experiments, but here the primate goes without any doubt to my **Petra** who was such an important person for me during this years, always present and ready to cheer me up.

And, last, but certainly not least, thank you to my **Hadi**. You were there for me and with me during all the ups and downs this journey brought and together (with **Bibi** as well) we crossed also this finish line. Thanks for your support, motivation, presence and trust which always give me the strength to move on and never ever give up.

Table of Contents

LIST OF FIGURES

INTRODUCTION

Orthoflaviviruses

Flavivirus, recently renamed by the International Committee on Taxonomy of Viruses (ICTV) *Orthoflavivirus* in 2023 (Postler et al., 2023) is a genus of positive-strand RNA viruses (+ssRNA) belonging to the *Flaviviridae* family. Annually more than 400 million people worldwide get infected by Orthoflaviviruses. Orthoflaviviruses are arthropod-borne viruses, i.e. transmitted by arthropod like mosquitoes or ticks and are responsible of severe diseases, in some cases leading to death. Orthoflavivirus infection can be neuroinvasive leading to several neurological symptoms and conditions (De Vries and Harding, 2023).

Some of the main representatives of the genus are the Dengue (*Orthoflavivirus dengue,* DENV), West Nile (WNV), Zika (*Orthoflavivirus zikaense,* ZIKV), Yellow Fever (*Orthoflavivirus flavi,* YFV), Japanese Encephalitis (*Orthoflavivirus japonicum,* JEV), Tick-borne encephalitis (*Orthoflavivirus encephalitides,* TBEV) and Usutu (*Orthoflavivirus usutuense,* USUV) viruses (Pierson and Diamond, 2020). Dengue virus, transmitted by *Aedes aegypti and A.albopictus* mosquitos, is presenting a real threat worldwide, mainly in the tropical area. In 2013, a study conducted by Bhatt et al. (Bhatt et al., 2013), predicted 96 million apparent dengue infections globally in 2010, with other more than 200 million inapparent infections. Those data show and indicate the huge infection ratio given by DENV and importance in its surveillance and research. ZIKV and WNV are other mosquitoes borne viruses which are exponentially spreading nowadays therefore presenting a rising risk (Pierson and Diamond, 2020). Moreover, the uncontrolled phenomenon of global warming is having a strong impact on allowing arthropods to spread and as consequence favour viral spread as well (Whitehorn and Yacoub, 2019). In addition, the currently rising problem of deforestation, forest degradation and urbanization are factors of big impact in the transmission of arthropod borne diseases, like it was observed from recent Zika and dengue epidemics (Ortiz et al., 2021). In Italy, TBEV is endemic in the Northern part at the border with Slovenia and Austria (Caracciolo et al., 2015), while WNV and USUV are endemic (Caracciolo et al., 2020) . In recent years the country experienced autochthonous transmission of Dengue (Branda et al., 2024).

Tick-borne encephalitis virus

Overview

Tick-borne encephalitis virus (TBEV) is one of the members of the *Orthoflavivirus* genus. It is spread mainly in Western Europe and North-eastern Asia (**Fig. 1**).

Figure 1 Approximate distribution of tick-borne encephalitis virus

Approximate distribution of tick-borne encephalitis as of January 20, 2024., CDC. TBEV is mainly spread in western and northern Europe to northern and eastern Asia.

The virus is mainly transmitted through the bite of an infected *Ixodes* tick. Ticks themselves get infected by feeding on small rodents infected by TBEV. People, on the other hand cannot transmit TBEV, except in very rare cases such as blood transfusion, organ transplant or breastfeeding, and are therefore referred to as dead hosts. Despite ticks being the main source of infection, people can get infected by the consumption of unpasteurized milk or cheese from infected goats, sheep or cows as well (CDC, 2024).

Being it a member of the Orthoflaviviruses, its genome is a 11 Kb +ssRNA which translates in a single polyprotein at the level of the endoplasmic reticulum (ER). The polyprotein, composed by three structural and seven non-structural proteins gets further cleaved and modified by host and viral enzymes (**Fig. 3**). Novel viruses are then formed in the ER, mature through the Golgi to get finally released in the extracellular environment and infect neighbouring cells.

It is known that upon infection in humans, dendritic cells (DC) and neutrophils skin localized are getting infected and virus replicates within them. Probably other cell types get infected as well, but it is not known by now. However, upon DCs infection, they transport the virus to the lymph nodes, where viremia occurs and transmission of the virus to different organs, including the CNS (Robertson et al., 2009).

Indeed, TBEV is a neurotropic virus able of crossing the blood brain barrier (BBB) therefore the risk of a severe disease, further described in detail the next paragraph 'TBEV caused disease', upon infection is high, occurring in 35% of symptomatic patients.
Available vaccines are based on inactivated whole virus, however, no drugs have been approved for the treatment of infected patients (Kubinski et al., 2020).
It is therefore of crucial importance deepening the knowledge about TBEV to identify promising pathways or proteins to be targeted by drugs.

Molecular structure of TBEV (genome, polyprotein, virion)

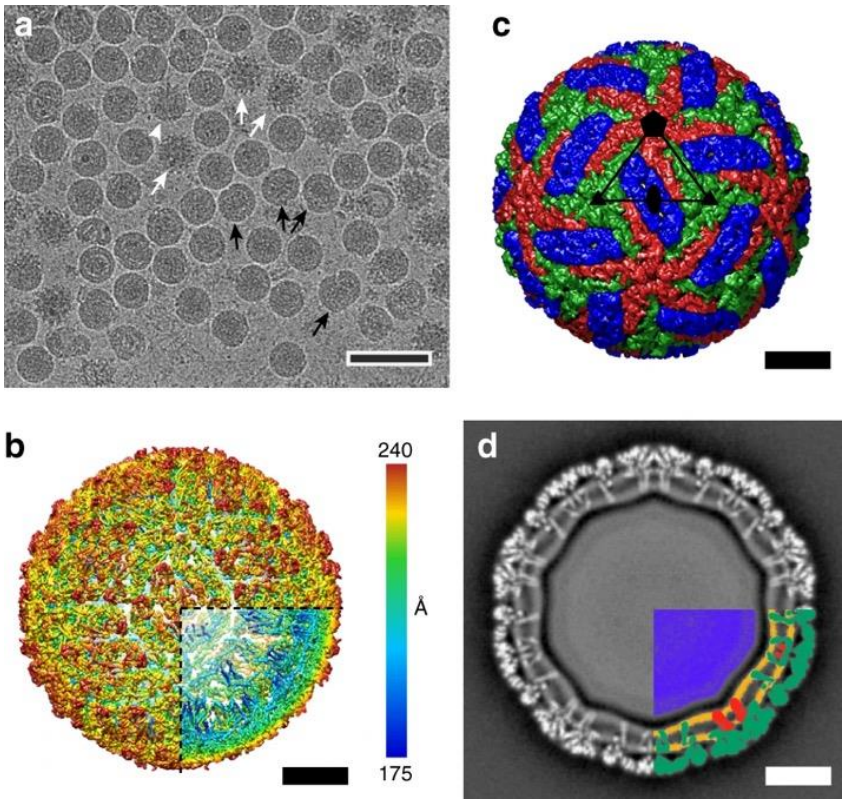

Figure 2 Structure of TBEV virion

a) Cryo-EM image of TBEV virions. White arrows are immature, black arrows are damaged.

b) B-factor sharpened electron-density map of TBEV virion

c) Molecular surface of TBEV virion

d) Central slice of TBEV electron density map perpendicular to the virus 5-fold axis (Füzik et al., 2018)

TBEV is an 11 Kb +ssRNA virus. The genome is formed by two non-coding sequences at the 5' and 3'-ends, and one open-reading frame (ORF). Once the viral genome undergoes translation, ten proteins get produced: three structural proteins (C, prM, and E proteins) and seven non-structural proteins (NS1, NS2A, NS2B, NS3, NS4A, NS4B and NS5). The non-coding regions are fundamental in forming secondary structures which participate as cis-regulatory elements during replication, translation and assembly of viral particles. A type-I cap of 130 nts is found on the 5'-short non-coding region, followed by two AG dinucleotides. The 3' non-coding region on the other hand is a bit longer, with its length varying from 450 to 800nts, and it might contain an internal poly-A.

TBEV +ssRNA acts at different levels in the viral replication steps:

1. mRNA for direct translation and polyprotein formation
2. template for RNA amplification and formation of dsRNA
3. genetic material stored in novel viral particles (Pustijanac et al., 2023)

Structurally, mature TBEV are enveloped and show a smooth, spherical morphology with a diameter of 50nm. TBEV envelope is formed by icosahedral asymmetric units, each formed by three E proteins and three M proteins. Being E protein glycosylated, small protrusions are formed on the viral surface (Fuzik et al., 2018) (**Fig. 2**). The inside contained nucleocapsid is formed by the C-protein and in the core of the virion the viral RNA is contained (Kofler et al., 2002).

The viral polyprotein (cca. 3400 aa) (**Fig. 3**) is co-translationally and post-translationally cleaved by host and viral proteases, therefore forming three structural and seven non-structural proteins. After the cleavage of the polyprotein, the ten proteins are produced (Pulkkinen et al., 2018). Detailed characterization of the role of each of the proteins known so far is described as follow. Detailed literature will be reported for the non-structural proteins NS2B, NS4B and NS5 since the focus of this study is to decipher the role of the abovementioned proteins.

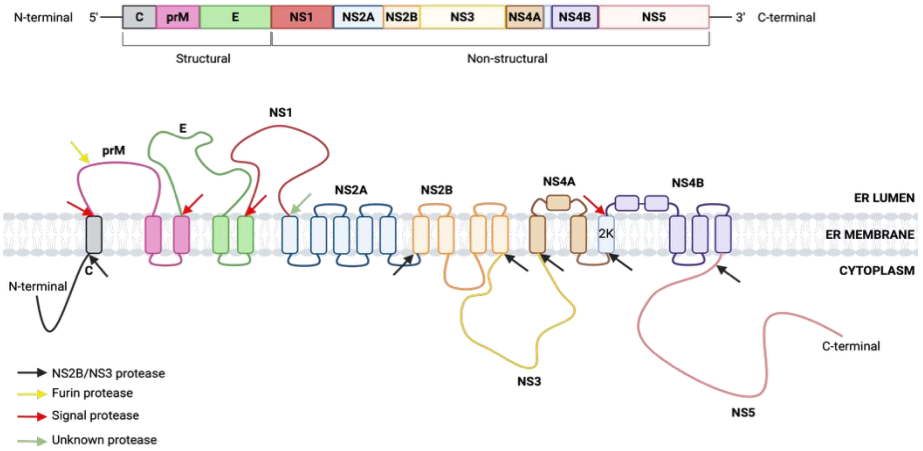

Figure 3 The TBEV polyprotein

C protein

C protein is a 11kDa (120aa) protein which forms a structural component of the nucleocapsid. A C protein dimer is the core of the nucleocapsid. Four helixes are forming each of the C monomers (Kofler et al., 2002). It is presumed that the highly positively charged a4 - helix is the one binding to the RNA (Pulkkinen et al., 2023). NS2B/3 cleaves between the C protein and the trans-membrane prM protein.

PrM protein

The prM protein is a 26kDa (cca 165aa) protein, which acts as a precursor of the structural M protein (8kDa, cca 75kDa). While the virus is still immature, prM forms a heterodimeric complex with the E protein, inhibiting therefore the fusion with the trans-Golgi network. In this way prM acts as a chaperon to allow for the proper folding of E protein before release in the cytoplasm. Once E protein is mature, the prM undergoes a cleavage which leaves attached only the C-terminal domain of the prM, forming therefore the mature M protein (Pulkkinen et al., 2018).

E protein

E protein is a 52 kDa (cca. 496aa) protein, the main protein of TBEV's envelope, being thereafter the main target of neutralizing antibodies. E protein is responsible for attaching to the cell membrane via receptor binding or membrane fusion, allowing therefore the virus to enter the cell. Before fusion E protein appears as a dimer, where the two monomers are oriented opposite one to the other, upon lowering of the pH, after fusion in the endoplasm, the E dimer dissociates and forms a trimeric form, thus allowing the genome to enter the cytoplasm. The protein is formed by four different domains. The N-terminal domain I acts as the central core of the protein. Domain II is the one needed for dimerization and contains a unique glycosylation site. Domain III with an immunoglobulin-like shape binds to the host receptors. The last domain, domain IV has a stem region with three peripheral membrane helicases and a transmembrane region. The C-terminal is the one anchored at the ER (Bressanelli et al., 2004; Pulkkinen et al., 2022)

NS1

NS1 is a glycosylated, highly conserved, 46kDa protein (351aa). After processing it translocates to the ER. It serves as a cofactor in viral RNA replication (Muller and Young, 2013). Its importance is given by the fact that it is released in patients' serum in its hexameric ring-like form, which is composed by three structural homodimers (Chuansumrit et al., 2011). NS1 gets internalized by hepatocytes where it plays immunomodulatory activities. It

accumulates there and forms lates endosomes where data suggest it leads to increased endocytic activity of hepatocytes and allows for the virus to replicate more (Alcon-LePoder et al., 2005).

NS2A

NS2A is a 22kDa (229aa) protein. Not much is known about its role upon infection, even though some evidence suggest it has a role in binding RNA to the ER membrane within the replication complex (Leung et al., 2008)

NS2B

NS2B is a 16kDa (130aa) protein. NS2B is a transmembrane protein which stably interacts with NS3 and acts as its cofactor for the NS3 serine protease activity.

Apart from playing a crucial role as cofactor of the viral protease NS3, NS2B has recently been demonstrated to play different roles during viral replication and host response to the infection. Interestingly, different roles of NS2B have been reported for Orthoflaviviruses.

A recent study on Japanese Encephalitis Virus (JEV) NS2B protein published by Yuan et al. in 2024 identified JEV NS2B as a protein able to cause the superinfection exclusion phenomena with ZIKV (Yuan et al., 2024). Indeed, the authors claim that the presence of JEV NS2B protein inhibits Zika virus replication. In addition, the authors confirmed that the cytoplasmatic domain of NS2B is the one responsible for the inhibition (Yuan et al., 2024). Moreover, a study performed by Nie et al. in 2023, on the role of NS2B during DENV-2 infection identified NS2B as a direct interactor of MAVS and IKKε. The authors link this event with an inhibition of the activation of the RIG-I/MAVS pathway (Nie et al., 2023). In addition, a new article published by Wu et al. in 2024 shows that ZIKV's NS2B protein has a role in inhibiting stress granules formation, thus allowing for the virus to replicate better and escape host cell response (Wu et al., 2024)

Finally, several articles have been published for different Orthoflaviviruses with the aim of identifying drugs which would target the NS2B3 protease to block its proteolytic activity (Constant et al., 2018).

However, no data are currently available for the independent role of NS2B in the context of TBEV infection.

NS3

NS3 is a 70kDa (621aa) protein. Several pivotal roles of NS3 in TBEV replication have been described so far. It acts as a helicase, an RNA triphosphatase, and, in complex with NS2B as a serine protease. Most of the non-structural proteins of the polyprotein are cleaved by the NS2B/3 protease (Bollati et al., 2010).

NS4A

NS4A is a 16kDa (149aa) small hydrophobic protein connected to NS4B by a 2K transmembrane domain. So far, its role has been linked to membrane remodelling, antagonism of the host cell response and induction of autophagy. Importantly, following ZIKA infection of pregnant women, reports suggest NS4A had a critical role in foetal development defects (Klaitong and Smith, 2021)

NS4B

NS4B is a 27kDa protein (252aa) linked to NS4A by a 2K loop. It is formed by four domains, from which three are transmembrane on the endoplasmic reticulum (ER), and the fourth one is facing the ER lumen. Only the so-called C-loop is the cytoplasmic domain of the protein. The role of NS4B during infection is not clearly understood so far, however, it has been shown to have a role in viral replication and host immunomodulation. Given this roles, it is an appealing target for orthoflavivirus drug discovery (Gao et al., 2022). For instance JNJ-1802 was described as a potent antiviral against DENV infection targeting NS4B (Kesteleyn et al., n.d.), as well as JNJ-A07 which targets NS4B C-loop to inhibit the formation of the replication complex and disrupt DENV replication (Kiemel et al., 2024). NS4B sequence is conserved between different orthoflaviviruses, indeed the NS4B sequence similarity between different flaviviruses is above 54% (Wang et al., 2022). Different studies have identified NS4B's role in different orthoflaviviruses as an innate immune response inhibitor, thus favouring viral replication. For instance, Zeng et al., published a work in 2023, where they identified JEV's NS4B protein as inhibitor of interferon beta production by a direct interaction/inhibition of TLR3 and TRIF (Zeng et al., 2023). In line with the previous study, Sarratea et al. showed, in 2023., that ZIKV NS4B inhibits IFN-β production as well, this time by interacting with TBK1 (Sarratea et al., 2023). Additionally, in 2022 Arakawa et al., published a work in which they prove JEV's NS4B has a role in stress granules (SGs) disassembly. They observed that the formation of the NPL4-VCP complex avoids the formation of stress granules, and in addition they demonstrated that JEV's NS4B protein is mediating this inhibition by the recruitment of the NPL4-VCP complex to the viral replication organelle. SGs are generally formed by the recognition of dsRNA by PKR, but they show that even in a context of a constitutively active form of PKR, named PKR-D328A, which generally induces high SGs formation, in the case of a co-expression with NS4B, the SGs formation decreases. They therefore suggest that NS4B together with VCP suppresses SGs accumulation, thus allowing for the virus to replicate.

The authors claim NS4B directly interacts with NPL4, which is VCP cofactor. Upon activation, VCP allows for viral propagation, as well as acts on SGs disassembly (Arakawa et al., 2022).

NS5

NS5 is a 103kDa (902aa) protein, the largest TBEV protein. It is the most important protein in viral RNA replication, since it acts as the viral RNA-dependent RNA polymerase. It has as well a methyltransferase activity, fundamental for stabilizing and translating RNA. In addition, it has an active role in the suppression of the immune response, being therefore a crucial pro-viral protein. Indeed, it has been reported by Garcias et al. in 2023 that TBEV infection antagonizes IFNα2 signalling. The authors report a direct binding by NS5 to TYK2 thus inhibiting the JAK/STAT pathway (Garcias et al., 2023). Previously, other reports indicated a general role of several orthoflaviviruses NS5 proteins, TBEV included, in antagonizing IFN-I (Best, 2017). In line with the previous studies, Biswal et al., published recently a work in which they show DENV and ZIKV's NS5 interacting with hSTAT2 by entering in the detail of the conformational changes allowing the interaction (Biswal et al., 2024).

TBEV life cycle

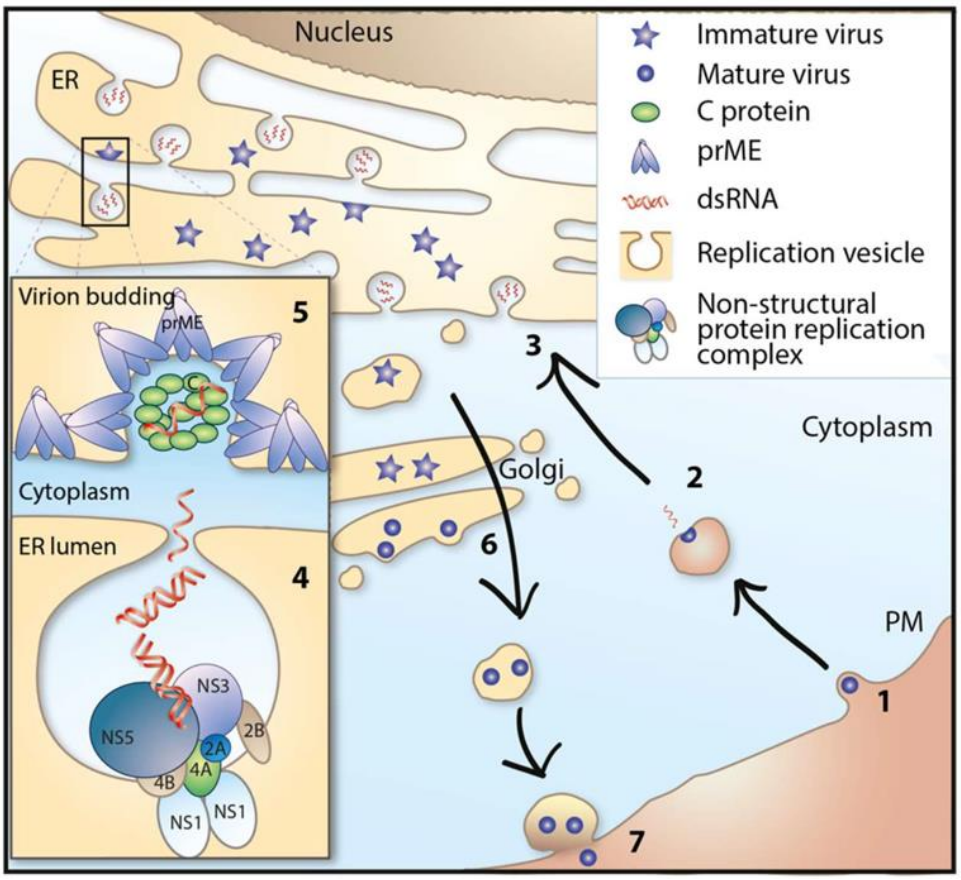

Figure 4 Life cycle of tick borne flaviviruses; (Lindqvist et al., 2018)

TBEV life cycle is schematically shown in **Fig. 4**. Like other Orthoflavivruses, TBEV enters the cells mainly through receptor-mediated endocytosis. The virus attaches to the cellular membrane by the linkage of E protein and the glycosaminoglycan heparan sulphate present on cellular membranes. Entry occurs mainly occurs *via* endocytosis, but micropinocytosis is possible as well. Upon localization in the endosome characterized by a low pH, E protein undergoes conformational changes, eventually leading to a change in its organization, which finally causes the fusion of viral and endocytic vesicles. The fusion allows for the nucleocapsid containing viral RNA to get released in the host cytoplasm, NC gets degraded, so the RNA is at that point found free in the cytoplasm. Initially there is a first amplification of the positive RNA strand to form the negative RNA strand as well, which then acts as a template for further genome amplification. The positive RNA strand is then used as a template for the translation into the viral polyprotein. The translation occurs at the ER level, where the single polyprotein gets processed as well. After processing, prM and E get internalized in the ER. On the other hand, C protein faces the cytoplasm its anchor to the ER membrane gets cleaved, rendering it a soluble protein.

The non-structural proteins get translated in the following order: NS1, NS2A, NS2B, NS3, NS4A, NS4B and finally NS5. NS5, the RNA-dependent RNA polymerase is responsible for genome replication, which occurs in proximity of the ER, rearranged in specific replicative invaginations. The assembly of novel particles occurs at the ER invagination level, where the soluble C protein surrounds novel ss+RNA particles thus forming the nucleocapsid. By budding in the ER, the lipid envelope is obtained, and this process allows for the incorporation of E and prM proteins thus forming the viral envelope. Viruses travel then from the ER to the Golgi network where they undergo through a process of maturation given by the low pH which causes cleavage at the pr site of the prM. However, the pr remains still associated to the virion, and detaches completely only after the virus reaches the extracellular space. The final detachment of the pr makes the virus ready for fusion to a neighbouring cell, rendering it finally infectious. (Lindqvist et al., 2018)

TBEV transmission

TBEV is mainly transmitted to humans *via* tick bites which acts as the main transmission vector. Ticks get infected principally by feeding on animals such as small rodents which act as a reservoir host (Michelitsch et al., 2019). Infected ticks then transmit the virus upon feeding to another animal (**Fig. 5**).

Two types of viral transmission exist: the vertical and the horizontal one. The vertical transmission consists in the maintenance of infection during the tick life cycle. This kind of transmission can be trans-ovarial, meaning that an infected tick passes the virus to the offspring via the eggs, or trans-stadial, meaning that the virus persists in the different stages of tick development. On the other hand, horizontal transmission occurs when an a tick gets infected by feeding on an infected animal, which can then be passed to a human host, which is referred as dead-end host, since it is not allow the transmission from the human to an uninfected tick (Labuda et al., 1997) (Ijaz et al., 2023) . Moreover, a third method of transmission is referred as co-feeding, where an infected tick and an un-infected tick co-feed on the same animal which acts as a bridge for the transmission of the virus (Labuda et al., 1997). Moreover, TBEV can also persist in alimentary products such as unpasteurized milk and dairy products thus allowing for infection of people consuming those products (Ličková et al., 2021).

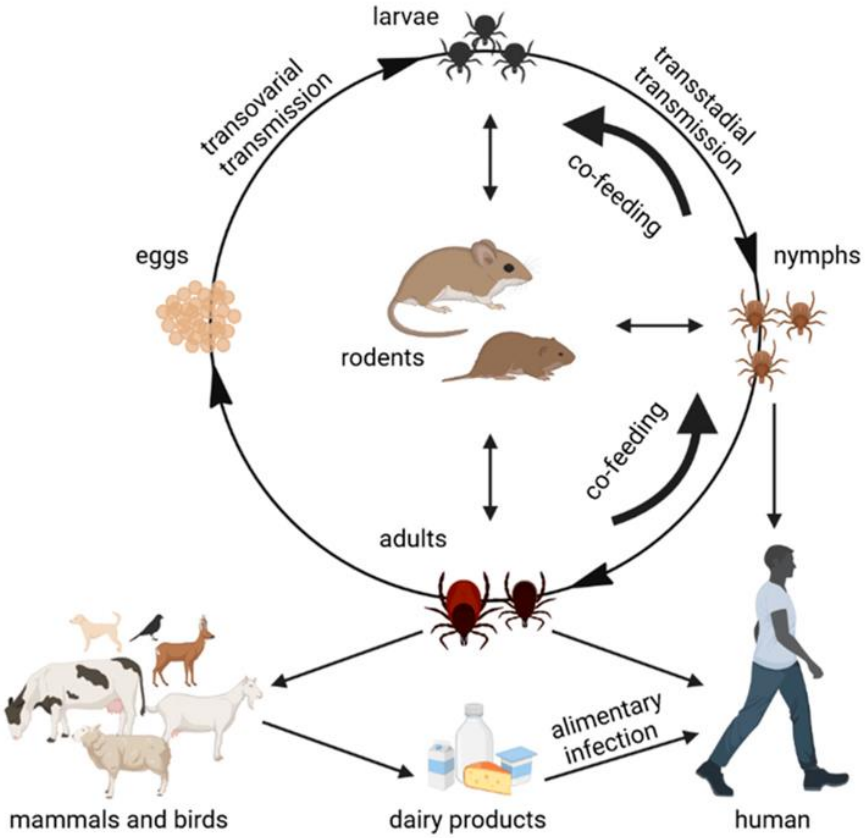

Figure 5 TBEV transmission cycle. (Ličková et al., 2021)

TBEV caused disease

TBEV infection is known to cause tick-borne encephalitis, a viral infection affecting the central nervous system (CNS) with neurological symptoms.

The disease has a biphasic course (**Fig. 6**). The first viraemic phase starts after the incubation time of approximately 8 days. This phase is characterized by influenza-like symptoms (fever, fatigue, body pain etc). In 65% of cases, after the first phase the virus gets cleared. However, for the remaining 35% an asymptomatic phase of approximately 7 days follows, which is further followed by a second phase with no detectable virus. This second phase can last months and is characterized by more severe, neurological symptoms, such as cranial nerve paralysis, spinal nerve paralysis, ataxia, tremor, altered consciousness. The mortality rate varies based on the strain, the Far Eastern strain (TBEV-FE) has the highest mortality rate of 5-35%, while in the case of the European and Siberian strains the mortality rate is lower 1-3%.

While there is a vaccine given in three doses available for prevention, there are no antivirals approved for the treatment of infected patients.

Since TBEV infection induces humoral and cell-mediated immune response, patients get diagnosed by the detection of specific IgM and IgG from the serum. IgM are detectable at early phases of infection, while IgG presents a peak at the convalescent phase of the disease and persists for a lifetime (Blom et al., 2018).

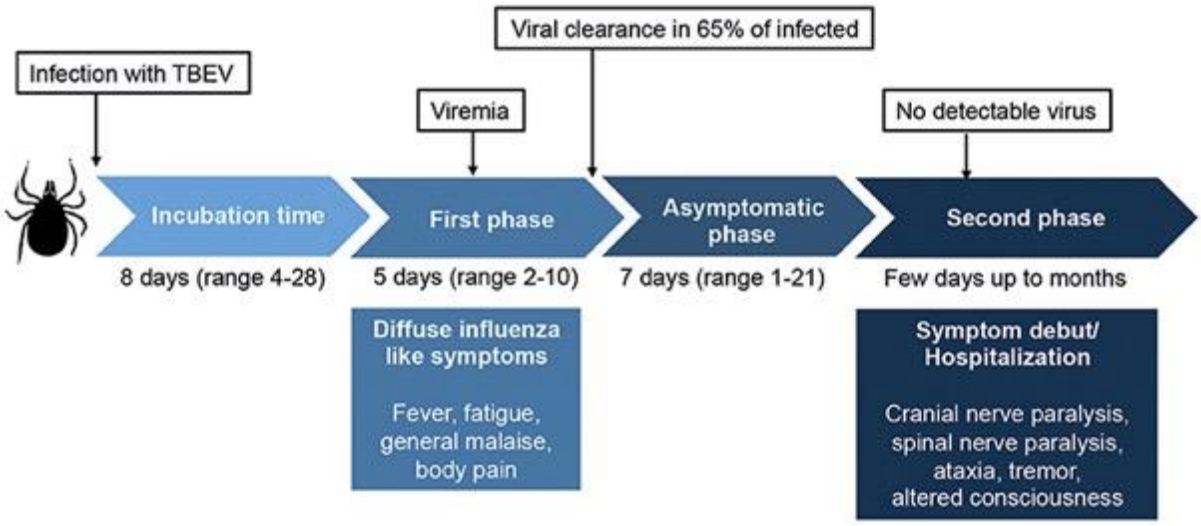

Figure 6 Biphasic course of TBEV infection (Blom et al., 2018)

The unfolded protein response (UPR)

The endoplasmic reticulum (ER) is a cellular organelle in which homeostasis is highly challenged by several processes, including proper protein folding and assembly, lipid and sterol biosynthesis, signalling and Ca^{2+} reservoir. In a condition of ER stress, where there is an uncontrolled accumulation of proteins in ER, which are therefore more prone to an incorrect folding, the unfolded protein response (UPR) pathway located at the ER level gets activated to

restore homeostasis. Activation of UPR acts by reprogramming gene transcription, mRNA translation and protein modifications, and inducing protein degradation (Hetz, 2012).

UPR is characterized by three main signalling branches. Each of them initiates the signalling cascade by the activation of the three ER transmembrane proteins:

- Inositol-requiring enzyme type 1 (IRE1α)
- (PKR)-like endoplasmic reticulum kinase (PERK) and
- Activating transcription factor 6 (ATF6)

Every protein has a luminal and cytoplasmic domain: the luminal domain senses stresses such as unfolded proteins in the ER, while the cytoplasmic domain is engaged in the interaction with the cellular components, triggering the pathways. Luminal BiP protein is fundamental for maintaining the inactive state of IRE1, PERK and ATF6, indeed, in an inactive condition, it is bound to the luminal domains of the proteins, inhibiting their activation. Upon the sensing of unfolded proteins, BiP behaves like a chaperon and binds the accumulating proteins to facilitate their proper folding. The detachment of BiP from PERK, IRE1 and ATF6 causes their activation and subsequent UPR signalling pathway.

Once activated, UPR can lead to protective or pro-apoptotic pathways. If the ER stress gets resolved a homeostatic condition is restored and UPR signalling is shut off. On the contrary, if the stress persists UPR can lead to apoptosis (Chen et al., 2023).

Upon UPR activation and induction of the three UPR branches, cells try to restore a homeostasis by acting at the following levels: ERAD, protein synthesis, autophagy, oxidative stress, mitochondrial dysfunction and metabolism.

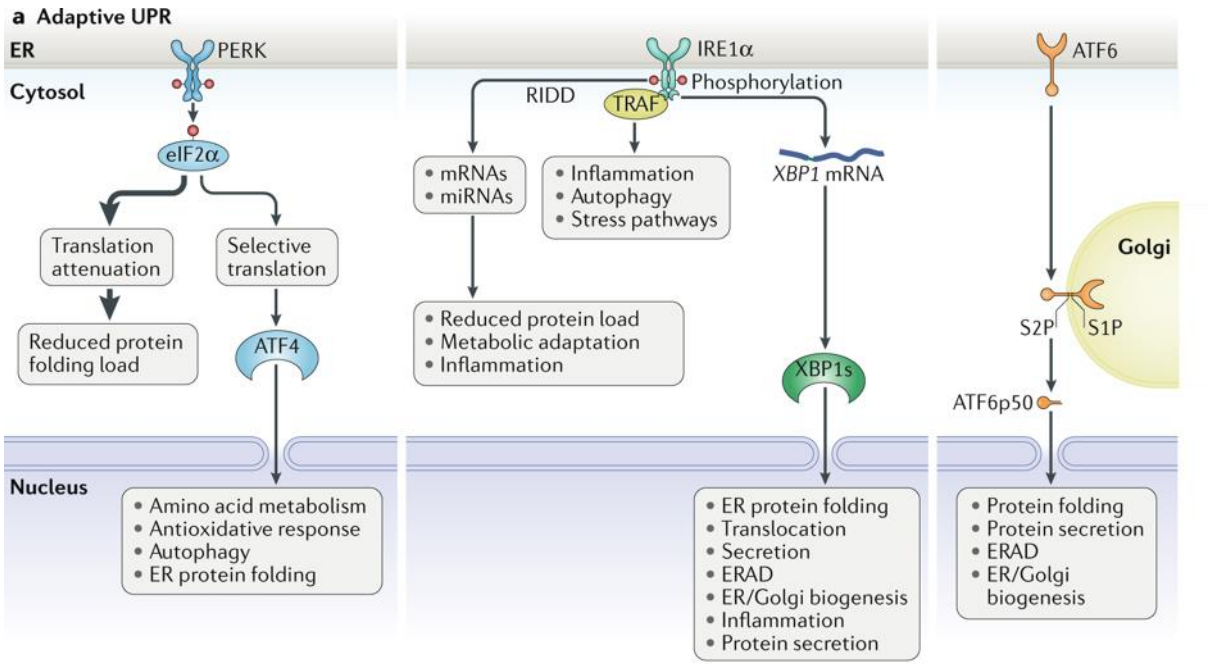

Figure 7 UPR signalling pathway. Adapted from (Hetz et al., 2020)

PERK signalling

The first reaction to UPR stress is given by PERK (Feng et al., 2021). Upon sensing of unfolded proteins in the ER, PERK dimerizes and auto-phosphorylates and in turn mediates the phosphorylation of the eukaryotic translation initiation factor 2 alpha (eIF2). When phosphorylated, eIF2α leads to a temporary attenuation of protein synthesis, being implicated in the ternary complex formation (described more in details in the integrated stress response-ISR paragraph). By inhibiting mRNA translation and protein synthesis, the ER is relieved from overlad allowing recovery form stress. On the other hand, P-eIF2α also coordinates a preferential translation of specific mRNAs which contain open reading frames (ORFs) in their 5' untranslated region (UTR), among which the mRNA of the activating transcription factor 4 (ATF4). ATF4 activates genes which regulate protein synthesis, redox homeostasis, amino acid metabolism, apoptosis and autophagy. Finally, ATF4 induces a negative feedback loop aimed at re-activating eIF2α, by removing its phosphate group *via* expression of growth arrest and DNA damage-inducible protein (GADD34) and constitutive repressor of eIF2α phosphorylation (CReP) proteins, cofactors of Protein phosphatase 1 (PP1). PP1 removes the phosphate group from the activated eIF2a, thus rendering it active again in the ternary complex. Additionally, ATF4 induces CHOP mRNA transcription, which is known to be involved in apoptosis triggering (Harding et al., 2000a).

IRE1α signalling

IRE1α is an ER transmembrane protein which upon activation dimerizes and mediates autophosphorylation. The luminal domain is responsible for sensing of unfolded proteins, while on the cytoplasmic the kinase and RNAse domain are found.

When unfolded proteins are sensed in the ER lumen, BiP detaches from the luminal side of IRE1, thus allowing for its dimerization. The dimerization brings in proximity the N-terminal luminal domains (NLDs) of IRE1, which in turn juxtaposes the kinase domains, allowing for a transphosphorylation of the dimers (Siwecka et al., 2021).

The RNase activity performs an unconventional cytoplasmic splicing of the X-box-binding protein1 (XBP1), by excising a 26-nt intron from its mRNA. XBP1 splicing is needed for the expression of an active form of the protein, which is then able to act as a transcriptional factor. XBP1s induces the expression of genes involved in ER protein translocation, folding and secretion. Moreover, degradation of misfolded proteins is also regulated by XBP1. Overexpression of XBP1 mRNA is given, in a context of ER stress, by the third branch of UPR, ATF6 (Yoshida et al., 2001).

IRE1α has also a role in the regulation of lipid metabolism. This regulation is given by the increase of XBP1s which acts on the transcription of lipid related genes (Moncan et al., 2021). On the other hand, IRE1α RNase domain has also a role in the regulated IRE1-dependent decay (RIDD), a process in which cleavage of a small set of mRNAs or miRNAs occur, with the aim, like in the case of PERK signalling, of lowering protein load of the ER. Every mRNA, including that of XBP1, has a consensus CUGCAG sequence accompanied by a stem-loop motif as target for IRE1α (Oikawa et al., 2010).

There is evidence about a role of a IRE1-RIDD-RIG-I pathway which connects the RIDD pathway to the antiviral RIG-I. Indeed, cleavage of some mRNA by the RIDD activity activates RIG-I pathway which in turn induces NF-kB and IFN pathways (Lencer et al., 2015). A direct connection between the RIDD pathway implication in the context of viral infection, and activation of an antiviral RIG-I signalling is hypothesized to be occurring *via* this path, however no evidence has still been shown in this context (Bhattacharyya, 2014).

ATF6 signalling

ATF6, like PERK and IRE1α, is an ER transmembrane protein activated upon ER stress. However, differently from the previous two, which dimerize and auto-phosphorylate upon infection, thus activate, ATF6 mechanism of action is different. Indeed, upon stress the full

length ATF6, referred as ATF6p90 transits from the ER to Golgi. At the Golgi level it gets cleaved by site-1 protease (S1P) and site-2 protease (S2P) to finally release the ATF6p50, a basic leucine zipper (bZIP) transcription factor to induce transcription of specific genes. Most of the genes induced by ATF6 overlap with the ones induced by XBP1, aiming therefore in restoring a homeostasis at the ER level (Hillary and FitzGerald, 2018).

UPR in viral infection

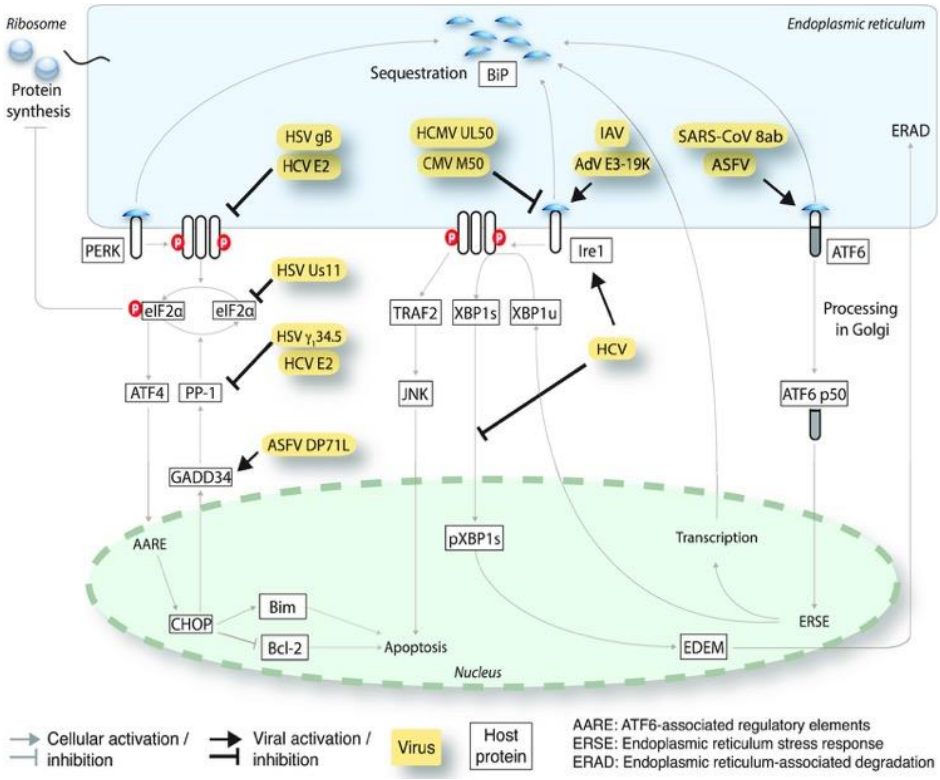

Figure 8 Viral proteins interfering with signal transduction along the three UPR branches IRE1, PERK and ATF6. (Prasad and Greber, 2021)

Several viruses have evolved mechanisms to favour their own replication and attenuate antiviral response. Some of those acts at the UPR level, where some viruses induce UPR activation, while others inhibit its activation. In figure 2 a representation from *Prasad et. Al 2021* of different viruses acting at the UPR level.

Enveloped viruses, such as TBEV, generally induce an ER overload, since there is the need for proper folding of viral proteins and glycosylation of specific proteins. Knowing this, it is easy to assume that upon infection, there is a global activation of the three UPR branches. (Prasad and Greber, 2021)

The activation of UPR *via* different mechanisms has been reported for several enveloped viruses, among which some *Orthoflaviviruses*. DENV infection is known to induce UPR

activation (Umareddy et al., 2007). A splicing at the Xbp1 level was seen as well (Yu et al., 2006). JEV infection has been reported to induce the activation of each of UPR branches (Sharma et al., 2017; Yu et al., 2006).

UPR in TBEV infection

In 2019 Carletti et al. from Molecular Virology lab in ICGEB, Trieste where I am conducting my PhD studies published a paper about the role of TBEV in UPR activation upon infection. RNAseq analysis conducted upon TBEV infection of U2OS cells at 24 hours post infection (h p.i.) vs 10 h.p.i., indicated several UPR related genes among the most strongly overexpressed ones. These data were further confirmed by RTqPCR. Moreover, treatment with tunicamycin, a well-known UPR activator, during TBEV infection reduced TBEV replication and induced expression of antiviral genes, meaning that activation of UPR prior infection helps in inhibiting virus replication. In addition, silencing of each of UPR's arm, indicated IRE1 as the main branch involved in the abovementioned role, since its downregulation allowed TBEV to replicate more compared to a control silencing (Carletti et al., 2019).
All together this data indicated a fundamental role of UPR during TBEV infection and more detailed studies might explain more precise mechanisms through which UPR activation occurs.

The Integrated stress response (ISR)

Upon changes in the cellular physiological condition caused by a range of different stressors, cells activate a pathway named integrated stress response (ISR). The stressors include cell extrinsic and intrinsic signals. Hypoxia, aminoacidic deprivation, glucose deprivation and viral infection belong to the extrinsic stressors, while the abovementioned UPR activation caused by an ER stress is listed as an intrinsic stress factor. Interestingly, all those factors converge on the activation of a common protein, termed as eukaryotic translation initiation factor 2 (eIF2α). Indeed, upon ISR activation, eIF2α gets phosphorylated thus inducing a global reduction in protein synthesis but allowing still for the preferential translation of specific mRNA, such as ATF4. Based on the severity of the stress stimuli, p-eIF2α might get de-phosphorylated, restoring a normal homeostatic status of the cells, or, when stress persists, could lead even to apoptosis. Four main kinases are responsible for the activation of the ISR: PKR-like ER kinase (PERK), double-stranded RNA-dependent protein kinase (PKR), heme-regulated eIF2α kinase (HRI) and general control non-derepressibile 2 (GCN2). Each of the kinases responds to different stress stimuli, dimerizes, auto-phosphorylates and in turn phosphorylates eIF2α (Feng et al., 2021; Lavoie et al., 2014; Lemaire et al., 2008; Misra et al., 2024; Ricketts et al., 2022).

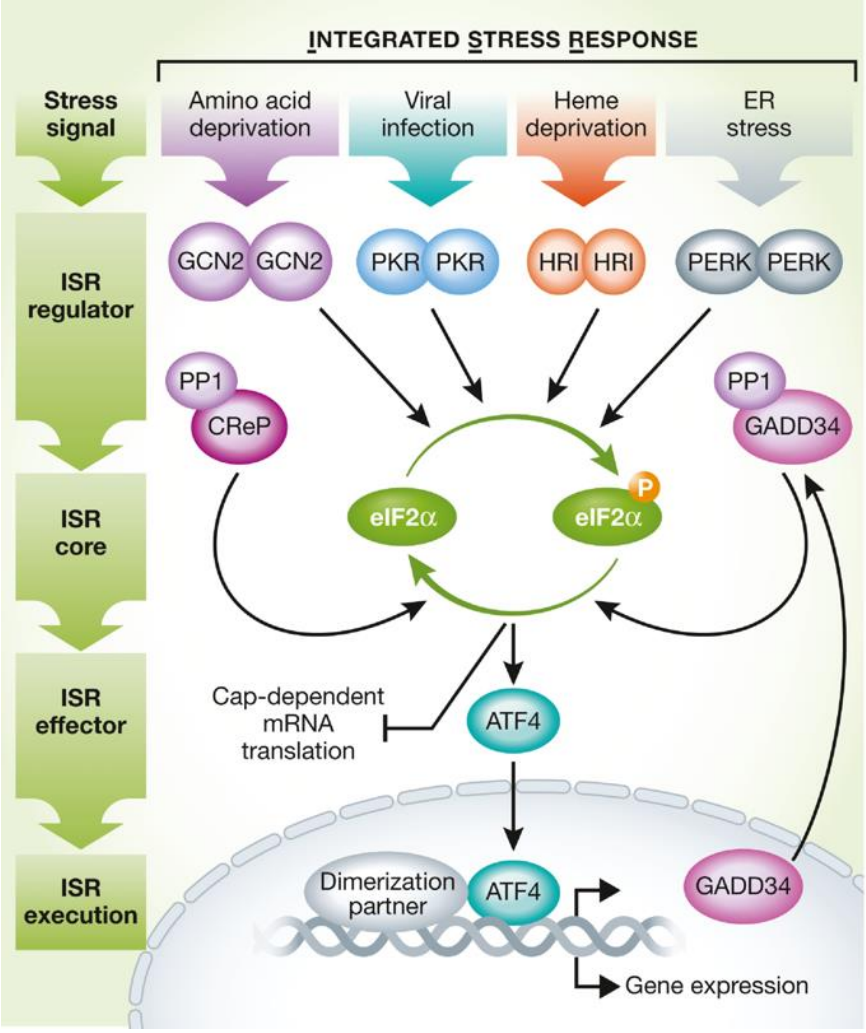

Figure 9 The integrated stress response (Pakos-Zebrucka et al., 2016)

ISR branches

Mechanistically, PERK activation has been discussed in the previous paragraph; what follows is the presentation of the detailed role of PKR, HRI and GCN2.

GCN2

GCN2 is a protein with high conservancy from yeast to human. It responds and activates upon amino acid deprivation via its binding to tRNAs. Moreover, its activity has been reported also by prolonged glucose deprivation in cancer cells, as well as in a context of UV radiation (Misra et al., 2024). Evidence suggests this kinase gets also activated upon viral infection in HIV-1 infection (Del Pino et al., 2012).

HRI

While the other kinases have a wide tissue distribution, HRI is mainly expressed in erythroid cells and has a role in erythropoiesis. It senses heme presence and couple globin mRNA translation. Indeed, in a therefore allowing for the translation of globin mRNA. However, upon its shortage and lack of interaction with HRI, HRI gets activated to inhibit globin mRNA translation. Indeed, accumulation of globin aggregates in cells is cell toxic. Presence of heme covalently binds to HRI, thus inhibiting its activation; on the other hand, the lack of heme, allows for the formation of an HRI dimer which therefore gets activated (Chen, 2007).

Arsenite-induced oxidative stress, heat shock, osmotic stress, 26S proteosome inhibition and nitric oxide are additional factors able to induce HRI activation. However, on contrary of heme deprivation which activates HRI in absence of heme itself, the abovementioned additional stressors induce HRI with the help of heat shock proteins such as HSP90 and HSP70, however the exact mechanism of this action is still unknown (Ricketts et al., 2022).

PKR

PKR is, together with PERK, the main ISR kinase activated upon viral infection. Indeed, it gets activated by sensing dsRNA, a hallmark of +ssRNAs viruses' replication (including TBEV). PKR contains an RNA binding domain (RBD) which binds the dsRNA, subsequently PKR dimerizes and autophosphorylates via its C-terminal kinase domain becoming therefore active. Once active, the kinase domain directly induces eIF2α phosphorylation (Nanduri et al., n.d.)

Like it was observed for HRI, also PKR can get activated by stimuli different than dsRNA in a dsRNA independent way. Those include oxidative and ER stress, growth factor deprivation, cytokine or bacterial infection and other (Pakos-Zebrucka et al., 2016)

eIF2α and its role in mRNA translation

eIF2α, together with eIF2β and eIF2γ form the eIF2 complex, which has the role of mRNA translation initiation and recognition of the AUG codon (Merrick, 1992). eIF2α has the main role in this complex since it is the only protein of the complex which owns a phosphorylation site, together with the RNA binding site. It gets phosphorylated at the S51 position (Harding et al., 1999). Indeed, mutations at this site have shown that inhibition of phosphorylation of eIF2α results in a loss of translation inhibition. In mice that are homozygous for the mutation at this site, a lethal effect was shown shortly after their birth, indicating the importance of the block of translation given by eIF2α (Scheuner et al., 2001)

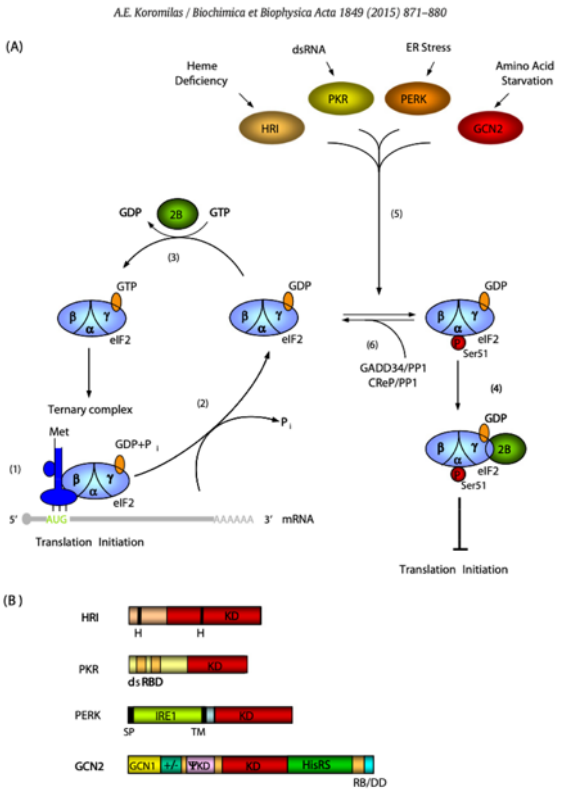

Figure 10 Regulation of mRNA translation by eIF12aS51P (Koromilas et al., 2015).

Moreover, the eIF2 complex, together with GTP and Met-tRNA$_i$ which binds to the 40S ribosome unit, forms the ternary complex. With the addition of two small initiation factors, eIF1 and eIF1a, to this complex, the 43S pre-initiation complex is formed. This complex is then recruited to the 5'methylguanidine Cap of mRNA, facilitated by the eIF4F complex. Several passages follow in this process, leading finally to an exchange of GDP to GTP by a protein named eIF2B, which in turn repristinates the eIF2 complex in its active form.

Upon eIF2α phosphorylation this GDP to GTP transition mediated by eIF2B is inhibited, blocking the formation of the active ternary complex and the consequent attenuation of 5'Cap-dependent protein synthesis (Komar and Merrick, 2020). In these conditions only some specific mRNAs, containing a short 5'UTR ORF are translated by re-initiation mechanisms or recruitment of ribosomes to IRES sites. Among these unconventional mRNA are ATF4, ATF5, CHOP and GADD34.

ISR and stress granules

As previously described, ISR activation leads to eIF2α phosphorylation, which results in mRNA inhibition of translation. This inhibition leads to an accumulation of un-translated mRNA in the cytoplasm. Those mRNA are bound by proteins of translation initiation as well as other RNA binding proteins (G3BP and TIA-1/TIAR) to form stress granules (Gilks et al., 2004; Kedersha et al., 2016).

Stress granules are membrane-less organelles formed by messenger ribonucleoprotein (mRNPs) complexes. Their composition includes 40S ribosomal subunit, translation initiation factors, poly(A)+ mRNAs and RBPs. Moreover, protein kinases, RNA helicases, structural constituents of ribosomes, calcium-binding proteins, hydrolases and cytoskeletal proteins are also part of stress granules. The composition of stress granules varies depending on the type of stress inducing their formation (Kedersha et al., 1999)

To start their formation, eIF2α must get phosphorylated by one of the four above-described kinases (GCN2, PERK, PKR and HRI). P-eIF2α induces the stall of translation thus accumulation of cytoplasmic mRNA, translation factors, RBPs and other proteins which promote some electrostatic interactions eventually forming stress granules which contain a stable core and a dynamic shell (Marcelo et al., 2021).

The role of stress granules is to act as foci for arrested translation during a stress event. However, their role has been extended also to a more active function in stress response and signalling, apoptosis, and others.

Stress granules in viral infection

SGs formation can be triggered in response to viral infection. They confer the cells a mechanism of fighting virus replication by blocking its mRNA translation (Marcelo et al., 2021). As reviewed by White and Lloyd, virus-SGs interaction show different phenotypes in the context of diverse viruses. Some viruses can induce and then inhibit SGs, such as Hepatitis C virus (HCV). For HCV it has been also shown that SG have an oscillatory phenotype which allows the cell to avoid a permanent translational shut-off and prolong cell survival, allowing thus the virus exploit this mechanism to sustain its replication (Ruggieri et al., 2012). Other, including West Nile and dengue virus have been reported to inhibit directly SGs formation by an interaction with TIAR, a SG marker (Emara and Brinton, 2007). Finally, some viruses have been reported to tolerate or exploit SGs to induce a more powerful replication, such as Respiratory syncytial virus (White and Lloyd, 2012). In 2012, Onomoto and colleagues described for the first time the localization of viral RNA in SGs. Unlike it was known until that

moment, that SGs contain only cellular mRNA stalled in translation, they showed that also viral RNA might get trapped in SGs giving a strong indication about the role of antiviral platform attributed to the SGs. Indeed, what they have seen is that upon infection with NS1-deficient Influenza A virus, there is an accumulation of RIG-I protein and viral RNA at the SGs level, allowing thus for the induction of an antiviral response. Additionally, they found that those SGs are generated by the activation of the PKR arm of ISR. (Onomoto et al., 2012). Also in the case of TBEV infection SGs get formed (Albornoz et al., 2014), it was observed that in virus induced SGs there is a colocalization between G3BP1, a SG marker, and RIG-I, giving an indication again about a possible role of SGs as antiviral platforms (Carletti et al., 2017).

However, as previously described in the paragraphs dedicated to the single viral proteins, there is evidence on how viruses manage to avoid/block/inhibit the SGs induced antiviral activity. For orthoflavivral NS4B, NS2B and NS5 there are evidence indicating several mechanisms through which those viral components modulate SGs formation, by inhibiting their formation or inducing their disassembly to allow the virus avoiding an antiviral response. (Arakawa et al., 2022; Wu et al., 2024)

Stress granules in Orthoflaviviruses infection

Studies have revealed the role of some *Orthoflaviviruses* in stress granules inhibition upon infection as a mechanism of host cell response escape.

For ZIKV it has been shown that upon infection there is a low percentage of cells with SGs (cca 10%). It was further demonstrated that ZIKV is able of inhibiting arsenite induces SGs, but interestingly the abundancy of SG proteins remained unvaried. A redistribution of HuR SG protein was further observed, and authors confirmed a localization of G3BP1 and HuR protein with ZIKV replication complexes. Finally, a colocalization between G3BP1 and ZIKV E protein was found. This data are in line with the idea that some viruses, ZIKV included, subvert the activation of the ISR to form SGs in order to escape a cell response and continue replicating their genome. (Bonenfant et al., 2019).

In line with the previous study, a recent paper confirmed stress granules inhibition in ZIKV infection and attributed to NS2B a role in this inhibition. Indeed, they show that upon ZIKV NS2B overexpression, eIF2α phosphorylation is lost upon the induction of ISR pathways *via* Dithiothreitol (DTT), arsenite and PolyIC treatment. This NS2B mediated phosphorylation occurs by the interaction between NS2B and the eIF2α phosphatase PP1 (Wu et al., 2024).

Moreover, for JEV and DENV it has been also shown that they share a mechanism by which they induce the disassembly of SGs. In addition, they linked this function by the action of the viral NS4B protein which initiates the whole process. The findings of this paper have been explained more in the detail in the NS4B paragraph (Arakawa et al., 2022).

From our laboratory, we have evidence that upon TBEV infection SGs are formed, also in this case reaching not a high percentage of infected cells, no more than 30% of TBEV infected cells show G3BP positivity. Moreover, TIA-1 and TIAR were found to be recruited to the site of viral infection, however, by counting each single TIA-1 induced granule, and comparing their induction by infection or a stressor such as heat, what was found is that less TIA-1 granules are found in infected cells. On contrary, G3BP granules were increased in number upon TBEV infection. Additionally, TIA-1 was found to be binding TBEV RNA and to act as a negative regulator of TBEV replication (Albornoz et al., 2014).

Innate immunity

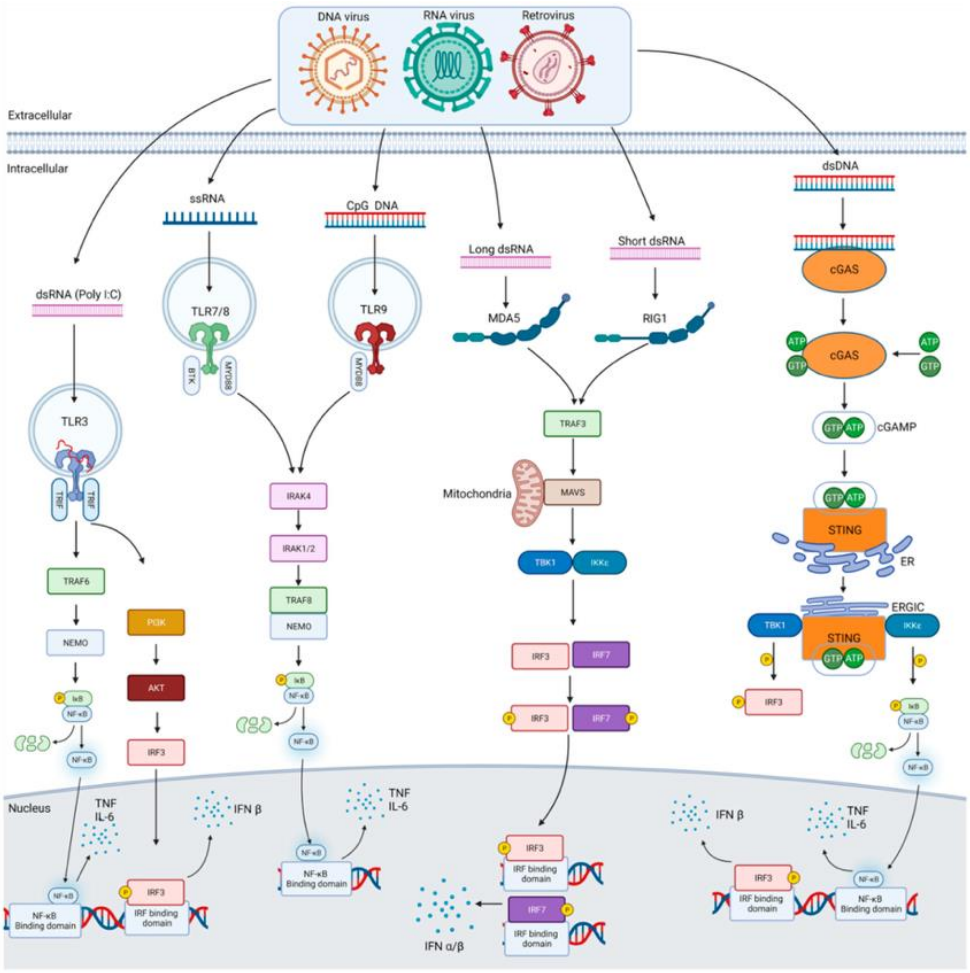

Figure 11 Antiviral pattern recognition receptors. (Hennessy and McKernan, 2021)

Upon viral infection, the first line of defence is given by the host innate immune response to fight against infection before the adaptive immunity gets activated. The key players in this process are the pattern recognition receptors (PRRs) which's role is to detect specific viral components and to induce an immune response via type I interferons (IFNs) and pro-inflammatory cytokines. PRRs include:

- Toll-like receptors (TLRs)
- Retinoic acid-inducible gene I (RIG-I)-like receptors (RLRs)
- Nucleotide-binding oligomerization domain (NOD)-like receptors (NLRs) (Koyama et al., 2008)

In view of orthoflaviviral infection, RLRs play a crucial role in the recognition of viral RNA and activation of the immune response. Mainly, the role of RIG-I is fundamental and has been shown to directly interact with several orthoflaviviral RNAs, including DENV and ZIKV (Chazal et al., 2018).

Toll-like receptors (TLRs)

TLRs are type I transmembrane proteins which recognize pathogen-associated molecular patterns (PAMPS) and damage-associated molecular pattern molecules (DAMPS) thanks to a 20-27 extracellular leucine-rich repeat. Upon activation, they induce downstream signalling pathways. 10 TLR members have been identified in humans. Functionally, they are subdivided in two classes:

- Cell membrane TLRs
- Intracellular TLRs

Upon activation by sensing of DAMPs and PAMPs, they induce antimicrobial activity and produce inflammatory cytokines (Tang et al., 2012).

NOD-like receptors (NLR)

NLRs are expressed mainly in the cytoplasm of immune cells, but not only. They sense stimuli of microbial infection and damage, like reactive oxygen species (ROS) or ion fluctuation. Mainly, they activate the Nuclear factor-κB (NF- κB) pathway, the mitogen-associated protein kinase (MAPK) and inflammasome (Franchi et al., 2009)

RIG-I-like receptors (RLRs)

RLRs are localized in the cytoplasm and are cytosolic sensors of RNA. Upon activation they initiate signalling cascades culminating in the type I interferon (IFN) and pro-inflammatory gene expression. They are formed by three members, RIG-I, melanoma differentiation-

associated protein 5 (MDA5) and laboratory of genetics and physiology 2 (LGP2). The three members are characterized by having a helicase domain and a so-called carboxy domain (CTD). The two domains together detect non-self RNA. Additionally, RIG-I and MDA5 have two amino-terminal caspase activation and recruitment (CARDs) needed to mediate downstream transduction. LGP2 is believed to regulate RIG-I and MDA5 (Rehwinkel and Gack, 2020). Additionally, RIG-I and MDA5 have been shown to have fundamental role in viral RNA recognition and downstream IFN signalling to induce an antiviral response (Kato et al., 2006).

The retinoic acid-inducible gene I (RIG-I) pathway

RIG-I, together with MDA5 and LGP2, belongs to the RIG-I like receptor family (RLR).

The RIG-I receptor is generally inactive in the cytoplasm. Upon interaction with the 5'-triphosphate (5'-PPP) or diphosphate (5'-PP) terminus of blunt-ended viral RNA duplex, a conformational change of the receptor occurs, exposing two signalling domains (CARDs). MDA5 on the other hand recognizes preferentially long dsRNA (>1-2 kb), such as some replication intermediates of certain RNA viruses. Host RNAs are generally capped and methylated, and do not have a 5'-PPP. These differences allow the RLR to detect only non-self RNA.

Once undergone the conformational change and exposure of the CARDs, these interact in turn with Mitochondrial antiviral-signalling protein (MAVS), an adapter protein located on the ER membrane, which triggers a phosphorylation cascade that leads to the expression of interferon stimulating genes (ISGs).

In detail: upon activation of RIG-I and MAVS, a phosphorylation cascade starts, causing the activation of Interferon regulatory factor 3 (IRF3) and NF-κB. This event is given by three main kinases:

- TNFα associated recruitment factors (TRAFs),
- Tank-binding kinase1 (TBK1) and
- Ikk kinase complex (IKK). (Rehwinkel and Gack, 2020)

Upon interaction with MAVS, it undergoes prion-like polymerization into fibril-like filaments which acts as a platform for downstream signalling. Indeed, they recruit TRAF adaptor proteins: TRAF3 for the IRF3/7 – IFN axis and TRAF6 for the NF-κB axis.

For the MAVS-TBK1/IKKε axis, MAVS associates also with TANK, NAP1 and SINTBAD – scaffold proteins that bridge MAVS to TBK1 and IKKε. Upon formation of these complexes, TBK1 and IKKε get trans-autophosphoylated at Ser172, which can then activate downstream

transcription factors. IRF3 and IRF7 get thus phosphorylated at specific C-terminal serine residues (i.e. S396-S405 in IRF3) leading to a dimerization, exposure of the nuclear localization signals (NLS) and translocation to the nucleus where they interact with CBP/p300 coactivators, bind promoters/enhancers of typer I IFN genes and induce ISGs expression.

In the case of the MAVS-NF-κB pathway, MAVS-TRAF6 activate the IKK complex formed by IKKα, IKKβ, and NEMO/IKKγ, which following ubiquitination of NEMO recruits TAK1 which phosphorylated IKKβ leading to the activation of the IKK complex. This active complex releases NF-κB dimers which translocate to the nucleus and promote pro-inflammatory gene expression (such as TNF, IL-6, IL-1β).

Together we can say that the IRF3/IRF7 branch induces activation of IFN-β, IFN-α and ISGs, while NF-kB induces pro-inflammatory cytokines. (Rehwinkel and Gack, 2020)

MATERIALS AND METHODS

Materials

Cells and media

The following mammalian cells were used:

- U2OS: Human osteosarcoma cell line (ECACC No. 92022711);
- Vero: African green monkey kidney cells (ECACC No. 84113001) were used for plaque assay;
- U2OS_IRF3-GFP: U2OS constantly expressing IRF3, under Geneticin selection (Maistriau et al., 2017)
- U2OS_PKR: U2OS constantly expressing PKR following transduction, under Puromycin selection
- U2OS_NS2B-HA: U2OS constantly expressing NS2B-HA following transduction, under Puromycin selection
- U2OS_EGFP: U2OS constantly expressing EGFP following transduction, under Puromycin selection
- BHK21 cells (ATTC CCL10) were used for the generation of reverse genetic viruses
- HEK-293T (ATCC number: CRL-3216): human embryonic kidney tissue

For bacterial work XL10-Gold Ultracompetent Cells (Stratagene) cells were used, as well as DH5α.

Mammalian cells were grown in Dulbecco's Modified Eagle Medium (Gibco –cat.num. 31885-023) supplemented with 10% foetal bovine serum (FBS) (Euroclone – cat.num. ECS0180L). For selection of stable cell lines Geneticin, also called G418 Sulfate (Invitrogen – 10131035), or Puromycine Dihydrochloride (Invitrogen – A1113803) were added at a concentration of 1.2 mg/ml and 1 µg/ml respectively. For transfection experiments with Lipofectamine OptiMEM: Reduced-Serum Medium (Gibco – cat.num 31985-070) was used. For transfection experiments with Calcium Phosphate DMEM, high glucose, GlutaMAX™ Supplement (Gibco – cat.num. 10566016) was used. For freezing cells for long-term storage cells were resuspended and stored in 90%FBS+10%DMSO at -80°C or in liquid nitrogen.

Bacteria were grown in Luria-Bertani (LB) Medium: 10 g bacto-trypton, 5 g bacto-yeast extract, 10 g NaCl per 1 litre medium. Ampicillin was added at a concentration of 100µg/ml. For hardening 1.5% agar-agar was added to the liquid medium.

Antibodies and antisera

In the following table the list of primary antibodies used:

Reactivity	Species	Subtype	Source	Dilutions
eIF3	Mouse		Santa Cruz; ref.sc-137214	
FLAG	Mouse	IgG Monoclonal	Sigma; ref.F1804-200UG	1:500 IF 1:1000 WB
FLAG	Rabbit	IgG Monoclonal	Sigma; ref.SAB4200119-200UL	1:500 IF
FLAG-HRP	Rat	IgG Monoclonal	Sigma; ref.SAB4200119	1:5000 WB
GFP	Mouse	IgG Monoclonal	Roche; ref.11814460001	1:1000 WB
HA	Rabbit	Polyclonal	Abcam; ref. ab9110	1:1000 WB 1:500 IF
Human b-actin-HRP	Mouse	IgG Monoclonal	Sigma; ref.A3854-200UL	1:50000 WB
Human eIF2a	Rabbit	Polyclonal	Cell Signaling; ref.9722S	1:1000 WB
Human eIF4B	Rabbit	Polyclonal	Abcam; ref.ab68474	1:100 IF
Human G3BP1	Mouse	IgG Monoclonal	BD transduction laboratories; ref.611126	1:100 IF
Human IFIT1	Rabbit	IgG	Cell Signaling; ref. 14769S	1:1000 WB
Human IKKε	Rabbit	Polyclonal	Cell Signaling; ref.2690	1:1000 WB
Human IRF3	Mouse	IgG Monoclonal	Cell Signaling; ref.10949	1:1000 WB 1:200 IF
Human p-eIF2a (Ser51)	Rabbit	Polyclonal	Cell Signaling; ref.9721S	1:500 WB
Human p-IRF3	Rabbit	IgG Monoclonal	Cell Signaling; ref.4947S	1:500 WB

Human p-PKR	Rabbit	IgG Monoclonal	Abcam; ref. ab32036	1:1000 WB
Human PKR	Rabbit	IgG Monoclonal	Cell Signaling; ref. 3072S	1:1000 WB
Human p-TBK1	Rabbit	IgG Monoclonal	Cell Signaling; ref.5483S	1:1000 WB
Human TBK-1	Rabbit	IgG Monoclonal	Cell Signaling; ref.3504S	1:1000 WB
PERK	Rabbit	IgG Monoclonal	Cell Signaling; ref.3192S	1:1000 WB
TBEV E	Rabbit	Polyclonal	Produced in the laboratory; whole serum not purified	1:500 IF 1:1000 WB

Following the list of secondary

Reactivity	Species	Fluorophore/HRP	Source	Dilutions
Mouse IgG	donkey	Alexa Fluor 488	Molecular Probes	1:500
Mouse IgG	donkey	Alexa Fluor 594	Molecular Probes	1:500
Mouse IgG	donkey	Alexa Fluor 647	Molecular Probes	1:500
Rabbit IgG	donkey	Alexa Fluor 488	Molecular Probes ref. A21206	1:500
Rabbit IgG	donkey	Alexa Fluor 594	Molecular Probes	1:500
Rabbit IgG	donkey	Alexa Fluor 647	Molecular Probes	1:500
Rabbit	goat	HRP	DakoCytomation ref. P0448	1:5000
Mouse	rabbit	HRP	DakoCytomation Ref. P0447	1:5000

Plasmids

The following plasmids were used:

Plasmid	Relevant characteristics	Reference
pl.18_NS2B-FLAG3X	AMP resistance; Hypr	Provided by Dr. Anna Overby
pl.18_NS4B-FLAG3X	AMP resistance; Hypr	Provided by Dr. Anna Overby

pl.18_NS5-FLAG	AMP resistance; Hypr	Provided by Dr. Anna Overby
pwpi_NS2B-HA	AMP resistance; Hypr	Generated during this study
pwpi_EGFP	AMP resistance;	Generated during this study
pl.18_hTBK-1-FLAG	AMP resistance;	Provided by Dr. Takashi Fujita
pl.18_hIKKε-FLAG	AMP resistance;	Provided by Dr. Takashi Fujita
pl.18_hMAVS-FLAG	AMP resistance;	Provided by Dr. Takashi Fujita
pl.18_RIG-I(N)-FLAG	AMP resistance;	Provided by Dr. Takashi Fujita
pl.18_IRF3-5D-HA	AMP resistance;	
pcDNA		
pl.18_GFP		
pl.18_NS2B3-FLAG	AMP resistance;	Provided by Dr. Anna Overby
pl.18_NS2B3-S135A-FLAG	AMP resistance;	Generated during this study
pl.18_NS4B_M1-FLAG	AMP resistance;	Generated by Dr. Lais Nascimento
pl.18_NS4B_M2-FLAG	AMP resistance;	Generated by Dr. Lais Nascimento
pl.18_NS4B_M3-FLAG	AMP resistance;	Generated by Dr. Lais Nascimento
Fragment 1-mCherry	/	Provided by Dr. Daniel Ruzek
Fragment 1-tGFP		Provided by Dr. Daniel Ruzek
Fragment 2		Provided by Dr. Daniel Ruzek
Fragment 3		Provided by Dr. Daniel Ruzek
Fragment 2_M1		Generated during this study
Fragment 2_M2		Generated during this study
Fragment 2_M3		Generated during this study
psPAX	Packaging Vector	Addgene
pMDG.2	Encodes VSV-G Envelope protein	Addgene

Primers

The following primers were used for PCR and RT-qPCR:

Primers	Sequence 5' – 3'
BiP FW	CCC GAG AAC ACG GTC TTT GA
BiP RV	TCA ACC ACC TTG AAC GGC AA
CHOP FW	TAA AGA TGA GCG GGT GGC AG
CHOP RV	CTG CCA TCT CTG CAG TTG GA
DNAJC3 FW	CGT TTG CGT TCA CAA GCA CT
DNAJC3 RV	CCC GAA CTT CAC TGA GGG AC
EDEM1 FW	AGG ACC AAG GGG GAA AGT CT
EDEM1 RV	GTA CAC GAT TGC AGT TGG AGC
GADD34 FW	CCC AGA AAC CCC TAC TCA TGA T
GADD34 RV	CTC GGA GAA GCG CAC CTT T
GAPDH FW	CAT GAG AAG TAT GAC AAC AGC
GAPDH RV	AGT CCT TCC ACG ATA CCA AAG
IFI44 FW	AGA CGA ATG CTA TGG GCT GC
IFI44 RV	CCT CCC TTA GAT TCC CTA TTT GCT C
IFI44L FW	TCA AAG CCG GGT CAT GAA TG
IFI44L RV	CCT TCA TGG GGT CCA GTT CC
IFIT1 FW	GAA ATA TGA ATG AAG CCC TGG A
IFIT1 RV	GAC CTT GTC TCA CAG AGT TCT CAA
OASL FW	TAC CAG CAG TAT GTG AAA GCC A
OASL RV	GGT GAA GCC TTC GTC CAA CA
TBEV 5' NCR FW	GCG TTT GCT TCG GA
TBEV 5' NCR RV	CTC TTT CGA CAC TCG TCG AGG
VIPERIN FW	CCC CAA CCA GCG TCA ACT AT
VIPERIN RV	TTG ATC TTC TCC ATA CCA GCT TCC
XBP1S FW	CTG AGT CCG CAG CAG GTG
XBP1S RV	GGC TGG TAA GGA ACT GGG TC
XBP1U FW	AGC CAA GGG GAA TGA AGT GAG G
M1_FW (RG)	GGCACTCCA TCTGGCCATTGTGGAGGCTGA ATTGACACAGAGAG
M1_RV (RG)	CTCTCTGTGTCAATTCAGCCTCCACAATGGC CAGATGGAGTGCC
M2_FW (RG)	GGCCAT TGTGGTGTCTGGTCTGACACAGAGAGC TCATAAGGTCT
M2_RV (RG)	AGACCT TATGAGCTCTCTGTGTCAGACCAGACAC CACAATGGCC
M3_FW (RG)	GGTGTCTGG TCTGGAGGCTGAATTGCATAAGGTCTTTTTCTCTGCA ATGGTGC
M3_RV (RG)	GCACCATTG CAGAGAAAAAGACCTTATGCAATTCAGCCTCCAGAC CAGACACC

Solutions and buffers

2X HBS - In water, 42 mM HEPES (Sigma-Aldrich), 274 mM NaCl, 1.5 mM Na2HPO4 • 12H2O, 15 mM D-glucose and pH adjusted to 7.0 (final volume: 1 Liter).

3.7 % Paraformaldehyde (PFA) - 10mL of 37% PFA: 3.7gr of PFA powder, reagent grade crystalline (Sigma-Aldrich) dissolved in 10 mL of distilled water, 10µl 10M KOH. 37% PFA was diluted in 2X PHEM buffer (18.14g PIPES (ChemCruz); 6.5g HEPES; 3.8g EGTA; 0.99g MgSO4; pH adjusted to 7.0 with 10M KOH) to produce 3.7% PFA.

8% carboxymethylcellulose sodium salt (CMC) - Sterile 80g CMC powder (Sigma-Aldrich) was dissolved in 1liter of 1X PBS.

1% Crystal violet solution - 1L; 10g Crystal violet powder (Sigma-Aldrich), 200mL PBS and 800mL Methanol (Sigma-Aldrich).

RIPA buffer - 50mM Tris-Cl pH 7.5, 150mM NaCl, 1% NP-40, 0.1% SDS, 1mM EDTA, 1mM EGTA, 1mM PMSF, 0.5% Sodium deoxycholate (Sigma-Aldrich) and Proteinase Inhibitors Cocktail (Roche) and Phosphatase Inhibitors: Sodium Fluoride (Riedel-deHaën) and Sodium Orthovanadate (Sigma-Aldrich).

Laemli Buffer (5X) - Tris (1M) pH 6.8, 2-β-mercaptoethanol, 10% SDS, 70% glycerol, bromophenol and H2O.

SDS electrophoresis buffer (10X) - 30.2g Tris, 188g Glycine (Sigma-Aldrich), 50 mL 10% SDS (Sigma-Aldrich), add water to 1 Liter. Final concentration used is 1X.

Transfer Buffer (10X) - 30gr Tris, 144gr Glycine, add water to 1 Liter. The working concentration was 1X: 100mL, 200 mL methanol and 700ml water.

TBS (10X) - 60g Tris, 2g KCl, 80g NaCl, pH adjusted to 8.5 with 37% HCl, add water to 1 Liter. The working concentration was 1X: 100mL 10X TBS, 900mL water plus 1mL Tween20 (Sigma-Aldrich).

Stripping solution – 15g Glycine (Sigma-Aldrich), 1g SDS powder (Sigma-Aldrich), 10mL Tween20 (Sigma-Aldrich), pH adjusted to 2.2 with HCl, add water to 1 Liter.

Methods – Protocols

Cell culture

Cells were grown in a cell-culture incubator at 37°C with 5% CO_2 with the suitable media. Cells were passaged when 90% confluent (approximately every 2 or 3 days) by detaching with Trypsin 0.05% - 0.02% EDTA and seeded at the appropriate dilution.

Cloning

To change vector encoding for the NS2B protein and changing its tag form FLAG to HA, the pl.18_NS2B_FLAG3x was used as template. FW primer was designed containing BamHI restriction enzyme, while the RV contained the HA tag at the 3' followed by MluI restriction enzyme sequence. PCR was performed with the following protocol: 4uL pl.18_NS2B_FLAG3x, 5uL PFU buffer; 2uL FW (10uL); 2uL RV (10uL) 1uL Polymerase; 1uL dNTPs; 35uL H_2O. Amplification was done 94°C 5 min, 94°C 30 sec; 65°C 30 sec; 72 °C 1 min; 72°C 5 min. Cycling reaction was performed 40X. The PCR product was then gel purified on a 1% agarose gel. The product (insert) as well as the pWPI vector were digested with BamHI and MluI. After digestion is done, the vector and the insert get ligated. After ligation and generation of the new construct, bacteria need to be transformed to amplify the plasmid.

Bacterial Transformation and Plasmid extraction

To amplify plasmid, DH5a competent bacteria cells were used. 50 of bacteria were thawed on ice. After thawing, bacteria were added to 5ng of plasmid and let on ice for 30 min. Heat shock followed for 30 sec at 42°C. 950 uL of LB were added to the bacteria and let on 1 h in the thermomixer at 37°C with the shaker on (250RPM). Transformation protocol was then plated on the desired plate containing the antibiotic resistance of interest and incubate O/N at 37°C. The next day colonies were picked and inoculated O/N in LB with antibiotic. Then, dependently it was possible to proceed by generation of a midi-prep or directly extracting the plasmid from bacteria with the usage of the kits. For mini-prep plasmids were extracted with the NucleoSpin Plasmid (Macherey-Nagel cat.num.1801/003), while for midi-preps NucleoBond Xtra Midi (Macherey-Nagel cat. num. 1803/009) was used. Extracted DNA was authenticated by restriction endonuclease digestion and sequencing. Restriction endonucleases and their specific buffers were purchased from New England Biolabs (NEB).

Production of infectious Lentiviral particles

Lentiviral (LV) particles were produced in HEK 293T cells using calcium phosphate transfection method. 1 x 10^6 HEK 293T cells were plated in 10 cm dishes one day prior to transfection. The following mix was prepared in 450 µl of sterile dH2O:

- 5 µg expression plasmid of interest (pWPI),
- 3.75 µg psPAX2 packaging plasmid
- 1.25 µg pMD2.G envelope plasmid

50 µl of sterile 2.5 M CaCl2 was added to each tube.

This mixture was incubated for 5 min at room temperature and then added dropwise to 500 µl sterile 2X HBS (Hepes Buffered Saline: 50 mM HEPES pH 7.05, 280 mM NaCl, 1.5 mM Na2HPO4) by gently vortexing and incubated at room temperature (r.t.) for 30 min. The transfection mixture was added dropwise to the cells and incubated O/N for 16h.

The day after, media was changed to remove the transfection reagent and replaced with fresh DMEM GlutaMax + 10% FBS. Cells were then incubated at 37 °C, 5% CO2 for 24 h. Following day, media containing the lentiviral particles were collected and centrifuged at 2250 rpm (Eppendorf Centrifuge 5804R) for 10 min at 4 °C to pellet any HEK-293T cells accidentally collected during harvesting. The surnatant was filtered with 0.45 µm sterile filters. The filtered lentiviral stocks were aliquoted and kept at -80 °C until needed for transduction experiments.

Transduction with lentiviruses

To obtain a cellular population expressing the gene of interest in a high number of cells or to produce a stable cell line expressing NS2B_HA or the experimental control EGFP, $1x10^5$/one 6-well plate well cells were resuspended with 0.5mL of lentiviruses and 0.5mL DMEM GlutaMax, seeded and incubated for the desired timing. In case selection needed to be applied Puromycin was used until the moment the control cells without resistance completely died and we could assume the population was selected (approximately one week). To confirm the overexpression protein levels were checked by Western blot and by cytofluorimetric analysis.

Transfection with Lipofectamine

Cells were transfected with Lipofectamine LTX (ref. 12343593**)** reagent with the plasmids of interest based on the manufacturer's instruction.

Flow cytometry analysis (FACS)

To determine the number of transduced cells, cells were resuspended, fixed in 3.7% PFA and stained with the antibodies of interest to detect NS2B_HA positive cells, while no staining was needed for the EGFP control. The anti-HA antibody used is the ref. ab9110. Cells stained only with primary, only with secondary and with the combination of the two on non-transduced cells were conditions used as controls. Gating strategy is shown in Fig.35. Briefly, we firstly selected cells that were alive (A), then cell doublets were removed from the population under analysis (B), followed by the draw of a gate indicating cells positive for the fluorophore of interest (C). Finally in D we see the percentage of the cells positive for the HA tag in the control and test samples.

Immunofluorescence

Cells were seeded onto microscope coverslips. The desired experiment was performed in cell-culture. For IF analysis cells were washed three times with PBS and fixed in 3.7 % paraformaldehyde (PFA) solution (3.7% PFA in PHEM buffer: 60 mM PIPES, 25mM HEPES, 10 mM EGTA, 2 mM MgCl2) for 15 minutes at room temperature. Thereafter, cells were again washed three times with PBS containing CaCl2 and MgCl2 (PBS+S) and incubated 5 minutes with 100 mM Glycine in PBS+S to saturate excesses of PFA and to stop the fixation reaction. Cells were permeabilized for 5 minutes with 0.1 % Triton X-100 in PBS and washed three times, 5 min each. Before incubation with antibodies, a blocking step was performed at 37°C for 30 minutes with 1 % bovine serum albumin (BSA, Roche – cat.num 10735078001) and 0.1 % Tween 20 (Sigma Aldrich – cat.num P2287-500ML). Primary antibodies were diluted to the desired concentration in blocking solution to prevent a-specific binding of the antibodies. After one hour incubation at 37°C, or overnight incubation at 4°C, coverslips were washed three times with PBS+S 0.1 % Tween 20 (washing solution) and incubated with secondary antibodies for 1 hour at 37°C. Coverslips were finally washed three times with washing solution and mounted on slides using Vectashield mounting medium with addition of DAPI (Vector Laboratories – cat.num H-1200). When TO-PRO3 was used to stain nuclei, it was used at the 1:1000 dilution with the secondary antibodies incubation – therefore for 1h at RT.

Imaging of fixed cells

Fluorescent images of fixed cells were captured with the Zeiss 880 Airyscan confocal microscope (Carl Zeiss Microimaging, Inc.). Images were acquired with the 63X Plan-Apo/1.4 NA Oil objective. The pinhole of the microscope was adjusted to get an optical slice of less than 1.0 µm for any wavelength acquired. The fluorophore Alexa488 as well as EGFP were excited with 488 nm line of the Argon Laser, the fluorophore Alexa594 was excited with the HeNe Laser 543 nm, while the Alexa647 was excited with the HeNe 633 nm Laser. Their emissions were collected using the appropriate filters.

Co-localization analyses were performed with ImageJ software by calculating the Pearson's coefficient or the Manders coefficient.

Cell lysis

Depending on experimental need cells were lysed in different lysis buffer:

- Laemmli Buffer (50 mM Tris-Cl pH 6.8, 2% SDS, 10% glycerol, 100 mM DTT, 0.1% bromophenol blue);

- RIPA buffer (50 mM Tris HCl pH8, 150 mM NaCl, 1% NP-40, 0.5% Sodium Deoxycholate, 0.1% SDS additioned with Proteinase Inhibitors (Roche - 11836170001) and Phosphatase Inhibitors: Sodium Fluoride and Sodium Orthovanadate;

Co-immunoprecipitation (Co-IP)

For co-immunoprecipitation cells were lysated in the following lysis buffer: 0.5% NP-40 (PanReac AppliChem, cat. nr. A1694); 150 mM NaCl (Roth, art. nr. 3957.2); 50 mM TrisCl pH 8.0 (PanReac AppliChem, cat. nr. A1086); 1X Protease Inhibitor (Complete, Roche, ref. 11697498001). 1mL of buffer was added to each cellular pellet and incubated on ice for 30 min. Beads used are anti-FLAG beads (Sigma, ref. F2426-1ML). Beads need to be equilibrated in the lysis buffer prior usage. 20uL of beads are needed for each sample. The desired amount of beads get equilibrated in the lysis buffer, followed by centrifugation at 10000g at 4°C for 1 min. The procedure is repeated 4 times.

After 30 min on ice, the lysate needs to be centrifuged to remove excess of membranes for 15 min at 20000g and supernatant is transferred to a fresh tube. Next, 900uL of lysate is added to 20uL of equilibrated beads and is let rotating on a rotary mixer for 4h at 4°C. After 4h the IP product gets centrifuged, and SN is discarded, following by at least 4 washes in the IP lysis buffer. Once finished with the washes, the beads can get resuspended directly in the LB. Classical SDS-PAGE and Western blot analysis follow.

SDS-PAGE

After lysing cells in the appropriate buffer, quantification of the sample with the Bradford method was performed. Equal amount of each sample was used for loading and were prepared by adding the loading buffer. Once prepared, samples were boiled for 10min at 95°C and loaded on a 10% or 12% SDS-PAGE depending on the size of the protein of interest to detect. Proteins were then transferred from the gel to a nitrocellulose membrane by the western blot technique. Gels were run in SDS electrophoresis buffer (25 mM Tris, 190 mM glycine, 0.1% SDS), initially at 90 V into the stacking gel and later at 120 V into the running gel.

Western blot

For Western blotting, nitrocellulose membrane (GE Healthcare – cat.num 10600015) was used and membranes were blocked for 1 hour in 5% milk or 5% BSA (for detection of phosphorylated proteins) followed by incubation with the appropriate primary antibodies diluted in 5% milk (5% BSA)/ 0,5% Tween-20 at 4°C O/N. After three washing with TBS 0.5% Tween-20 secondary antibodies conjugated with HRP (DakoCytomation – cat.num

P0447/8) were diluted in 5% milk / 0,5% Tween-20 and incubated for 1 hour. Blots were developed using Immobilon Western Chemiluminescent HRP Substrate (Millipore – cat.num WBKLS0500) according to manufacturer's instructions or in the case of low abundant proteins Clarity Max^{TM} Western ECL Substrate (Bio-Rad, ref. 1705062) was used.

For densitometric analysis ImageJ software was used. Phosphorylated proteins were normalized on their total levels, while not phosphorylated proteins were normalized on the loading control (actin). The densitometric graph represents the quantification of the western blot panel showed in proximity.

Real-time quantitative reverse transcription PCR

To obtain total cellular RNA cells were lysed with TRiFast II (EuroClone cat.num. EMR517100) according to the manufacturer's instructions and extraction was performed with the phenol/chloroform method. After treatment with DNase I (Life Technologies – cat.num 18060-015), RNA was quantified using Nanodrop. 500 ng of extracted RNA was used as a template to synthesize cDNA using SensiFAST cDNA synthesis kit (Meridian Bioscience - Cat.num. BIO-65053). Quantitative Real-time PCR (qRT-PCR) using SensiFAST SYBR No-ROX (Meridian Bioscience – Cat.num. BIO-98005) was performed from cDNA samples. Signals of cellular mRNAs were normalized to the GAPDH mRNAsignal. The sequences of oligonucleotides used for this analysis are reported in the Primers session. Amplification and detection were carried out on a CFX96 Real Time System (Bio-Rad).

Statistical analysis

Statistical analysis was performed by using Prism GraphPad software. Data are presented as a mean of ± standard error of the mean (SEM). For the comparison of two groups, Student's t-test was performed. For the comparison of more than two groups, One-way ANOVA was performed. To choose if to use the parametric or non-parametric test, data were tested for Normality and Longemirity by the usage of the Shapiro-Wilk test. Tests performed for each experiment are listed in the figure legends. For all the statistical analysis, significance was accepted at *, p-value < 0.05 (** $p < 0.01$; *** $p < 0.001$).

Infectious experiments

All the experiments performed with TBEV were done in a BSL-3 facility.

Preparation of TBEV stock

TBEV Neudoerfl strain was used for my experiments, while for the experiments with the reverse genetic system the original Hypr strain was generated.

Viral stocks were prepared by infection of Vero cells at the low multiplicity of infection of 0.1. After cytopathic effect (CPE) was observed (approximately 5-6 days), cell culture supernatant was collected, clarified by centrifugation at 2250 RPM for 10min at 4°C and stored in aliquots at -80°C. Viral titres were determined by using a plaque-forming assay.

Plaque assay

120.000 Vero cells/well were seeded into 24-well plates on day one. Cells were infected the day after with a 10-fold serial dilution of TBEV in a total volume of 200 µl of serum-free medium. After 1 hour incubation at 37°C with 5% CO2, the inoculum was removed and a 500 µl overlay containing 1 volume of 6% carboxymethyl cellulose (CMC) to 1 volume of maintenance medium (DMEM supplemented with 4 % decomplemented FBS) was added. The plates were incubated for 5 days before fixation with 4 % PFA dissolved in PBS. Infected cells were stained adding 300 µl of 1% crystal violet solution in 80% methanol / 20% PBS. After 30 minutes the staining solution was removed, and cells were washed 3-4 times with water. Viral titres were determined by counting number of plaques formed and multiplying it for the dilution factor. The following equation is used to determine the PFU/mL.

$$\frac{PFU}{mL} = \frac{mean\ of\ plaques\ counted\ (PFU)}{volume\ of\ infection\ (mL)\ x\ dilution\ factor}$$

Infection with TBEV

For standard infection assays, U2OS cells were seeded on day one. 24 hours later, cells were infected at the appropriate multiplicity of infection (MOI) by adding the virus stock properly diluted in serum-free medium to get a final volume of 200uL for a 24-well plate, 400ul for a 12-well plate and 600uL for a 6-well plate. After 1 hour of incubation at 37°C with 5 % CO2, the inoculum was replaced with maintenance medium (DMEM supplemented with 4 % decomplemented FBS). The moment in which the virus is replaced with normal medium is considered time zero, 0 hours post infection (0 h.p.i.). Cells were then harvested at the appropriate time points.

To determine the volume of virus to use for infection at a desired MOI, the following equation needs to be used.

$$uL\,\frac{virus}{well} = \frac{n\ of\ cells\ per\ well\ at\ the\ moment\ of\ infection\ x\ MOI}{virus\ titer}$$

TBEV Reverse Gentics – Infectious subgenomic amplicons (ISA) method

To mutate TBEV in the region of interest the TBEV reverse genetic system detailly described in the papers by Haviernik and Berankova (Berankova et al., 2025; Haviernik et al., 2021) was

used. Briefly, three fragments defined as Fragment 1 (F1), Fragment 2 (F2) and Fragment 3 (F3) encoding the entire genome were transfected in BHK-21 cells to produce the viruses of interest. Following the detailed protocols of the experiments performed with the ISA.

Insertion of mutations in the fragments

To insert mutations of interest in the fragments which are linear DNA sequences, FW and RV primers containing the mutation of interest were designed. A first PCR is then performed by using the fragment as template and adding in one reaction the FW mutated primer and the RV used for the amplification of the original fragment, while in the other reaction the RV mutated primer and the FW for the original amplicon were used on the fragment of interest. From the two PCR we obtained two shorter fragments referred to as A and B. The PCR was performed with the Takara PrimeStar polymerase (Cat. # R045A/B) by adding: 1uL of FW primer (10uM), 1uL of RV primer (10uM), 0.5mL of template, 25uL of PrimeStar master mix and 22,5uL of H_2O. The amplification is performed at the following temperatures:

- 110°C lid for 90 sec
- 30-35 cycles: 98°C for 10sec; 55°C for 5 sec; 72°C for 5 sec per 1kbp (since F2 is cca 4 kbp, amplification step is 20 sec).
- Store at 4°C - 8°C

After PCR is done, samples need to be run on an agarose gel, gel purified form a 1% Agarose gel and sent for sequencing.

A second PCR is then performed in which fragment A and B obtained from the first PCR are added together with the original FW and RV primers and PCR is again performed. Since A and B have an overlapping region in the area of the mutation, those will anneal, and with several cycles of amplification the full mutated fragment will be obtained. Again, it has to be purified from agarose gel and sequenced.

Transfection and generation of infectious particles

To obtain replicative viruses, the three fragments are transfected on sub-confluent BHK-21 cells plated in 24-well plates. Transfection is done with XtremeGene HP Transfection reagent (Roche, ref. 6366244001) in the following way:

- Add 2,0 ug of DNA to 200 uL of OptiMem medium. If using two or more DNA parts (e.g. for homologous recombination), adjust the ratio of DNAs according to their length
- Add 2 uL of transfection reagent (XtremeGene HP DNA Transfection Reagent - Roche) to the mixture.
- Incubate for 15 mins at RT.

- Transfer the mixture to the well (24-well plate) with sub-confluent cells in 500 uL of cultivation medium.
- Watch for the cytopathic effect (CPE). When CPE occurs (usually 3 to 5 dpi), harvest infectious medium and prepare zero passage of the clone.

After collecting the viruses their titre is established by Plaque assay or Focus Formig Assay.

RESULTS

Introduction to the results part 1 – NS2B

These unpublished data were produced by Dr. Yvette Kazungu, a former PhD student in the laboratory and are a follow-up of the data published by Carletti *et al.* in 2019. I contributed to the data presented in this paragraph by performing biological replicates, generating the plots and performing statistical analysis.

TBEV prM, E, NS1, NS2A and NS2B proteins induce IRE1 activation

Since we previously observed (Carletti & Zakaria et al., 2019) that TBEV induces the unfolded protein response (UPR) early during infection, and that this UPR activation triggers the induction of the RIG-I dependent antiviral response, we decided to dig more in the detail of these events to understand the mechanisms connecting UPR activation and the subsequent upregulation of the genes belonging to innate immune response. IRE1α has been shown to be the branch of the UPR which acts as connector between UPR activation upon TBEV infection and induction of the response. Therefore, as is it known that XBP1 mRNA splicing is a

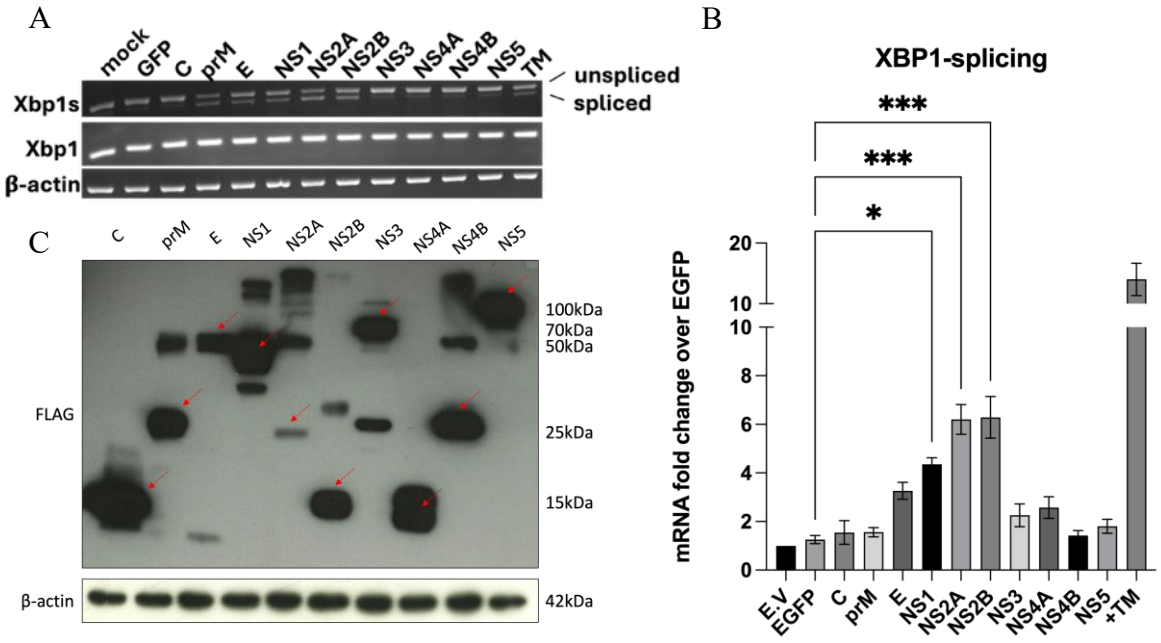

Figure 12 TBEV prM, E, NS1, NS2A and NS2B proteins induce IRE1 activation

U2OS cells were transfected with plasmids of interest with the Lipofectamine LTX reagent for 20h. Cells were lysed in Trizol for RNA analysis and in RIPA for protein analysis. RNA was extracted and retrotranscribed to cDNA. In a) a PCR was performed with primers amplifying both the spliced (double band) and unspliced (single band) version of XBP1, while in b) an RT-qPCR amplifying the spliced version of XBP1 was done. In c) western-blot confirming the overexpression of the FLAG tag proteins of interest by the usage of an anti-FLAG antibody.

hallmark of IRE1 activation, we screened the ability of all TBEV proteins to induce the UPR by overexpressing them in U2OS cells. We observed that prM, E, NS1, NS2A and NS2B

induce IRE1 activation since XBP1 mRNA is found in both the spliced and unspliced version **Fig. 12A**. Additionally, the same proteins were observed to induce XBP1-s RNA by RT-qPCR as seen in **Fig. 12B**. Western blot analysis is shown to confirm the overexpression of the proteins of interest **Fig. 12C**.

E, NS1, NS2A and NS2B induce UPR related genes

The next screenings were done by focusing only on TBEV proteins that induced IRE1 activation: E, NS1, NS2A and NS2B. Some of the UPR-replated genes which were observed to be overexpressed in the transcriptome analysis upon TBEV infection by Carletti et al. were used as targets. Those are: EDEM, GADD34, DNAJC3, CHOP/DDIT3, BiP. TBEV proteins were overexpressed in U2OS and then mRNA levels of genes of interest were determined by RT-qPCR. As expected, the viral proteins which were inducing IRE1 activation, induced an increased expression level of the UPR genes **Fig 13**.

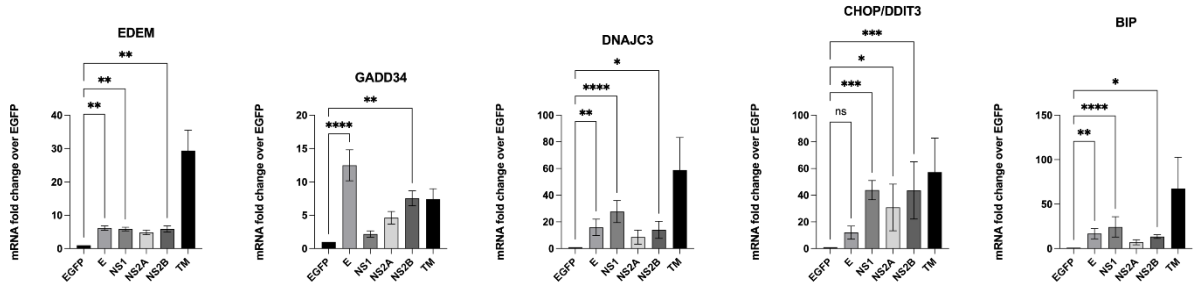

Figure 13 E, NS1, NS2A and NS2B induce UPR related genes

U2OS cells were transfected for 20h with the plasmids of interest using the Lipofectamine LTX reagent. Cells were lysed in Trizol and RNA was extracted, followed by cDNA synthesis. cDNA was used for RT-qPCR to determine mRNA levels of the genes of interest. Experiment was performed in 3 independent biological replicates, each in 2 technical replicas. Normalization was done on the mRNA level of the EGFP sample following the ΔΔCT method. Statistical significance was determined using the Kruskal–Wallis test with Dunn's multiple comparisons test. *, $P < 0.05$; **, $P < 0.01$; ***, $P < 0.001$*. Data are considered significantly different with a $p \leq 0.05$.

NS2A and NS2B proteins induce ISGs

Next, we wondered whether the overexpression of those viral proteins would have induced an increased expression level of ISGs as a readout of the antiviral response. The ISGs to test were selected based on the transcriptome results of TBEV infection generated and published in the Carletti and Zakaria et al., 2019 paper. We noticed that only NS2A and NS2B could induce several ISGs at different magnitude, while E and NS1 proteins were weaker **Fig. 14**.

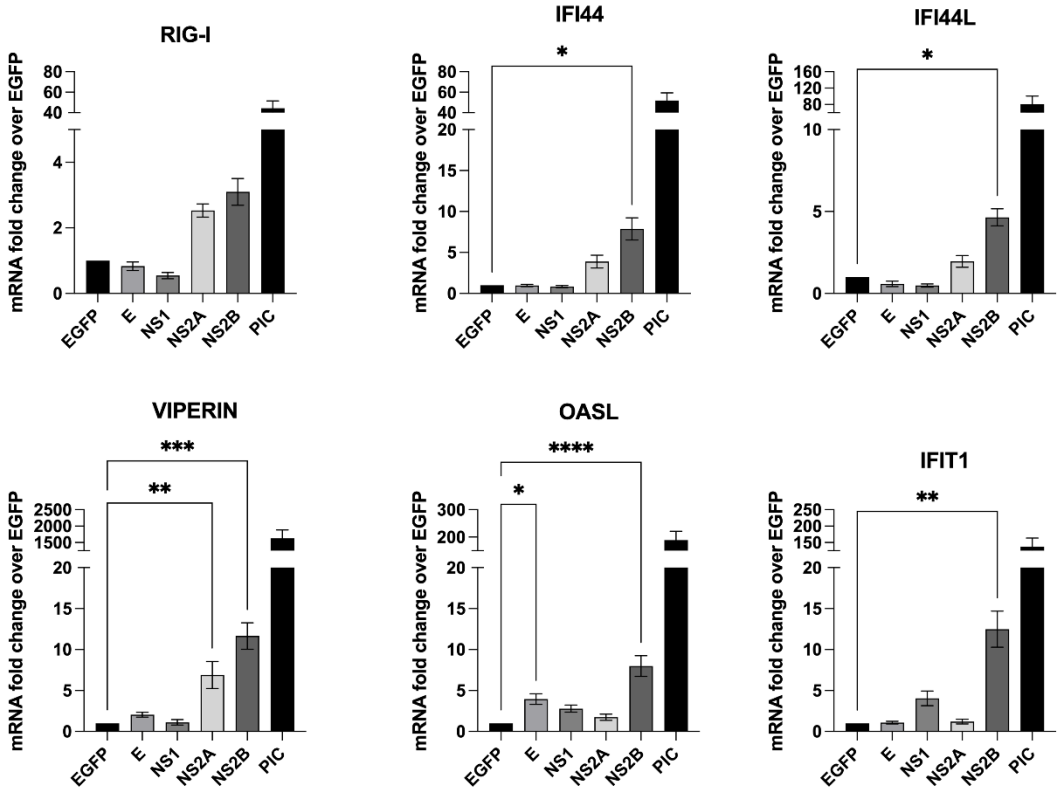

Figure 14 NS2A and NS2B proteins induce ISGs

U2OS cells were transfected for 20h with the plasmids of interest with the Lipofectamine LTX reagent. Cells were lysed in Trizol and RNA was extracted, followed by cDNA synthesis. cDNA was used for RT-qPCR to determine mRNA levels of the genes of interest. Experiment was done in 3 independent biological replicates, each in 2 technical replicas. Normalization was done on the mRNA level of the EGFP sample following the ΔΔCT method. For statistical purposes Statistical significance was determined using the Kruskal–Wallis test with Dunn's multiple comparisons test. *, $P < 0.05$; **, $P < 0.01$; ***, $P < 0.001$.

E, prM, NS1 and NS2A proteins fail to induce UPR-related genes in IRE1_KO cells, while NS2B still show a slight activation of UPR

Then, a U2OS cell-line was established in our laboratory which was knocked down for IRE1α. Since we observed previously (Carletti and Zakaria et al., 2019), that the TBEV given UPR activation and further ISGs upregulation were dependent on IRE1, we hypothesized that the

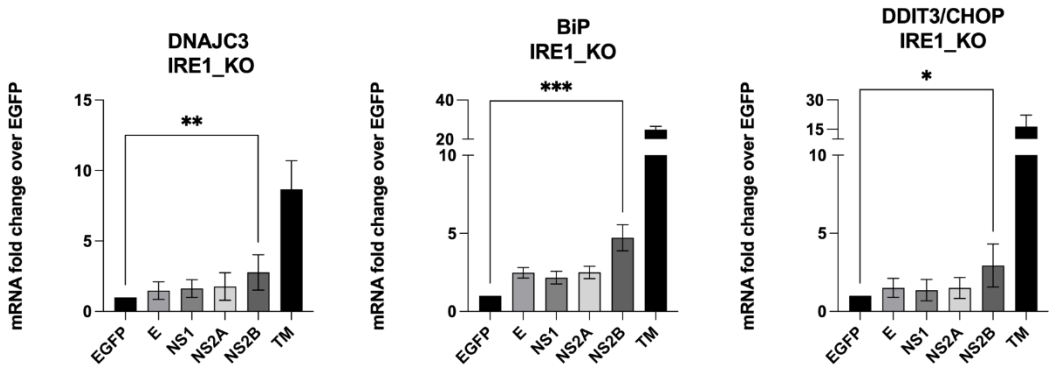

Figure 15 E, prM, NS1 and NS2A proteins fail to induce UPR-related genes in IRE1_KO cells, while NS2B still show a slight activation of UPR

U2OS cells were transfected for 20h with the plasmids of interest with the Lipofectamine LTX reagent. Cells were lysed in Trizol and RNA was extracted, followed by cDNA synthesis. cDNA was used for RT-qPCR to determine mRNA levels of the genes of interest. Experiment was done in 3 independent biological replicates, each in 2 technical replicas. Normalization was done on the mRNA level of the EGFP sample following the ΔΔCT method. For statistical purposes Statistical significance was determined using the Kruskal–Wallis test with Dunn's multiple comparisons test. *, $P < 0.05$; **, $P < 0.01$; ***, $P < 0.001$.

lack of IRE1 would have inhibited the upregulation of UPR and ISGs when overexpressing the selected TBEV proteins. Indeed, as expected we observed that the loss of IRE1 reduced drastically the upregulation of UPR-related genes as shown in **Fig. 15**. However, only NS2B was still able to slightly, but significantly induce their expression. This might mean that despite IRE1, NS2B is mildly activating also one of the other two pathways of UPR: PERK and ATF6.

NS2B induces ISGs upregulation in an IRE1 independent manner

Next, ISGs expression levels were addressed in IRE1 deficient cells upon the overexpression of TBEV proteins. In this case we again observed that, while E, NS1 and NS2A failed to induce ISGs in absence of IRE1, NS2B was still able of increasing the mRNA levels of those antiviral players (**Fig. 16**). These data suggest that NS2B protein play a role in the cell-antiviral response However, with this set of data we are proving that despite an obvious UPR activation, the induction of ISGs given by NS2B is not UPR dependent, suggesting a direct interaction with other cellular factors.

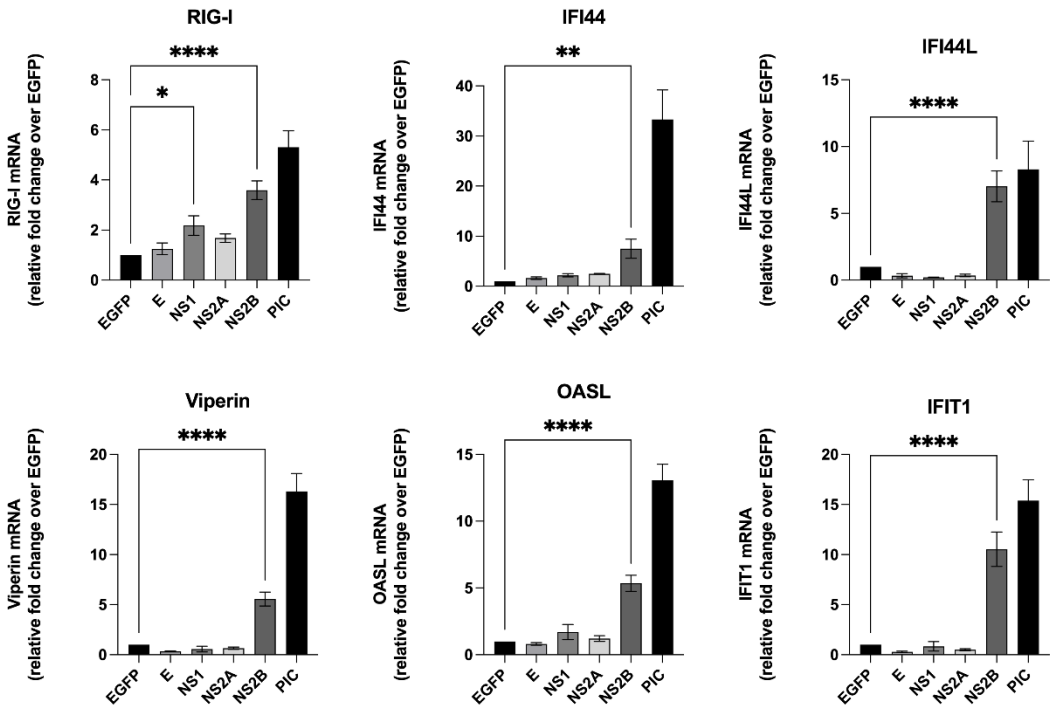

Figure 16 NS2B induces ISGs upregulation in an IRE1 independent manner

U2OS cells were transfected for 20h with the plasmids of interest with the Lipofectamine LTX reagent. Cells were lysed in Trizol and RNA was extracted, followed by cDNA synthesis. cDNA was used for RT-qPCR to determine mRNA levels of the genes of interest. Experiment was done in 3 independent biological replicates, each in 2 technical replicas. Normalization was done on the mRNA level of the EGFP sample following the ΔΔCt method. For statistical purposes Statistical significance was determined using the Kruskal–Wallis test with Dunn's multiple comparisons test. *, $P < 0.05$; **, $P < 0.01$; ***, $P < 0.001$.*

Expression of TBEV NS2B prior viral infection reduces viral replication

Given that expression of the selected TBEV proteins led to upregulation of interferon-stimulated genes (ISGs), we next investigated whether priming cells with these proteins—thereby inducing an antiviral state—could inhibit subsequent viral replication. To address this, cells were transfected to overexpress the selected viral proteins and, after 20 hours, infected with TBEV at a multiplicity of infection (MOI) of 0.5. Viral replication was assessed at 8 and 24 hours post infection (h.p.i.), representing early and prolonged stages of infection, respectively.

As shown in Fig. 17A, U2OS_WT cells exhibited a clear reduction in TBEV replication—approaching a one-log decrease—in the presence of all viral proteins as early as 8 h.p.i., which was maintained at 24 h.p.i. Notably, NS2B priming resulted in the strongest antiviral effect, reducing viral replication by approximately one log at 8 h.p.i. and by ~1.5 logs at 24 h.p.i. In contrast, in U2OS_IRE1_KO cells, this inhibitory effect was largely abolished at both time

points. However, NS2B overexpression still led to a significant reduction in viral replication during the early phase of infection (8 h.p.i.), as shown in Fig. 17B (left panel).

Collectively, these data support our hypothesis that TBEV proteins are sensed by host cells, triggering an antiviral response that is sufficient to suppress viral replication. This effect is largely dependent on IRE1, as it is lost in IRE1-deficient cells. The sole exception is NS2B, which retains a significant inhibitory effect at early time points even in the absence of IRE1. This observation is consistent with our earlier findings that NS2B induces the strongest ISG response, which remains intact in IRE1_KO cells. Together, these results suggest that NS2B is recognized by host sensing mechanisms that activate an innate antiviral response, ultimately limiting viral replication. Based on these findings, we therefore focused our subsequent investigations on elucidating the mechanism by which NS2B is sensed by the host cell to induce this antiviral state.

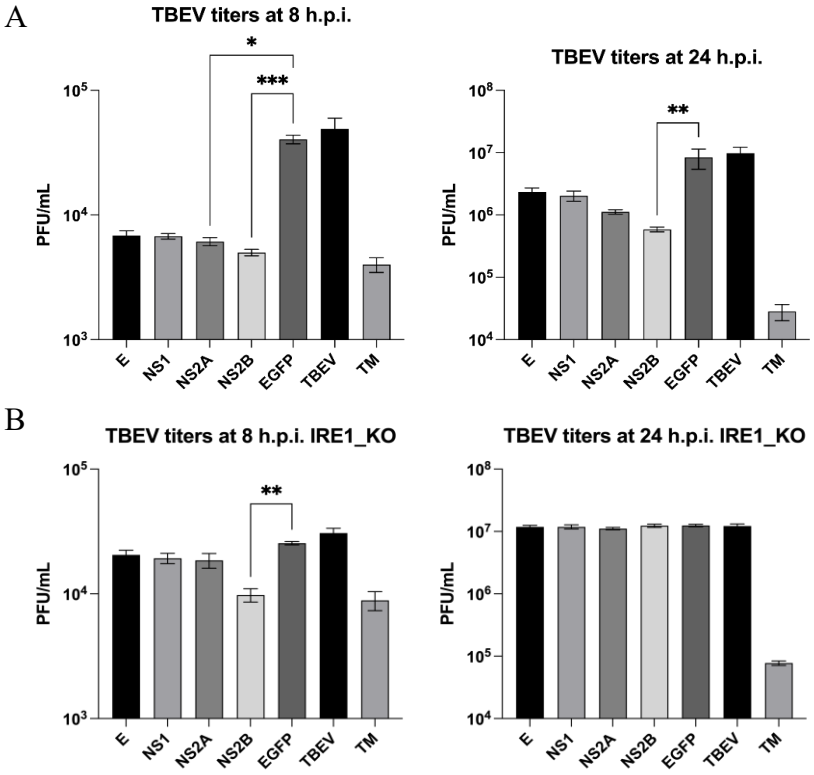

Figure 17 Expression of TBEV NS2B prior viral infection reduces viral replication

U2OS_WT (a) and (b) and U2OS_IRE1_KO (c) and (d) cells were transfected with plasmids of interest with Lipofectamine LTX for 20h, after 20h cells were infected with TBEV MOI 0.5 for other 24h. Supernatant was collected for plaque assay. Experiment was performed in ≥3 independent biological replicates. In a) and b) data of plaque assay are displayed as a readout of the PFU/mL count in the U2OS_WT cells. In c) and d) data of plaque assay are displayed as a readout of the PFU/mL count in the U2OS_IRE1_KO cells.

Results part 1 – NS2B

NS2B induces Interferon Stimulated Genes (ISGs) at the IKKε level

Since we observed that overexpression of NS2B was able to induce ISGs expression in an IRE1 independent way, it was important to understand the mechanism of ISGs induction given by NS2B. We hypothesized at this point that NS2B protein might be recognized by one of the components of the RIG-I pathway to induce the activation of the downstream effectors. We therefore focused on the dissection of the RIG-I pathway. A dual-reporter Luciferase assay was performed by transfecting HEK-293T cells with Lipofectamine. A plasmid encoding the Firefly Luciferase transcribed under the IFN-β promoter of interest, a plasmid encoding Renilla Luciferase under a constitutively active promoter as internal control were transfected together with NS2B and the different components of the RIG-I pathway. Of note that RIG-I(N) stands for the active form of RIG-I since the N-terminal domain of RIG-I is sufficient and necessary for the activation of the pathway, as well as IRF3-5D which stands for a constitutively active mutated version of IRF3 in which five serines are replaced by aspartates resulting in the generation of a constitutively active IRF3. Upon activation of the IFN-β promoter, the Firefly Luciferase gets transcribed, later translated and is then used to directly measure its abundance upon addition of the substrate. Renilla Luciferase, expressed under the constitutive promoter, is used as a transfection/expression control experimental control. EGFP transfection is used as

	plasmid →	Firefly luc	Renilla luc	NS2B	EGFP	RIG-I(N)	IPS1	TBK1	IKKε	IRF3-5D
	Sample									
	RIG-I(N)	X	X	X	X	X				
NS2B/EGFP	**IPS1**	X	X	X	X		X			
	TBK1	X	X	X	X			X		
	IKKε	X	X	X	X				X	
	IRF3-5D	X	X	X	X					X

Table 1

Description of transfection combinations used in the experiment of **Fig. 18.**

a control compared to NS2B. Overall, Firefly Luciferase signal gets normalized on the one of Renilla Luciferase. The ratios are then normalized on those of the mock EGFP signal. The different samples are obtained by co-transfecting the plasmids of interest as described in **Table 1**.

As visible in figure **Fig. 18**, we observed that co-overexpression of NS2B with each component of the RIG-I pathway is inducing a stronger activation of the INFβ promoter compared to

EGFP. In both TBK1 and IRF3-5D condition the difference in the Firefly luciferase signal between EGFP and NS2B is lost.

Expression of the transfected proteins has been evaluated by WB, **Fig. 19**. Proteins were lysed

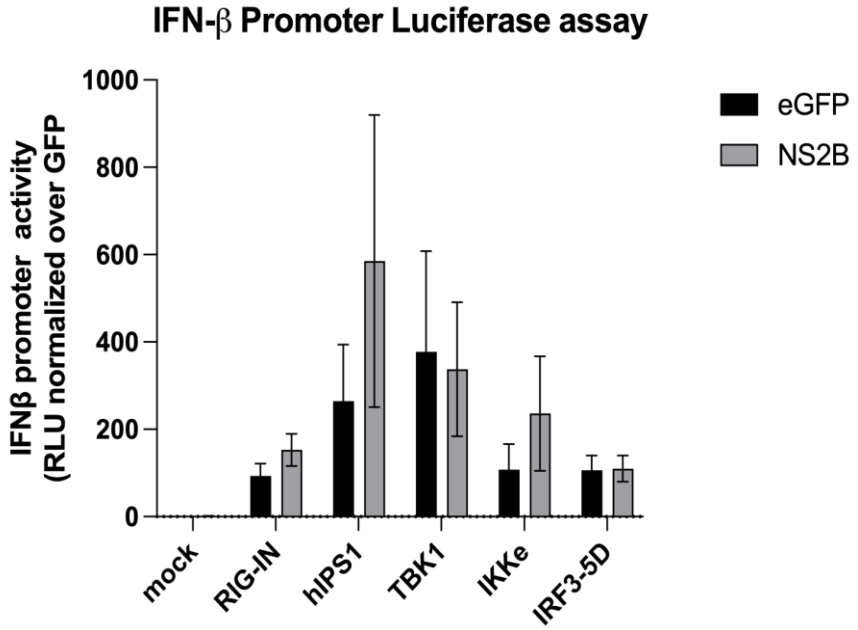

Figure 18 NS2B induces Interferon Stimulated Genes (ISGs) at the IKKε level – luciferase assay

HEK-293T cells were co-transfected with Lipofectamine LTX for 24h with the two components of the assay: luciferase and renilla encoding plasmids, as well as the plasmid encoding for NS2B or EGFP together with the plasmid encoding each of the component of the RIG-I pathway. Experiment was performed in ≥3 independent biological replicates. Normalization is performed for each sample on its own Renilla signal over the mock GFP. For statistical purposes the mean of two technical experiments was reported; multiple T-test was used for the comparison of each NS2B and EGFP condition. Only statistically significant results with a $p \leq 0.05$ is shown.

in the reagent coming with the Luciferase kit, resolved on a SDS PAGE and transferred on a nitrocellulose membrane. Anti-FLAG antibody was used to detect RIG-I(N), hIPS1, TBK1, IKKε and NS2B, while IRF3-5D was detected with anti-HA antibody. β-actin was used as loading control. This result led to the conclusion that the synergic effect of NS2B with the components of the pathway occurs until the moment the pathway is activated upstream of IKKε, since co-overexpression with TBK1 and IRF3-5d did not show a synergic effect of NS2B compared to the control. This led to the hypothesis that NS2B might be recognized by IKKε to induce IRF3 translocation to the nucleus and further transcription of genes regulated by the activation of this transcriptional factor.

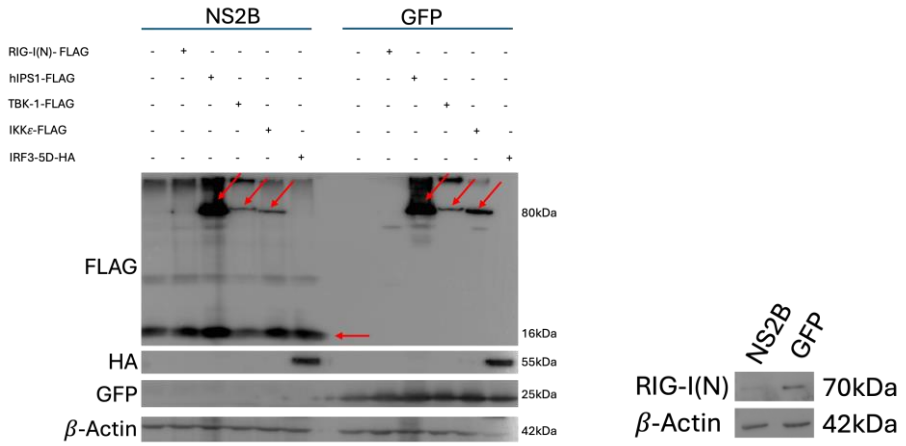

Figure 19 Western-blot analysis confirming overexpression of proteins of interest from Figure 18

Proteins collected for the luciferase assay were then run on a 12% SDS-page gel to prove transfection of plasmids of interest occurred. An anti-FLAG antibody was used for the detection of all the proteins but hIPS1 which was HA tagged. Actin was used as loading control. Red arrows indicate the correct FLAG signal bands.

IKKε recognizes and interacts with NS2B

Given our recent observation that NS2B may be recognized by IKKε, we decided to dig further into this mechanism. First, we investigated whether the two proteins interact. Since TBK1 and IKKε are similar kinases and are activated at the same level of the RIG-I pathway we used TBK1 as an experimental control. IKKε_FLAG and TBK1_Flag were co-transfected with NS2B_HA and immunoprecipitated (IP) with anti-FLAG beads. Results of the immunoprecipitation are shown in **Fig. 20**. Input indicates the whole protein lysate which was not undergone in the process of immunoprecipitation which acts as a control. Additionally, absence of β-actin detection in the IP indicates a clear pull-down without contamination of the input.

The data shows that by pulling-down IKKε, a strong band corresponding to NS2B protein is detected. In contrast, no comparable interaction was observed in the TBK1 pull-down, since in this case NS2B is not co-immunoprecipitated. This clearly indicates that TBEV NS2B interacts with IKKε but not with TBK1.

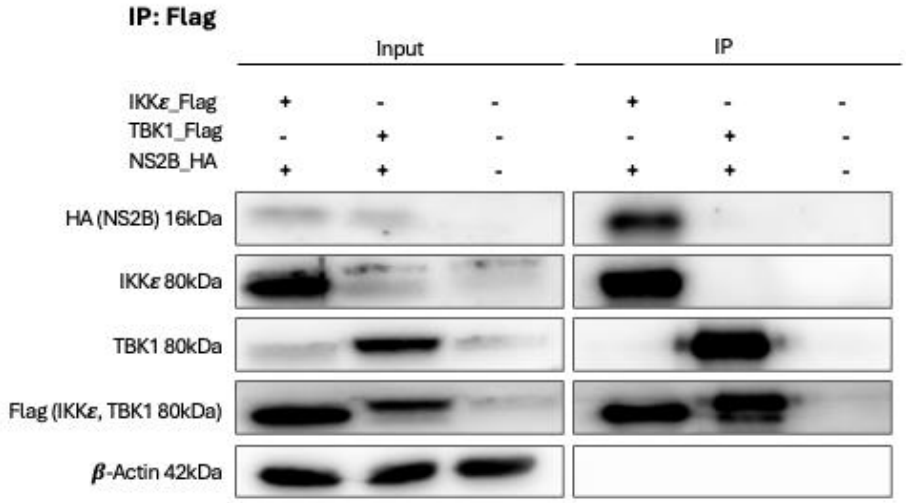

Figure 20 IKKε recognizes and interacts with NS2B by co-immunoprecipitation.

HEK293T cells were transfected with NS2B_HA and IKKε_FLAG or TBK1_FLAG with calcium phosphate for 24h. Proteins were collected with a mild buffer suitable for IP experiments as described in the materials and methods. Anti-FLAG beads were used for immunoprecipitation. Immunoprecipitated proteins were then loaded on a 12% SDS-page gel and transferred on a nitrocellulose membrane. Proteins of interest were detected with appropriate primary antibodies for 1h at RT or over-night at 4 degrees, secondary antibodies HRP tagged were then used for 1h at RT. Anti-FLAG antibody indicates wells were IKKε_FLAG and TBK1_FLAG are present, while an anti-HA antibody is used for detecting NS2B. Development of the immunoblotting was done with the usage of Millipore substrate or SuperECL. Experiment was done in 2 independent biological replicates, each in 2 technical replicas.

Next, immunofluorescence staining was done on cells co-transfected with IKKε and NS2B. TBK1 was used as a control in this case as well. We observed that NS2B co-localizes with IKKε. To better characterize the colocalization we calculated the Pearson's coefficient which resulted to be 0.5 indicating high co-localization, while for TBK1 the value was below 0.4. In **Fig. 21** microscope images are shown. Subsequently, we transfected PolyI:C, a synthetic double strand RNA molecule that mimic viral RNA, together with NS2B and IKKε or TBK1, to study if the proteins would have a different localization when the pathway is active. The treatment with PolyI:C shows that activation of IKKε and TBK1 results in the formation of protein aggregates. We wondered whether activating the pathway *via* PolyI:C treatment would have boosted the co-localization of NS2B with IKKε, but just a slight increase in the Pearson's was observed while no difference at all was observed for TBK1-NS2B colocalization.

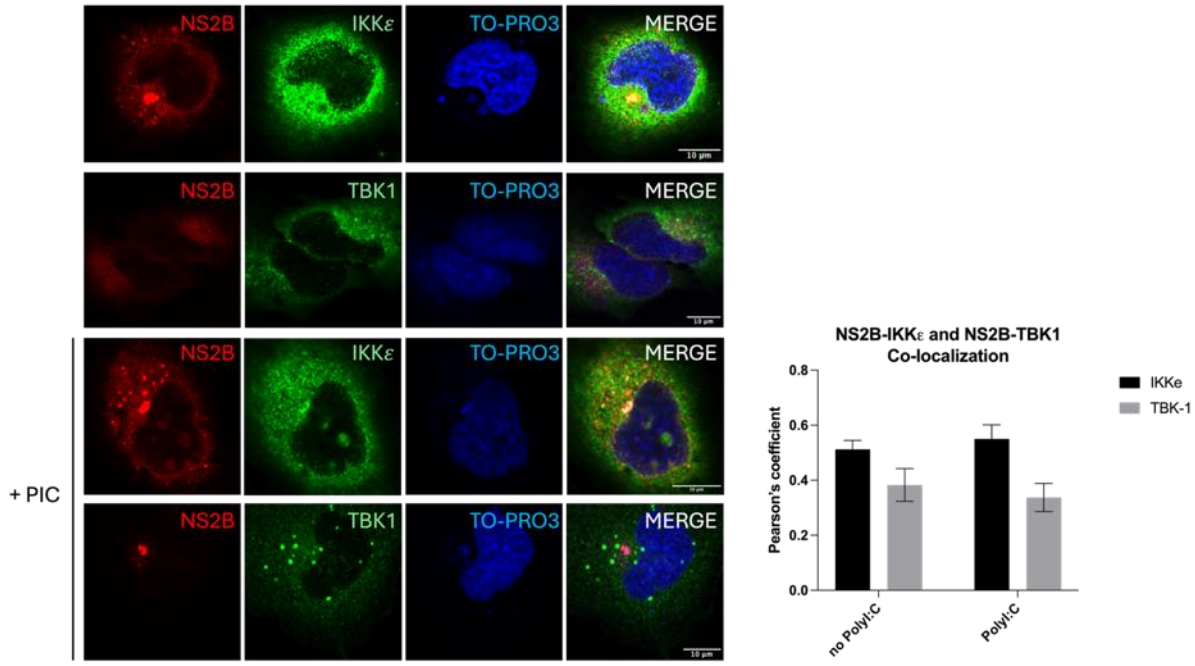

Figure 21 IKKε co-localizes with NS2B.

U2OS cells were co-transfected with NS2B_HA and IKKε_FLAG or TBK1_FLAG with Lipofectamine LTX for 20h. Half of the samples were treated with PolyI:C 4h before fixing the coverslips with 3.7% PFA, while the other half was not treated with PolyI:C. NS2B was stained with an anti-HA antibody, IKKε and TBK1 were stained with the anti-FLAG antibody. Proper secondary fluorophore-tagged antibodies were used for visualization. TO-PRO3 was used to stain nuclei. Images were taken in confocality with the pinhole set to 1 Air Unit, which allowed us to do co-localization analysis. Pearson's coefficient was calculated using ImageJ. Experiment was performed in 3 independent biological replicates. For statistical purposes every double positive Pearson's value was plotted; multiple T-test was used for the comparison of IKKε and TBK1 condition in presence or absence of PolyI:C. 10nm scalebar is set. Zeiss Airyscan 880, 63X Plan-Apo/1.4 NA Oil objective was used to acquire images.

NS2B induces IRF3 nuclear translocation

IKKε is known to induce IRF3 phosphorylation, which, once active, translocates to the nucleus to act as a transcriptional factor that regulates the expression of Interferon Stimulated Genes (ISG). IRF3 nuclear translocation is generally used as a marker of the active pathway and can be easily visualized by immunofluorescence. Since we have proven the interaction between NS2B and IKKε which probably led to the induction of ISGs, we hypothesized that the actor connecting those two events is IRF3. We therefore overexpressed again NS2B and checked this time at the IRF3 protein localization as well as at its phosphorylation status. The experiment was performed both in U2OS_WT and in U2OS_IRF3-GFP, a stable cell line expressing a GFP chimeric form of the IRF3 protein previously established in our laboratory (Maistriau et al., 2017). The experiment was firstly performed on the U2OS_IRF3-GFP cells since the readout of IRF3 activation is more straightforward in immunofluorescence. Therefore, we overexpressed NS2B in U2OS_IRF3-GFP, transfection of pcDNA was used as

an experimental control, while the condition of un-transfected cells was reported as well (reported in the panel as NT). PolyI:C transfection was used as a positive control to estimate the IRF3-GFP nuclear translocation upon treatment with this compound which activates the pathway of our interest.

Indeed, as visible in **Fig. 22**, we observed that the overexpression of NS2B induced a higher IRF3-GFP nuclear translocation compared to the overexpression of the negative control pcDNA. The quantification of the immunofluorescence was done in two ways:

a) by estimating a percentage of IRF3 translocation given by the ratio between the number of nuclear IRF3 positive cells on the total number of cells counted as displayed in **Fig. 22B**.
b) by determining the fluorescence intensity of the nuclear signal of IRF3-GFP in NS2B positive cells as displayed in the violin plots in **Fig. 22C**.

As we can see in the quantification as performed in **Fig. 22B** that NS2B induces a strong nuclear translocation on the overall cellular population, since almost 25% of cells were positive for the nuclear signal of IRF3-GFP. This level is only slightly lower than the one given by the positive control PolyI:C. Of note, we see a minor increase in the pcDNA transfected cells compared to the cells which were not transfected; we attribute that effect to the presence of the transfection reagents in the pcDNA, and those reagents might independently induce a stressful condition to the cells which respond by a mild activation of IRF3. However, the effect observed by NS2B is striking so we proceeded by characterizing it. In **Fig. 22C** we adopted a different quantification method in which nuclei were selected with the freehand tool in the ImageJ software and the Integrated density of the GFP signal corresponding to the nuclear IRF3 was measured in the respective cells. Also in this case we can see a significant increase in the nuclear IRF3 intensity coming from the NS2B transfected cells. In the violin plot every dot represents a single cell.

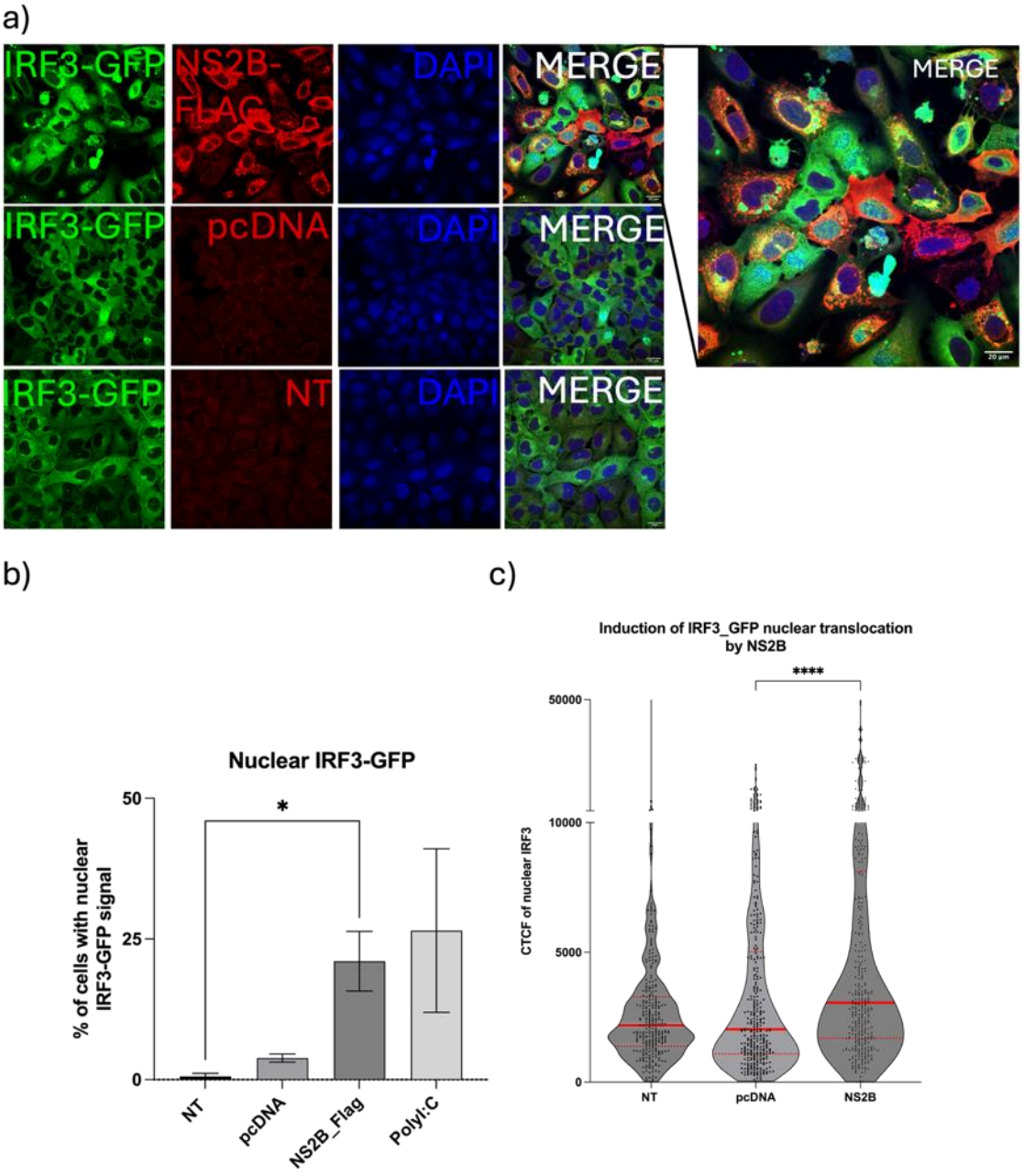

Figure 22 NS2B induces IRF3 nuclear translocation in U2OS_IRF3-GFP cells

U2OS_IRF3-GFP cells were transfected with NS2B_FLAG and a pcDNA control for 20h for immunofluorescence staining. Cells were fixed with 3.7% PFA, then permeabilized with 0.1% triton and stained with an anti-FLAG antibody, followed by a secondary tagged with a 549 fluorophore. Nuclei were stained with DAPI. Experiment was performed in ≥3 independent biological replicates. In a) the panel representing the immunofluorescence staining further quantified in b) and c). In b) the comparison of the total IRF3 nuclear translocation was considered in the different conditions. In c) every dot represents a cell, where in the NS2B condition only NS2B positive cells were considered and the intensity of their GFP signal was quantified then compared to the one of the control samples. For statistical purposes Statistical significance was determined using the Kruskal–Wallis test with Dunn's multiple comparisons test. *, $P < 0.05$; **, $P < 0.01$; ***, $P < 0.001$.* 20nm scalebar is set. Zeiss Airyscan 880, 63X Plan-Apo/1.4 NA Oil objective was used to acquire images.

To further determine the level of phosphorylation as another readout of IRF3 activation, western blot analysis was performed. In line with what was observed in immunofluorescence, overexpression of NS2B induced phosphorylation of IRF3-GFP, as well as that of the endogenous form of IRF3 present in the IRF3-GFP cells. Importantly, an increase of IFIT1, one of the ISGs tested previously at the mRNA level, is also clearly increased in the condition in which NS2B is overexpressed. Western blot data are shown in **Fig. 23**.

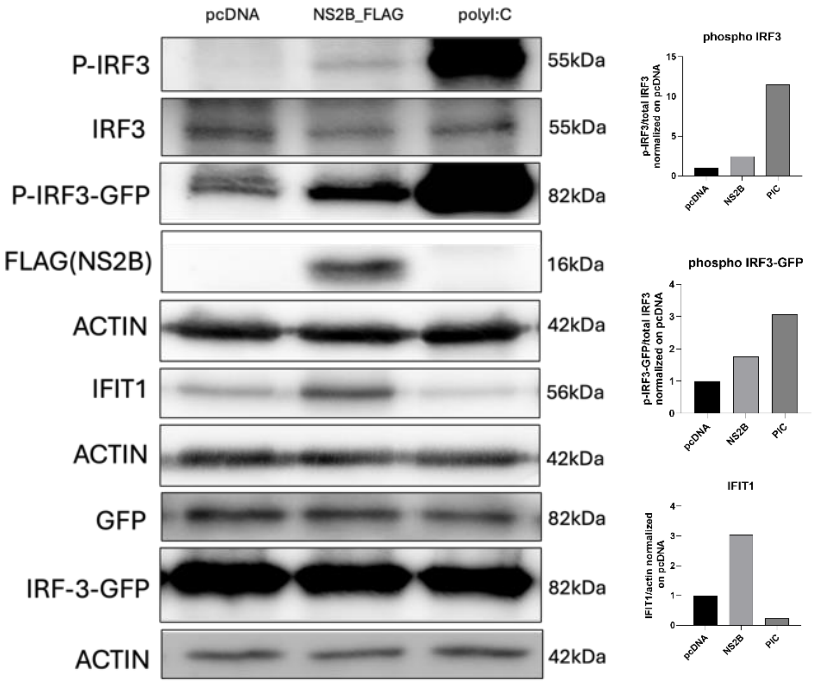

Figure 23 NS2B induces IRF3 phosphorylation and IFIT1 expression in U2OS_IRF3-GFP cells

U2OS_IRF3-GFP cells were transfected with NS2B_FLAG and a pcDNA control for 20h after which proteins were collected in RIPA buffer for western-blot analysis. Proteins were run on a 12% SDS-PAGE, then transferred on a nitrocellulose membrane and incubated with the primary antibodies for 1h at RT or over-night at 4 degrees against the proteins of interest, further incubated for 1h at RT with the appropriate secondary antibodies HRP tagged. Actin was used as loading control. Millipore or Super-ECL reagent were used for the detection of the proteins. Densitometric analysis of the Western blot bands is displayed on the right. Experiment was done in 3 independent biological replicates, each in 2 technical replicas.

Next, we wanted to confirm that the same would occur also in the U2OS_WT cells where we looked for the activation of the endogenous IRF3 protein. Immunofluorescence experiment recapitulated the results previously obtained on the IRF3-GFP cells. The experimental setup was identical to the one just described for **Fig. 22**. In fact, we could see an increase in the endogenous nuclear translocation of IRF3 in the samples where NS2B was over expressed (**Fig. 24**). IF data were quantified in two different ways, as explained above, and the result has the same trend as previously observed. The overexpression of NS2B increased both the percentage of overall nuclear IRF3 compared to the pcDNA and

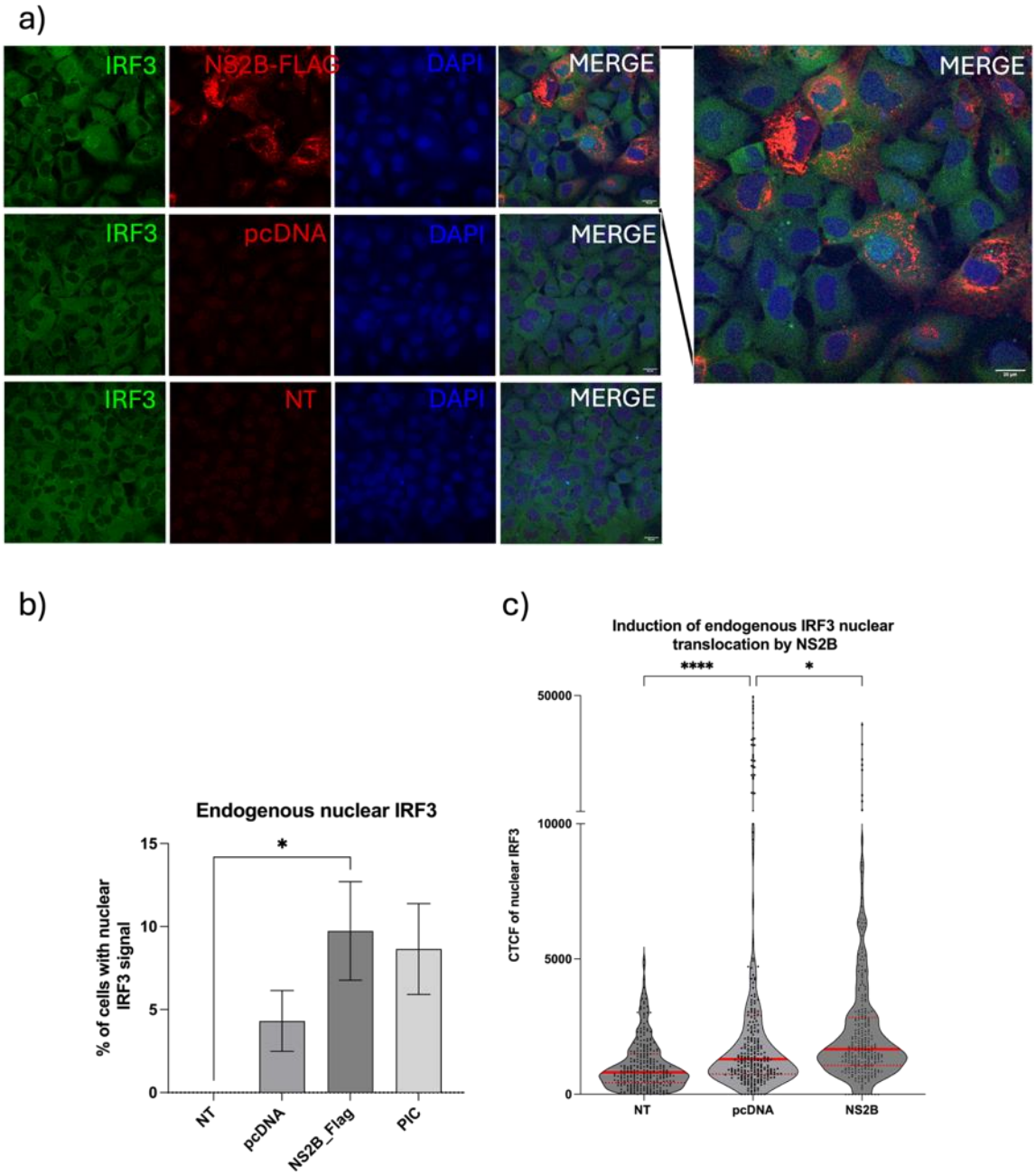

Figure 24 NS2B induces IRF3 nuclear translocation in U2OS_WT cells

U2OS_WT cells were transfected with NS2B_FLAG and a pcDNA control for 20h for immunofluorescence staining. Cells were fixed with 3.7% PFA, then permeabilized with 0.1% triton and stained with an anti-FLAG antibody and an anti-IRF3 antibody, followed by a secondary tagged with a 488nm fluorophore to stain IRF3 and a 549nm fluorophore to stain NS2B. Nuclei were stained with DAPI. Experiment was performed in ≥3 independent biological replicates. In a) the panel representing the immunofluorescence staining further quantified in b) and c). In b) the comparison of the total IRF3 nuclear translocation was considered in the different conditions. In c) every dot represents a cell, where in the NS2B condition only NS2B positive cells were considered and the intensity of their endogenous IRF3 signal was quantified then compared to the one of the control samples. For statistical purposes Statistical significance was determined using the Kruskal–Wallis test with Dunn's multiple comparisons test. *, $P < 0.05$; **, $P < 0.01$; ***, $P < 0.001$.* 20nm scalebar is set. Zeiss Airyscan 880, 63X Plan-Apo/1.4 NA Oil objective was used to acquire images.

NT control (**Fig. 24B**) as well as the intensity of nuclear IRF3 signal in NS2B transfected cells (**Fig. 24C**).

Western blot analysis showed, also in this case, an activation of IRF3 visible at the band level,

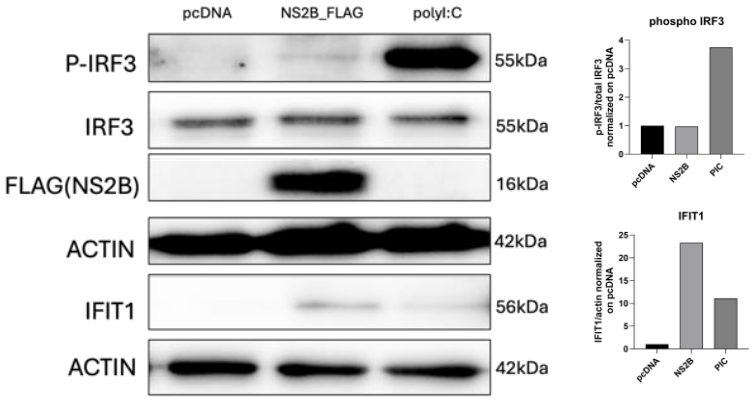

Figure 25 NS2B induces IRF3 phosphorylation and IFIT1 expression in U2OS_WT cells

U2OS_WT cells were transfected with NS2B_FLAG and a pcDNA control with Lipofectamine LTX for 20h after which proteins were collected in RIPA buffer for western-blot analysis. Proteins were run on a 12% SDS-page gel, then transferred on a nitrocellulose membrane and incubated with the primary antibodies for 1h at RT or over-night at 4 degrees against the proteins of interest, further incubated for 1h at RT with the appropriate secondary antibodies HRP tagged. Actin was used as loading control. Millipore or Super-ECL reagent were used for the detection of the proteins. Densitometric analysis of the Western blot bands is displayed on the right. Experiment was done in 3 independent biological replicates, each in 2 technical replicas.

even though the p-IRF3 band is fainter compared to the positive control PolyI:C, it is visible if compared to pcDNA control and the densitometric analysis of bands did not show an increase. In line as before, a strong increase was seen at the protein levels of IFIT1 when NS2B was present. (**Fig. 25)**.

Generation of the NS2B3 catalytic mutant

NS2B is known to act as the NS3 protease co-factor during TBEV replication. Other independent roles of TBEV NS2B protein are still not known, however, its independent role has been shown in two different DENV papers which describe its antagonistic role in the induction of the IFN response. The first shows NS2B induces the degradation of cGAS (Aguirre et al., 2017), while the second one indicates it inhibits the activation of the RIG-I pathway by sequestering MAVS/IPS-1 and IKKε (Nie et al., 2023). Interestingly, in both these papers the role of NS2B has been shown as a proviral factor capable of inducing an immune evasion, while in our case the opposite scenario is being observed. This will be fully discussed later.

We reasoned thus about mimicking a condition which would be more like the physiological TBEV infection in which NS2B interacts with the NS3 protease and decided to overexpress

the fully functional NS2B3 construct. Additionally, we wondered which would be the effect of the overexpression of the NS2B3 catalytic mutant not capable of cleaving the target cleavage sites. We needed to confirm that in a physiological scenario IKKε would still be able to detect NS2B and thus induce IRF3 phosphorylation and the downstream innate immune response. Experimental data will be shown in the next paragraphs.

The NS2B3 plasmid was kindly provided by Dr. Anna Overby's laboratory, while the NS2B3 catalytic mutant was generated in our laboratory. Mutation S135A in the catalytic domain of NS3 is sufficient to inhibit its protease activity (Chambers et al., 1990), therefore the NS2B3 protein was mutated at that position, and the mutant is referred as NS2B3_S135A.

The correct insertion of the mutation was verified by sanger sequencing. In **Fig. 26** we report the alignment of the WT plasmid NS2B3_Flag and the mutated one, showing the mutation was correctly inserted.

Figure 26 Alignment of the NS2B3 plasmid to the NS2B3 S135A mutant one

Alignment is shown in the Benchling tool. In the first row NS2B3_Flag sequence at the level of mutagenesis is shown, in the second row the sequence of the mutant version of NS2B3 is displayed indicating that the mutagenesis was successful since the correct mutation was inserted in position 135 of NS3 in which a Serine was mutated to Alanine.

Being NS2B3 an autocatalytic protein, meaning that a functional NS2B3 will cleave itself into the NS2B and NS3 proteins, another proof of the insertion of the correct mutation into the catalytic domain is the visualization by WB of NS2B3 in its un-cleaved version.

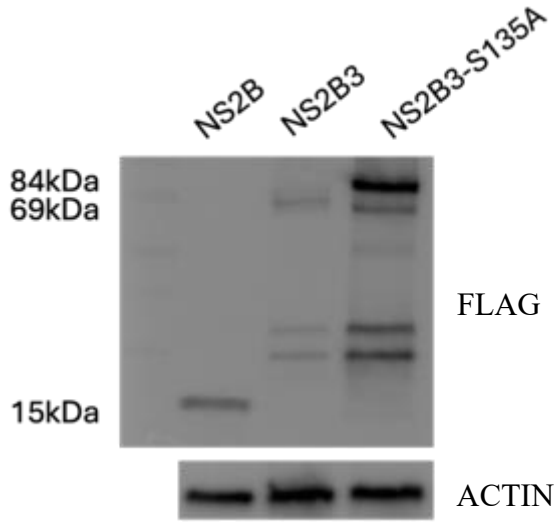

Figure 27 Western-blot analysis showing protein size of NS2B, NS2B3 and NS2B3 S135A

Western-blot analysis 20h past transfection on U2OS cells of NS2B_FLAG, NS2B3_WT and NS2B3_S135A. Proteins were collected in RIPA buffer. Proteins were run on a 12% SDS-page gel, then transferred on a nitrocellulose membrane and incubated with the primary anti FLAG-HRP antibody for 1h at RT or over-night at 4 degrees. Actin was used as loading control. Millipore reagent was used for the detection of the proteins.

Indeed, we observed by western-blot (**Fig. 27**) analysis that transfection of the active NS2B3_FLAG protein results in the visualization of a band of 69kDa size, the corresponding MW of NS3. The band correspondent to NS2B is not visible since the FLAG tag is present at the N terminal of NS3 in this protein and an antibody specific for TBEV NS2B is not available. However, when we transfect the protease-deficient version NS2B3_S135A, we are detecting another band as well – the one of a size of 85kDa corresponding to the size of the un-cleaved NS2B3 (NS2B size is 16kDa and NS3 is 69kDa) proving that this version cannot get cleaved into the two proteins. Overexpression of NS2B alone indicates a clear band at the level of 16kDa.

NS2B3 strongly induces ISGs overexpression, while its catalytic mutant induces levels comparable to NS2B

Having generated a catalytic mutant of NS2B3, we wanted to explore if the NS2B phenotype we have identified is conserved when NS2B is in its physiological NS2B3 status and if the catalytic domain might play a role. The 3 proteins were overexpressed in U2OS cells for 24h, after which samples were collected in Trizol and RNA analysed by RT-qPCR. The overexpression of the protease NS2B3 strongly induced ISGs, while the presence of NS2B3_S135A induced to a level comparable to the one of NS2B (**Fig. 28**). In addition to ISGs, we measured CCL5 and IL-6 expression to assess early innate immune activation. These genes are rapidly induced upon PRR engagement and serve as indicators of upstream signalling

events that precede interferon production and ISG induction. Together, this is a first indication that:

A) The overexpression of the active protease is a strong inducer of ISGs indicating that other mechanisms are involved as well.

B) The overexpression of the catalytic mutant loses most of the induction given by the active protease but still induces ISGs to a level comparable to NS2B alone. This data indicates that despite the loss of the effect given by the protease itself, NS2B is still actively recognized by IKKε in the context of the full NS2B3 construct. Hence, no shielding effect could be observed for the NS3 protein.

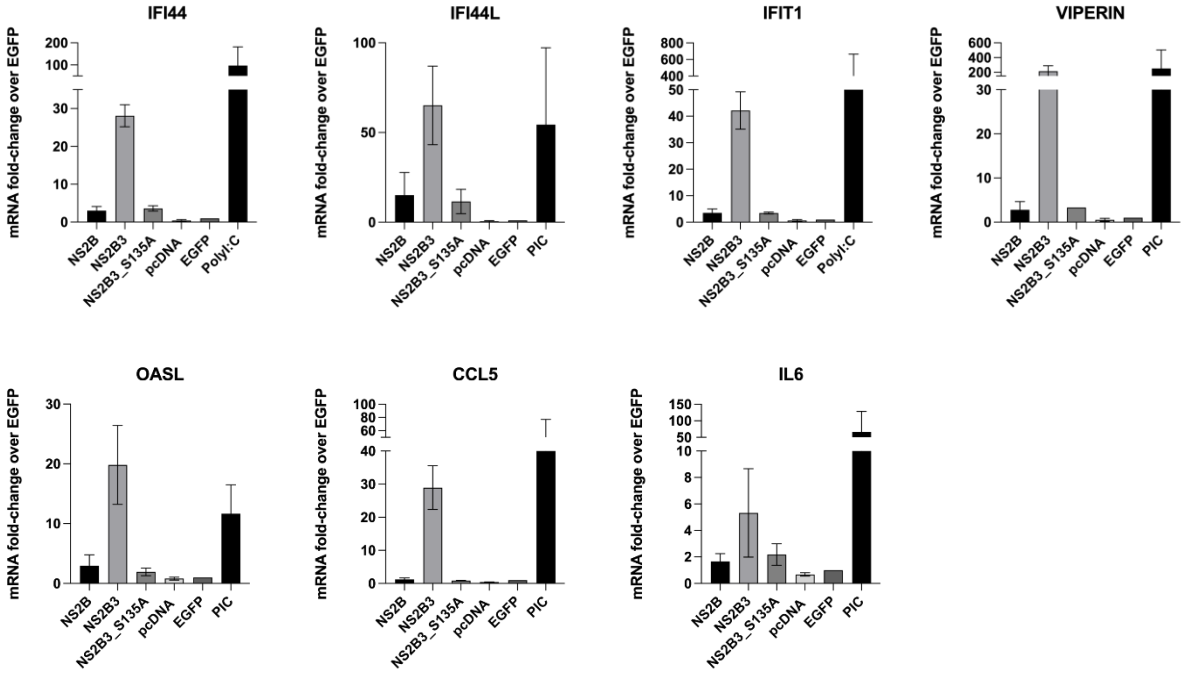

Figure 28 NS2B3 strongly induces ISGs overexpression, while its Catalytic mutant induces levels comparable to NS2B

U2OS cells were transfected for 20h with the plasmids of interest with the Lipofectamine LTX reagent. Cells were lysed in Trizol and RNA was extracted, followed by cDNA synthesis. cDNA was used for RT-qPCR to determine mRNA levels of the genes of interest. Experiment was performed in 2 independent biological replicates, each in 2 technical replicates. Normalization was done on the mRNA level of the EGFP sample following the ddCT method.

Priming cells with NS2B prior infection inhibit viral replication given by the activation of the innate immune response

Since the recognition of NS2B by IKKε leads to the translocation of IRF3 and consequent expression of antiviral genes, we wondered whether the magnitude of this antiviral response was sufficient to affect TBEV replication. Active NS2B3 and the mutated NS2B3_S135A were included in the experiment as well.

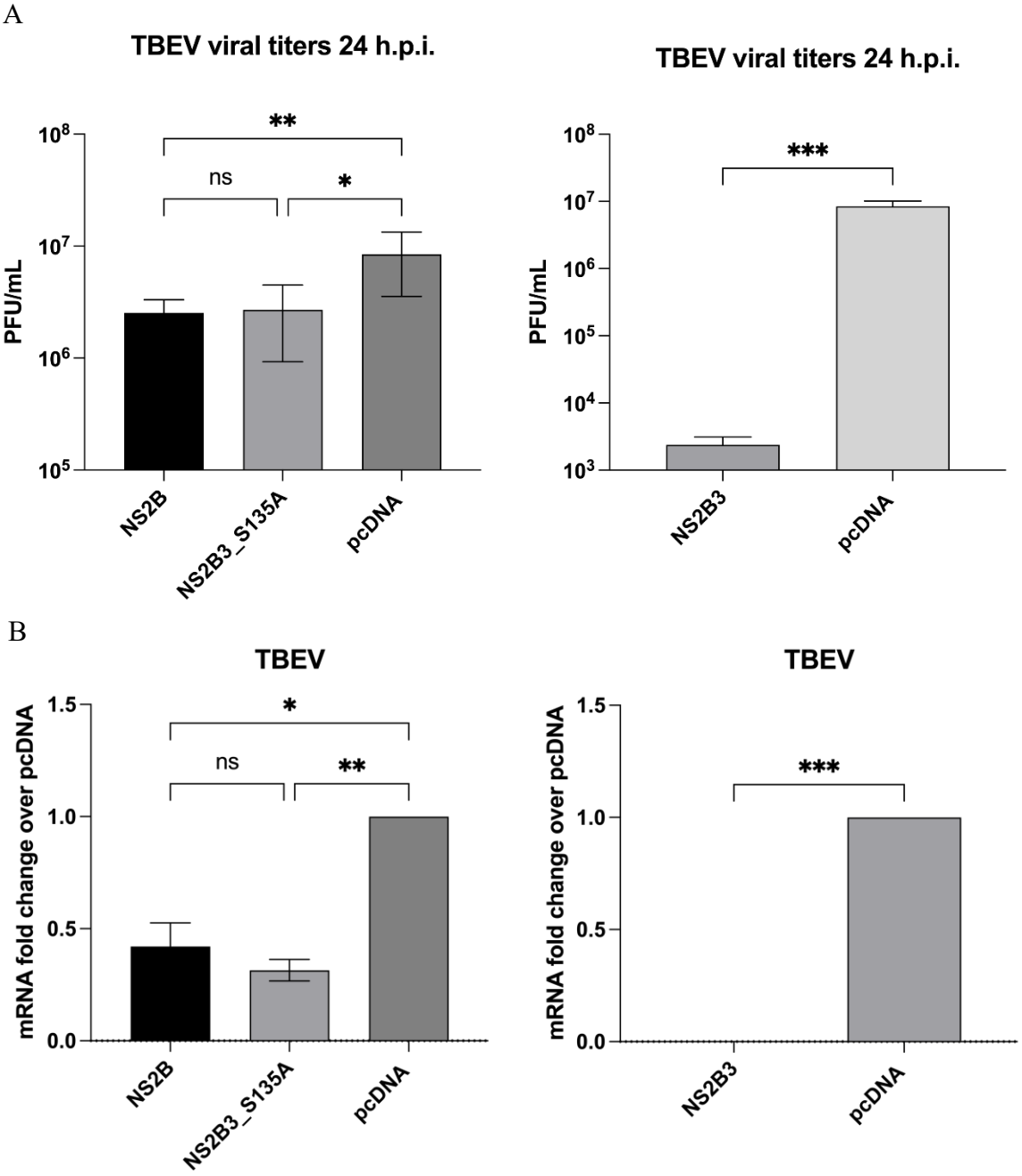

Figure 29 Priming cells with NS2B, NS2B3 S135A and NS2B3 prior infection inhibit viral replication at the viral titer

U2OS cells were transfected with plasmids of interest with Lipofectamine LTX for 20h, after 20h cells were infected with TBEV MOI 0.5 for other 24h. Supernatant was collected for plaque assay, while cells were lyzed in Trizol for mRNA analysis. Experiment was performed in ≥3 independent biological replicates. In a) and b) data of plaque assay are displayed as a readout of the PFU/mL count. In c) and d) RT-qPCR results of mRNA fold changes are shown – data are normalized on the mRNA levels of the pcDNA control. For statistical analysis in a) and c) Statistical significance was determined using the Kruskal–Wallis test with Dunn's multiple comparisons test. *, $P < 0.05$; **, $P < 0.01$; ***, $P < 0.001$. Comparison was done against the NS2B sample. For b) and d) Mann-Whitney t-test was performed. Data are considered significantly

Indeed, we observed an inhibition of the replication, both infectivity and RNA levels, when NS2B was overexpressed 20h before infection with TBEV at an MOI of 0.5. In line with the previous data, NS2B3_S135A behaved the same as NS2B (**Fig. 29B left**), while the

overexpression of the active protease prior infection almost completely inhibited viral replication (**Fig. 29B right**). In **Fig. 29A left** plaque assay results are displayed indicating that NS2B and NS2B3_S135A inhibit TBEV replication to an extent of approximately ½ LOG, while NS2B3 strongly inhibits TBEV replication of approximately 4 LOGs (**Fig. 29A right**). Viral mRNA levels were further quantified via RT-qPCR and this data showed, in line with the plaque assay data, that upon cell-priming with NS2B and the catalytic mutant NS2B3_S135A, the amount of cellular TBEV mRNA level is halved compared to the pcDNA transfected control. On the other hand, mRNA levels of TBEV in the samples overexpressing the active protease complex were not detectable by RT-qPCR.

Next, to have a visual indication of the infection occurring in the same conditions as just described in **Fig. 29** for mRNA levels and viral titers, an immunofluorescence was performed. Immunofluorescence again confirmed that NS2B3 was completely inhibiting viral replication as no signal for TBEV E-protein (red) was detected in the cells which were transfected with the NS2B3 plasmid. On the other hand, NS2B and NS2B3_S135A allowed for a higher TBEV infection ratio, which was anyway lower compared to the pcDNA transfected control. We observed as well that cells that were clearly overexpressing NS2B and NS2B3_S135A are getting less infected compared to the neighboring NS2B/NS2B3_S135A not overexpressed cells. Interestingly, the localization of NS2B seems to be much more perinuclear – ER localized compared to the one of NS2B3 which is much more spread in the cytoplasm (**Fig. 30**).

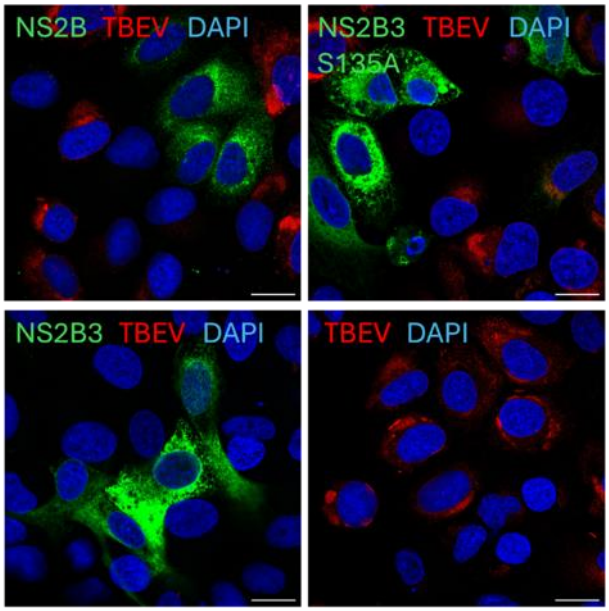

Figure 30 Priming cells with NS2B, NS2B3 S135A and NS2B3 prior infection inhibit viral replication in immunofluorescence

U2OS cells were plated on coverslips, transfected with plasmids of interest with Lipofectamine LTX for 20h, cells were then infected with TBEV MOI 0.5 for other 24h. Cells were fixed with PFA 3.7%, permeabilized with Triton 0.1% and stained with the antibodies of interest: an anti-FLAG to detect transfection and an anti-TBEV E-protein to detect infected cells, followed by an incubation with a secondary tagged with a 488nm fluorophore to stain FLAG-tag proteins and a 549nm fluorophore to stain TBEV-E protein. Nuclei were stained with DAPI. Images were acquired at the Zeiss Airyscan microscope with a 63X magnification. Experiment was performed once. 20nm scalebar

We proceeded by quantifying the infection in NS2B transfected cells. Indeed, for the determination of TBEV infection in NS2B positive cells the strategy adopted for quantification was the following: NS2B positive cells were selected with the freehand tool on ImageJ. The same area was then used for calculating the corrected integrated density (CTCF) of the TBEV E-protein signal (**Fig. 31 right**). We observed that cells which were NS2B positive showed a signal of infection which was much lower compared to the one of the control cells thus showing that not only in the whole population there is a smaller number of infected cells but that in the one expressing NS2B the virus struggles to replicate.

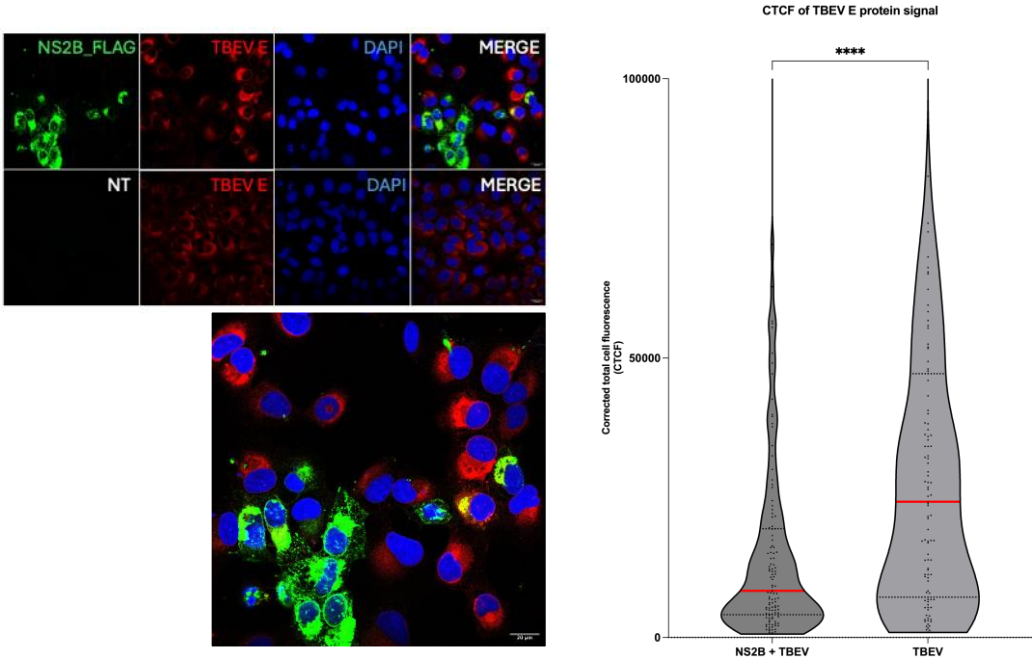

Figure 31 NS2B transfected cells show lower TBEV signal in immunofluorescence

Figure U2OS cells were plated on coverslips, transfected with plasmids of interest with Lipofectamine LTX for 20h and then infected with TBEV MOI 0.5 for other 24h. Cells were fixed with PFA 3.7%, permeabilized with Triton 0.1% and stained with the antibodies of interest: an anti-FLAG to detect transfection and an anti-TBEV E-protein to detect infected cells, followed by an incubation with a secondary tagged with a 488nm fluorophore to stain NS2B-Flag and a 549nm fluorophore to stain TBEV-E protein. Nuclei were stained with DAPI. In a) the representative images are shown, the magnification of the merged image of NS2B_FLAG infected cells is shown on the bottom. In b) the quantification of the Intensity signal corresponding to E-protein is showed. Cells positive for NS2B were selected with the freehand tool on ImageJ and the intensity of the same cells in the E-protein channel was measured and compared to the signal of neighboring infected cells which were not expressing NS2B. Experiment was performed in ≥3 independent biological replicates. Every dot of the violin plot represents a cell. Data were checked for normality to choose the proper test to perform – for statistical purposes Mann-Whitney t-test was performed. Data are considered significantly different with a $p \leq 0.05$. 20nm scalebar is set. Zeiss Airyscan 880, 63X Plan-Apo/1.4 NA Oil objective was used to acquire images.

A Western-blot analysis was performed to study TBEV protein levels of this experiment. As showed in **Fig. 32** a 55 kDa band, corresponding to E protein, appears strong in both non-transfected (MOCK – only infected) and pcDNA transfected control samples, while the same band appear fainter in NS2B samples, confirming that in these cells TBEV replication is inhibited. The band corresponding to E protein was not detectable in the sample where NS2B3 was overexpressed. Expression levels of NS2B and NS2B3 were also confirmed by WB. Actin was used as control.

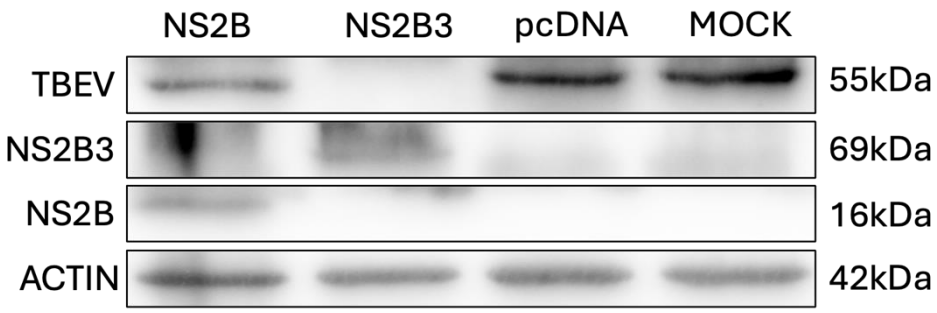

Figure 32 NS2B transfection shows lower TBEV E protein levels in western blot

U2OS_WT cells were transfected with Lipofectamine LTX for 20h and then infected with TBEV MOI 0.5 for other 24h. Proteins were collected in RIPA buffer for western-blot analysis. Proteins were run on a 12% SDS-PAGE gel, then transferred on a nitrocellulose membrane and incubated with the primary antibodies for 1h at RT or over-night at 4 degrees against the proteins of interest, further incubated for 1h at RT with the appropriate secondary antibodies HRP tagged. Actin was used as loading control. Millipore or Super-ECL reagent were used for the detection of the proteins.

Expressing NS2B and NS2B3 concomitantly with TBEV infection does not inhibit viral replication

We next wondered if cells transfected with NS2B or the active protease NS2B3 immediately after TBEV infection would still be able to mount an antiviral response and inhibit viral replication. Interestingly, we observed that cells that overexpressed NS2B and NS2B3 immediately following infection where not able to inhibit TBEV replication (**Fig. 33**).

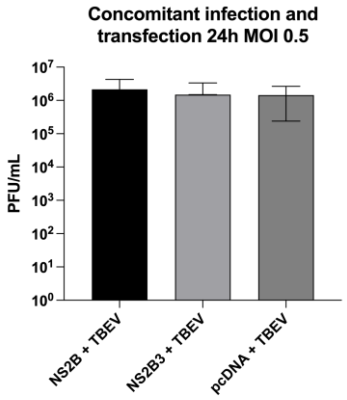

Figure 33 Transfection of NS2B and NS2B3 at the moment of infection does not inhibit viral replication

U2OS cells were infected with TBEV MOI 0.5, after 1h incubation with the virus, media was changed, and cells were transfected with plasmids of interest with Lipofectamine LTX for 20h. Supernatant was collected for plaque assay. Experiment was performed in ≥3 independent biological replicates.

Western-blot analysis showed that there is no major difference in the expression of TBEV E protein among the different samples (**Fig. 34**).

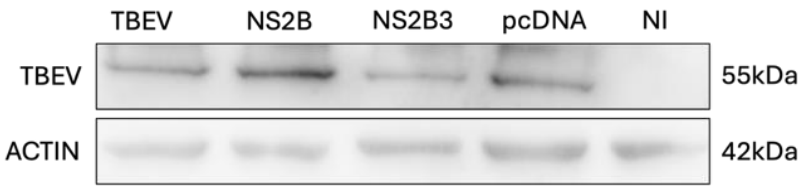

Figure 34 Transfection of NS2B and NS2B3 at the moment of infection does not reduce E protein levels

U2OS_WT cells were infected with TBEV MOI 0.5, after 1h incubation with the virus, media was changed, and cells were transfected with plasmids of interest with Lipofectamine LTX for 20h. Proteins were collected in RIPA buffer for western-blot analysis. Proteins were run on a 12% SDS-PAGE, then transferred on a nitrocellulose membrane and incubated with the primary antibodies for 1h at RT or over-night at 4 degrees against the protein of interest, further incubated for 1h at RT with the appropriate secondary antibodies HRP tagged. Actin was used as loading control. Millipore or Super-ECL reagent were used for the detection of the proteins.

The fact that the expression of the two proteins of interest, NS2B and NS2B3, did not reduce viral replication when transfected once infection has already started, reinforces the data previously seen. Meaning that, since we previously observed that upon recognition of NS2B by IKKε there is an induction of an antiviral response which reduces the following viral replication, the same is not true when infection starts before the cells have been primed by NS2B to induce the innate immune response. Activation of this pathway upon an already ongoing infection is not sufficient to block the viral replication which can in this case proceed normally. On the other hand, overexpressing NS2B when infection is already ongoing does not help in inhibiting the virus replication, since virus replication is progressing while the antiviral response needs still to be induced.

For what concerns NS2B3, it is known that in physiological infection conditions the cleavage of the polyprotein occurs in a specific order (Amberg and Rice, 1999; Chambers et al., 1991; Wahaab et al., 2021). We can therefore hypothesize that the overexpression of NS2B3 prior to infection has an impact on the cleavage of the polyprotein which, if cleaved unproperly, does not allow for the formation of mature viral proteins and thus infection cannot proceed. The same cannot be said when NS2B3 gets overexpressed upon an already ongoing infection. Moreover, it might be that additionally NS2B3 gets recognized by IKKε and other cellular anti-viral actors which strongly induce an antiviral response, as seen by the previous data. Again, when NS2B3 is transfected when viral replication is already ongoing, this effect gets bypassed, and viral infection can normally proceed as shown in **Fig. 33** and **Fig. 34**.

Stable overexpression of NS2B via a lentiviral system recapitulates NS2B effect observed in transfection

NS2B_HA transduction shows 99% HA positivity at 48 hours post transduction, a good signal in western blot and a perinuclear localization in IF

To obtain a better transfection efficiency of NS2B, we cloned NS2B-HA in the pWPI lentiviral vector to transduce U2OS cells. In addition, we needed a tag different than FLAG to use in co-transfection experiments with FLAG-tagged plasmids. EGFP was cloned in the same lentivector as a control. Cloning strategy is detailed in the Materials and Methods section.

Cytofluorimetric analysis indicated an increased positivity to the HA tag over time. Indeed, at 16 hours post transduction (h.p.t.) 91,6% of cells showed HA positivity, at 24 h.p.t. 95.4% of cells were positive, and lastly, at 48 h.p.t. 99,5% of cells were positive, indicating a high overexpression rate. FACS analysis results are shown in **Fig. 35**. Three timing conditions (16, 24 and 48h.p.t.) were tested, along with three control conditions, as summed up in the table below.

U2OS_WT only permeabilized (1)	**Control conditions**
U2OS_WT permeabilized and treated with primary and secondary AB (2)	
U2OS_WT permeabilized and treated secondary AB (3)	
U2OS_NS2B-HA 16h.p.t. (4)	**Test conditions**
U2OS_NS2B-HA 24h.p.t. (5)	
U2OS_NS2B-HA 48h.p.t. (6)	

Table 2 Description of Fig. 35 FACS analysis experimental setup.

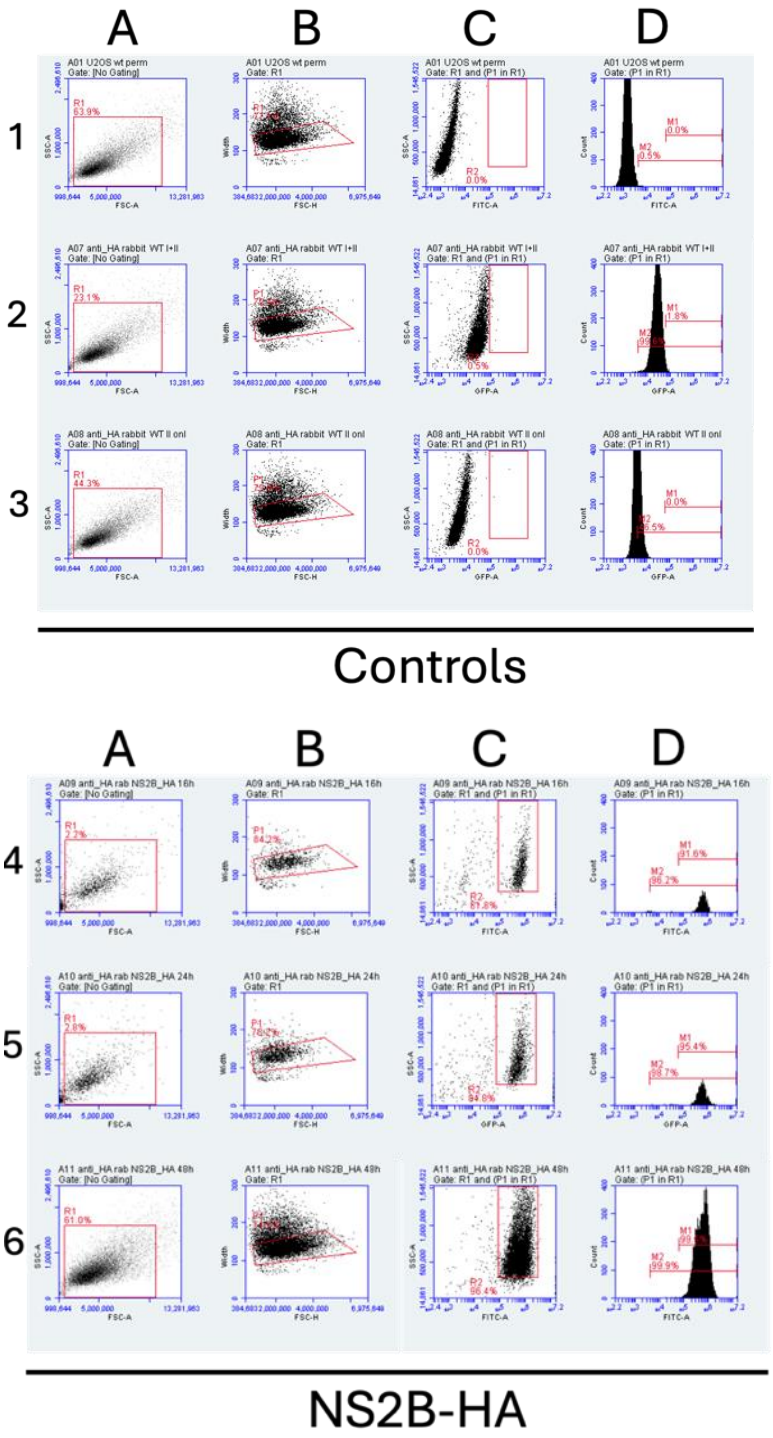

Figure 35 Determination of efficiency of NS2B_HA transduction by the usage of the cytofluorimeter

FACS analysis performed after NS2B_HA transduction indicates more than 90% of HA positivity starting at 16 h.p.t. Cells were fixed in 3.7% PFA and stained with a primary anti-HA antibody, followed by a secondary 488nm. Rows 1, 2 and 3 representing the three negative controls were used to set the parameters for HA-positive cells quantification. Column A indicates a first gating of selection of live cells, next in B the selection of single cells (exclusion of cell doublets), in C the selection of FITC positive cell population based on the negative controls (1,2,3), in column selection M1 the representation of the final HA-positive cells. In rows 4, 5 and 6 the transduction of NS2B_HA indicating 91,6% HA positivity at 16 h.p.t., 95,6% HA positivity at 24 h.p.t. and 99,9% HA positivity at 48 h.p.t.

NS2B_HA protein, as well as EGFP protein production were further confirmed by western blot analysis in which increased level of overexpressed proteins are visible over time **Fig. 36**. For this reason, the 48 h.p.t. was selected as the optimal timing for the following transduction experiments. In the western blot NAP1L1, a protein not related to this experiment, which was anyway HA tagged, was used as a positive control for the anti-HA antibody.

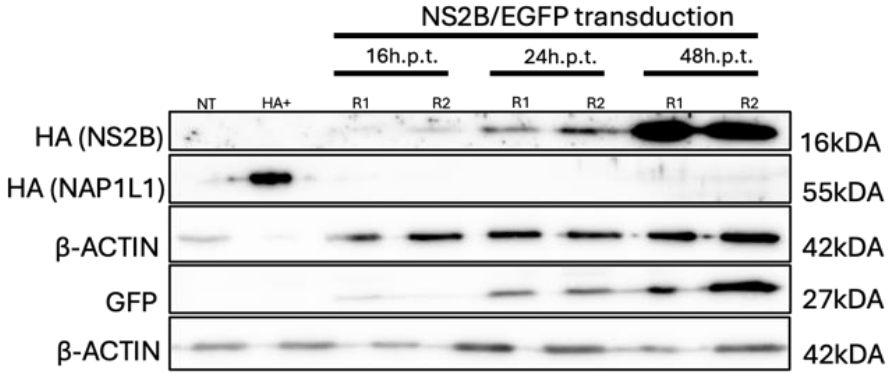

Figure 36 Determination of the transduction of NS2B and EGFP by western blot

U2OS_WT cells were transduced with the NS2B_HA lentivirus and the EGFP control for different times (16h, 24h and 48h). Proteins were collected in RIPA buffer for western-blot analysis. Proteins were run on a 12% SDS_PAGE, then transferred on a nitrocellulose membrane and incubated with the primary antibodies for 1h at RT or over-night at 4 degrees against the protein of interest, further incubated for 1h at RT with the appropriate secondary antibodies HRP tagged. NAP1L1_HA overexpression was used as a positive control for the anti-HA antibody. Actin was used as loading control. Millipore or Super-ECL reagent were used for the detection of the proteins.

Next, NS2B-HA and EGFP as control were expressed in U2OS cells by transduction and analysed by IF (**Fig. 37**). The perinuclear localization of NS2B was nicely appreciable following transduction.

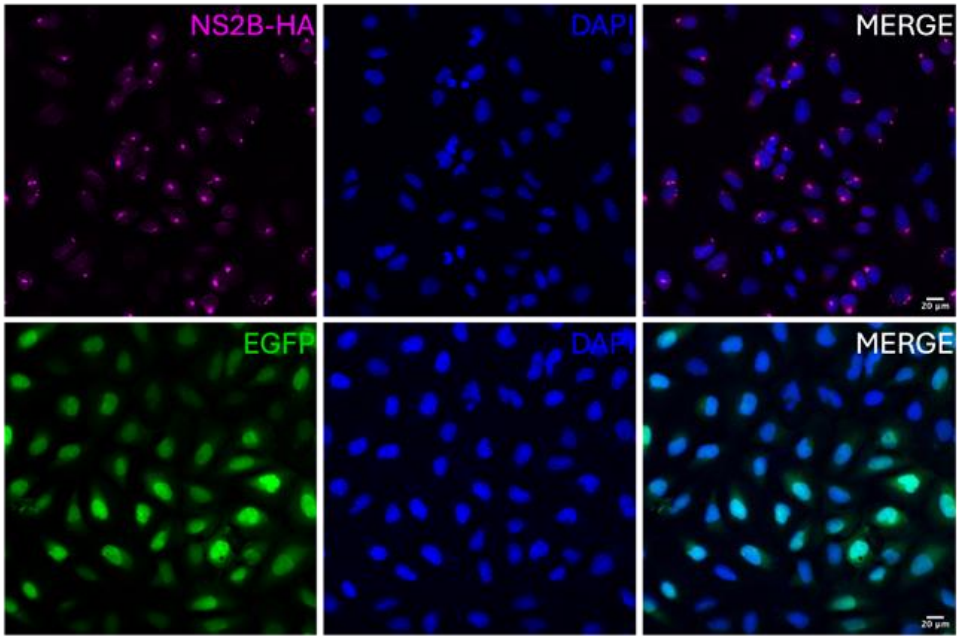

Figure 37 Determination of transduction efficiency of NS2B_HA and EGFP by immunofluorescence

Figure 26 Cells were transduced for 48h with NS2B_HA and EGFP lentiviruses. After 48h cells were fixed with PFA 3.7%, permeabilized with Triton 0.1% and stained with anti-HA to detect NS2B positive cells), followed by an incubation with a secondary tagged with a 594nm fluorophore to stain HA-tag proteins. EGFP transduced cells were not processed for Ab staining. Nuclei were stained with DAPI. 20nm scalebar is set. Zeiss Airyscan 880, 63X Plan-Apo/1.4 NA Oil objective was used to acquire images.

NS2B transduction inhibits TBEV replication

After having obtained functional NS2B_HA expressing lentiviruses, we overexpressed NS2B in a condition of TBEV infection to check the effect on the viral replication. Cells were transduced during plating by the addition of lentiviruses. On the next day cells were infected with TBEV MOI 0.5. for 16 and 24 hours. Supernatant was collected for plaque assay and RNA was extracted for addressing mRNA levels. Tunicamycin, a drug known to inhibit TBEV infection was used as a TBEV inhibitor control. EGFP overexpressing lentivectors were used as transduction control. In line with transfection experiments, a decrease in viral replication in cells overexpressing NS2B_HA was observed both at 16 h.p.i. and 24 h.p.i., both in plaque assay and mRNA levels **Fig. 38** and **Fig. 39** if compared to control cells. At 16 h.p.i. a half Log decrease in the viral replication is observed, while at 24 h.p.i. the decrease reaches one Log. At 24 h.p.i. the inhibition is a bit higher compared to the transfection experiment; this can be assumed to be because transduction induces a higher percentage of cells strongly expressing

NS2B thus better activating the innate immune response which is more prone to fight the replicating virus.

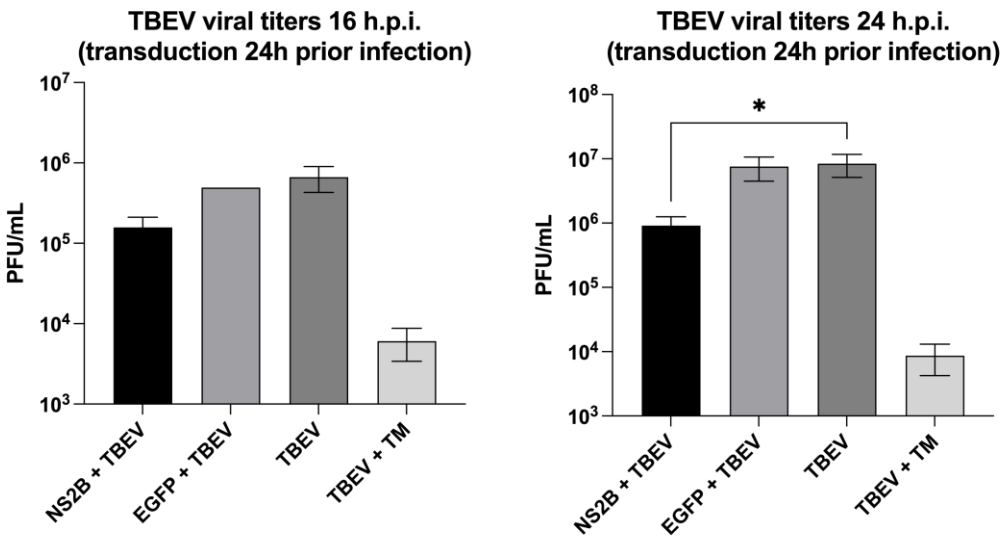

Figure 38 NS2B transduction inhibits viral replication at the titre level at 16 h.p.i. and 24 h.p.i.

U2OS cells were transduced for 24h before infection with TBEV MOI 0.5 for other 16h or 24h. Supernatant was collected for plaque assay. Experiment was performed in ≥3 independent biological replicates. In a) and b) data of plaque assay are displayed as a readout of the PFU/mL count. Statistical significance was determined using the Kruskal–Wallis test with Dunn's multiple comparisons test. *, P < 0.05; **, P < 0.01; ***, P < 0.001.* Comparison was done against the NS2B sample. Data are considered significantly different with a p≤0.05. Data were checked for normality to choose the proper

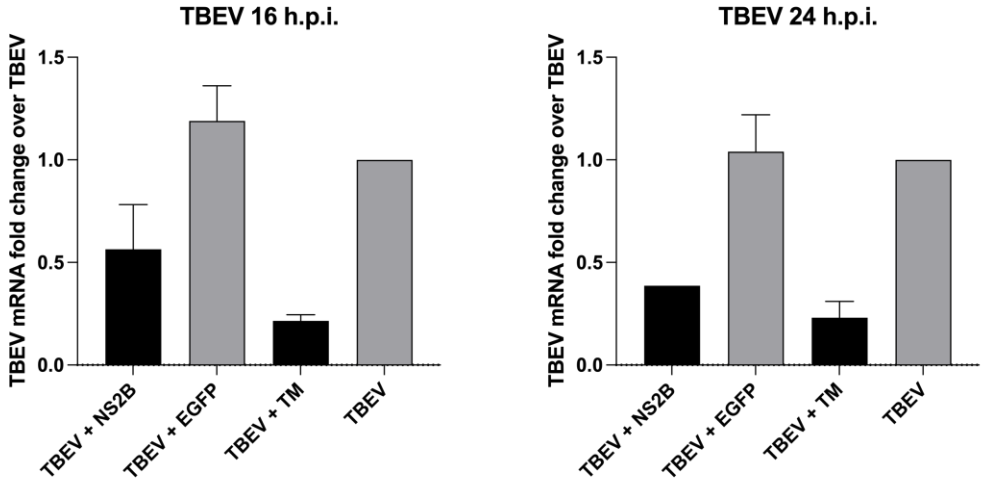

Figure 39 NS2B transduction inhibits viral replication at the mRNA level at 16 h.p.i. and 24 h.p.i.

U2OS cells were transduced for 24h before infection with TBEV MOI 0.5 for 16h or 24h. Cells were lysed in Trizol for mRNA analysis. Experiment was performed in ≥3 independent biological replicates. In a) and b) RT-qPCR results of mRNA fold changes are shown – data are normalized on the mRNA levels of the TBEV control. For statistical analysis in a) and b) Statistical significance was determined using the Kruskal–Wallis test with Dunn's multiple comparisons test. *, P < 0.05; **, P < 0.01; ***, P < 0.001.*Comparison was done against the NS2B sample. Data are considered significantly different with a p≤0.05. Data were checked for normality to choose the proper test to perform.

In line, the immunofluorescence displayed in **Fig. 40** shows that cells which strongly overexpress NS2B (green) allow much less for viral replication, displayed in red as a readout of TBEV E protein.

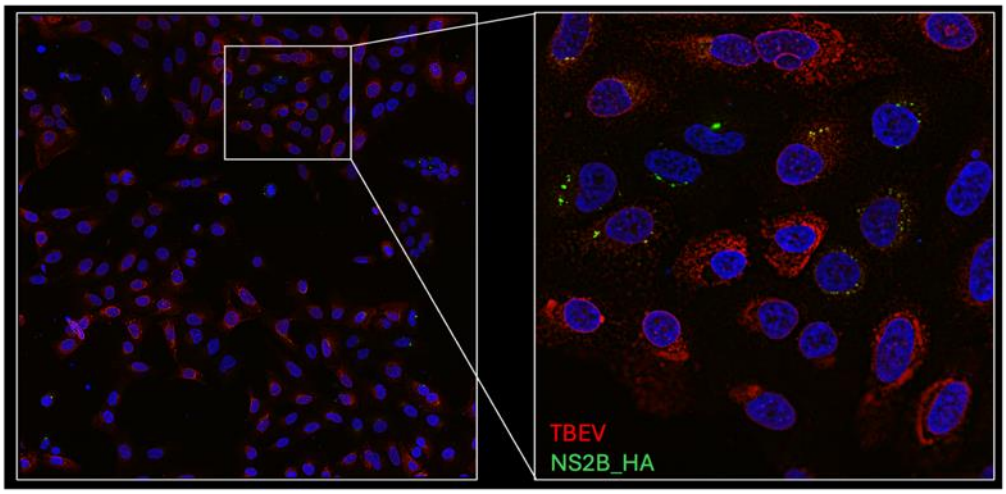

Figure 40 NS2B transduction inhibits viral replication at the as visible by immunofluorescence

U2OS cells were plated on coverslips, transduced with NS2B_HA expressing lentiviruses for 24h, after 24h cells were infected with TBEV MOI 0.5 for other 24h. Cells were fixed with PFA 3.7%, permeabilized with Triton 0.1% and stained with the antibodies of interest: an anti-HA to detect transfection and an anti-TBEV E protein to detect infected cells, followed by an incubation with a secondary tagged with a 488nm fluorophore to stain FLAG-tag proteins and a 549nm fluorophore to stain TBEV-E protein. Nuclei were stained with DAPI. Zeiss Airyscan 880, 63X Plan-Apo/1.4 NA Oil objective was used to acquire images.

NS2B_HA induces XBP1 splicing and UPR genes

Since we have seen before that NS2B_FLAG overexpression activates IRE1, leading to XBP1 splicing and UPR genes induction, we wanted to confirm the same phenotype in cells transduced with NS2B_HA lentivirus. Indeed, NS2B_HA at 48 h.p.t. induced XBP1 splicing, as visible on the agarose gel of **Fig. 41**. RNA was extracted from transduced and control cells and XBP1 mRNA was amplified with specific primers to determine the total XBP1 mRNA and the spliced form, visualized as double band in the gel. GAPDH was used as PCR control. As shown in fig X the negative control, as well as EGFP and NS2B_HA transduced for 16 or 24 hours do not show a double band while in the sample NS2B_HA at 48 h.p.t. is visible a second band that identifies the spliced form. In addition, the expression levels of a panel of UPR related genes (XBP1-s, XBP1-total, DNAJ, EDEM, BIP and DDIT3) were analysed by RT-qPCR, and at 48h.p.t. most of them were upregulated compared to the controls. This data indicates that the lentivirus system successfully recapitulates NS2B_FLAG UPR activation given by IRE1.

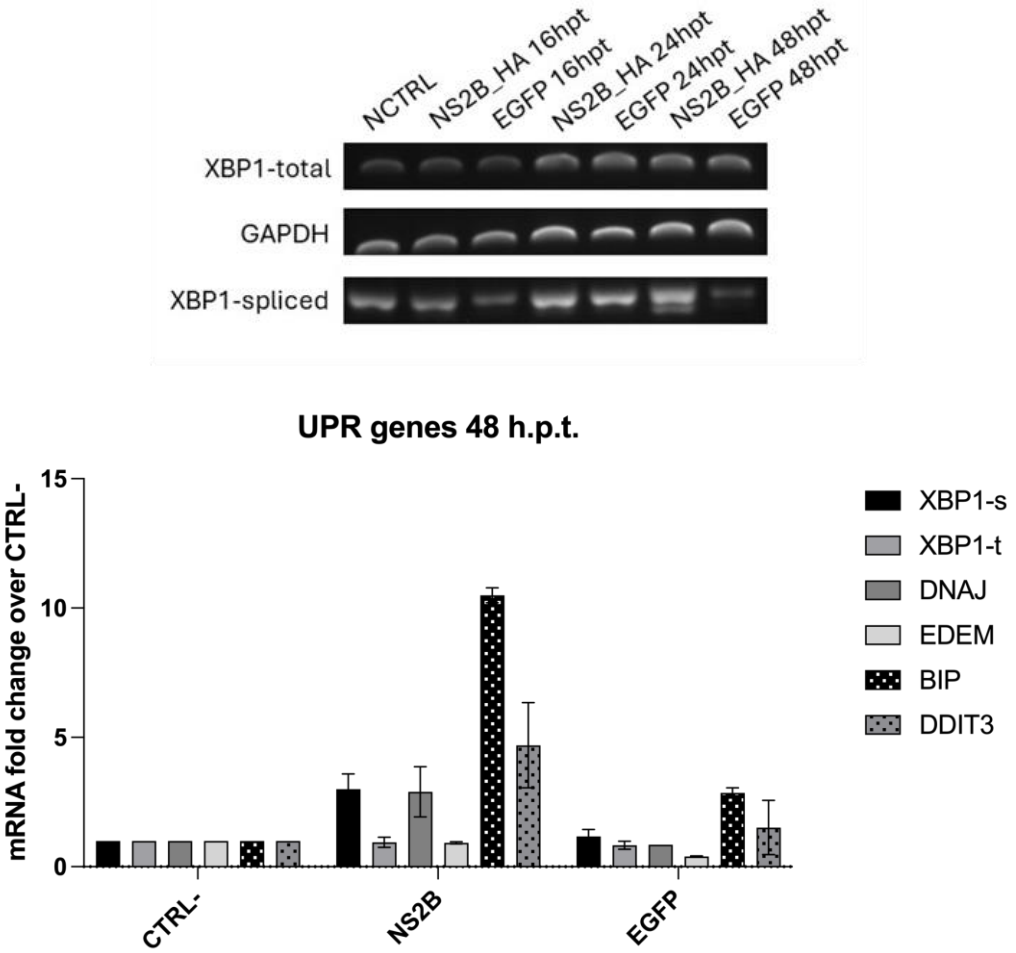

Figure 41 NS2B_HA transduction induces UPR activation at 48 h.p.t.

U2OS cells were transduced for 24h and 48h before collecting cells in Trizol for mRNA analysis. In the upper part of the figure a PCR run on a 1% agarose gel is represented indicating the splicing of XBP1. In the lower part, an RT-qPCR was performed to check the levels of some UPR related genes. Data are normalized on the negative control – not transduced cells. Experiment was performed in a single biological experiment.

Introduction to the results part 2 – NS4B

Some initial data were produced by Dr. Lais Nascimento Alves, a former PhD student in the laboratory. These data are shown here to contextualise my contribution to the project.

TBEV induces stress granules in less than 10% of infected cells

It is known that among the cellular responses adapted from the cells to fight infection there is the formation of stress granules which induce a general block of cellular translation and thus inhibits the formation of newly formed viruses. However, several viruses developed some mechanisms to avoid the formation of stress granules in favour of their replication. We addressed the formation of stress granules by TBEV by two different stress granules markers: eIF3 and G3BP1 (**Fig. 42**). We quantified that in the context of TBEV infection there are less than 10% of cells containing stress granules, suggesting that TBEV, like other members of the flavivirus group, might also be inhibiting the formation of stress granules.

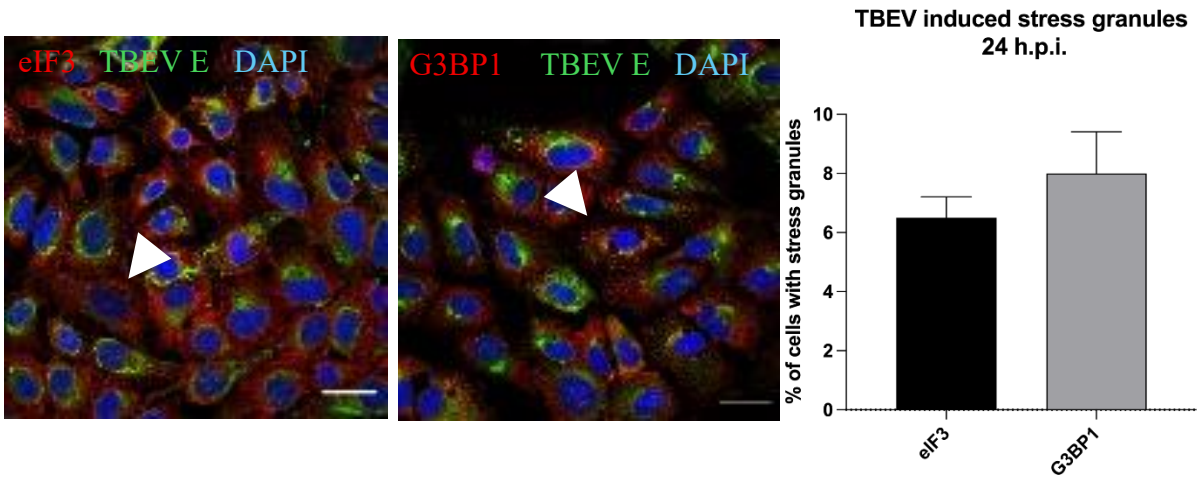

Figure 42 TBEV infection induces SGs in less than 10% of infected cells

U2OS cells were plated on coverslips, infected with TBEV at an MOI 0.5 for 24h. Cells were fixed with PFA 3.7%, permeabilized with Triton 0.1% and stained with the antibodies of interest: an anti-TBEV E-protein to detect infection and an anti-G3BP1 or anti-eIF3 to detect stress granules positive cells, followed by an incubation with a secondary tagged with a 488nm fluorophore to stain infected. Cells and a 549nm fluorophore to stain G3BP1 or eIF3. Nuclei were stained with DAPI. Acquisition was done at the Zeiss Airyscan 880 with a 63X magnification. 20nm scalebar is set.

TBEV induced stress granules are PKR dependent

There are four cellular kinases which, upon activation via different stressors, phosphorylate the protein eIF2a, inducing the formation of stress granules and stall of translation. Those are: PERK, PKR, GCN2 and HRI. GCN2 gets activated by aminoacid starvation (Dong et al., 2000), while HRI by stressors such as oxidative stress (Lu et al., n.d.). On contrary, PERK gets activated by an accumulation of unfolded proteins at the levels of the endoplasmic reticulum (Harding et al., 2000b) and PKR is known to recognize dsRNA to activate the integrated stress

response (ISR). Even though each of them has been shown to be active in the context of some viral infection, PERK and PKR are the ones mostly studied when we consider infection with +ssRNA viruses such as Orthoflavivruses. PERK is one of the three actors of the Unfolded Protein Response which is often activated during replication of viruses that exploit the Endoplasmic Reticulum, while PKR is a Pattern Recognition Receptor protein that binds dsRNA, a well-known replication intermediate of +ssRNA viruses. We therefore generated lentiviruses carrying a short hairpin RNA against PERK and PKR and that that we used to transduce U2OS cells, generating U2OS_knocked down cells named U2OS_shPKR. The aim was to decipher which of the proteins is the one responsible for the induction of stress granules

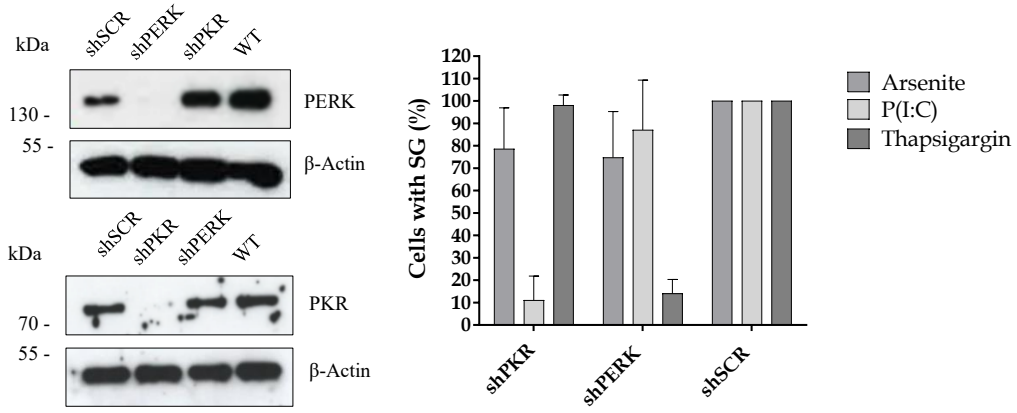

Figure 43 Knock down of PKR and PERK by shPKR and shPERK inhibits PolyI:C and Thapsigargin induced SFs

U2OS cells were treated with shPERK and shPKR lentivectors for knocking down. KD cells were selected by puromycin. a) and b) KD was demonstrated via western-blot analysis. In c) those cells were treated with the drugs known to induce SGs in different conditions and stress granules formation was quantified by IF. PolyI:C is a known activator of PKR and it is shown in c) that shPKR cells do not induce SGs when treated by PolyI:C, while PERK's activator Thapsigargin still successfully induces SG formation. The same is observed in shPERK cells which do not induce SGs when treating with

formation during TBEV infection. In **Fig. 43** the evaluation of the KD levels by WB. shSCR means shScramble, a control shRNA transduced in U2OS cells, WT are not transduced U2OS cells. For both shPERK and shPKR the silencing of proteins was efficient. Actin was used as loading control. To further validate the silencing of PERK and PKR in U2OS cells we quantified SG positive cells after stimulation with specific inducers of the kinases: PolyI:C for PKR, Thapsigargin for PERK and Arsenite for HRI. As shown in **Fig. 44** shPKR cells fail to induce SG in response to PolyI:C and shPERK cells fail to produce SG in response to Thapsigargin. In both cell lines the other inducers efficiently induced SG in 80-100% of cells. Next, knocked down cells were infected with TBEV at a MOI of 0.5, fixed at 24 h.p.i. and stained with a marker for stress granules. We observed that while the silencing of PERK was

still permissive for the stress granules to be formed, silencing of PKR resulted in a complete loss of SG formation. This result suggests that during TBEV infection the formation of stress granules is PKR dependent (**Fig. 44**)

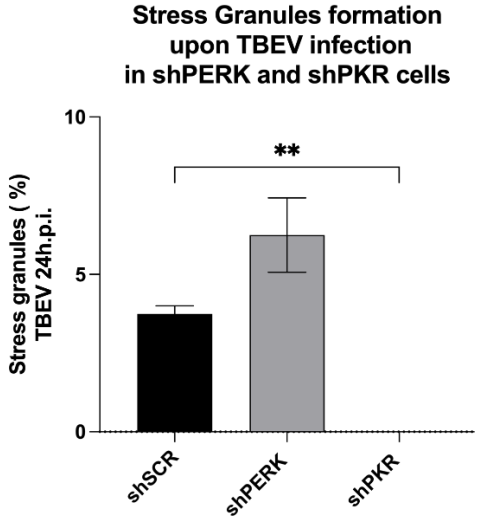

Figure 44 TBEV induced stress granules are PKR dependent

U2OS_shPERK and U2OS_shPKR were plated on coverslips and infected with TBEV MOI 0.5. for 24h. Cells were fixed in 3.7% PFA and stained with primary antibodies against TBEV E protein and G3BP1. Secondary antibodies tagged with fluorophores of interest were added and images were acquired at the Zeiss Airyscan 880 with the 63X magnification. Cells were manually counted and % of positive cells calculated. Statistical significance was determined using the Kruskal–Wallis test with Dunn's multiple comparisons test. *, $P < 0.05$; **, $P < 0.01$; ***, $P < 0.001$.*

NS4B and NS5 inhibit the formation of PolyI:C induced stress granules

It has been reported for several Flaviviruses that diverse non-structural proteins had an effect in the inhibition of the stress granules formation as a mechanism evolved by the virus to avoid the antiviral response. For ZIKV it has been proven that inhibition of SGs formation boosts viral replication (Wu et al., 2024), as well as for JEV and DENV for which a strategy of SG disassembly has been proposed (Arakawa et al., 2022). From our laboratory, Albornoz and colleagues showed that upon TBEV infection, the SGs component TIA-1 was recruited to sites of viral replication thus not entering in the SGs (Albornoz et al., 2014). We thus wanted to investigate the strategy used by TBEV to inhibit the PKR dependent SGs formation. We screened all the TBEV non-structural proteins in their ability to inhibit stress granules formation upon PolyI:C treatment (PKR activator). All the proteins were firstly overexpressed for a total of 20h, and 4h before closing the experiment PolyI:C was added to induce stress granules formation. NS4B had the strongest inhibitory effect, followed by NS5 that is also significantly inhibiting the PKR dependent SGs (**Fig. 45, left**), while all other NS proteins didn't show significant inhibitory activity. This was further confirmed at the protein levels by the phosphorylation level of PKR upon PolyI:C treatment, which was shown to be decreased

in the presence of NS4B and NS5 compared to the GFP control or NS2B (**Fig. 45, right**). Since the effect of NS5 may be linked to an activity already described and discussed later, we decided to focus our interest in understanding the mechanism exploited by NS4B to inhibit PKR activation.

NS4B C-loop interacts with PKR

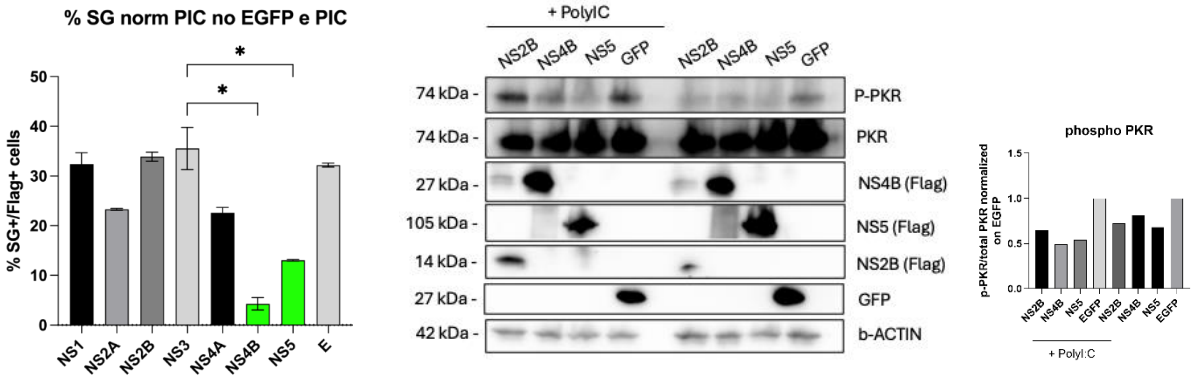

Figure 45 TBEV NS4B mostly inhibits PolyI:C induces stress granules

U2OS cells were plated on coverslips, plasmids were transfected using Lipofectamine LTX and 16 later 500ng of PolyI:C was transfected and incubated for 4h to induce stress granules. Cells were fixed with PFA 3.7%, permeabilized with Triton 0.1% and stained with the antibodies of interest: an anti-FLAG to detect transfection of the FLAG-tagged non-structural proteins and its mutants and an anti-G3BP1 to detect stress granules positive cells, followed by an incubation with secondary antibodies. Nuclei were stained with DAPI. Acquisition was done at the Zeiss Airyscan 880 with a 63X magnification. Quantification of immunofluorescence data is displayed. 200 cells were counted for each sample. Cells with stress granules were counted and normalized on the total cell number. Experiment was performed in ≥3 independent biological replicates. Statistical significance was determined using the Kruskal–Wallis test with Dunn's multiple comparisons test. Comparison was done against the NS3 sample. Data are considered statistically significant with a $p \leq 0.001$. Data were checked for normality to choose the proper test to perform.

Central, U2OS_WT cells were transfected with Lipofectamine LTX with the plasmids of interest for 20h, 16h after transfection PolyI:C was added for 4h to induce stress granules. Proteins were collected in RIPA buffer for western-blot analysis. Proteins were run on a 12% SDS-PAGE, then transferred on a nitrocellulose membrane and incubated with the primary antibodies for 1h at RT or over-night at 4 degrees against the proteins of interest, further incubated for 1h at RT with the appropriate secondary antibodies HRP tagged. Densitometric analysis of the Western blot bands is displayed.

Since we discovered that NS4B plays a major role in the inhibition of PolyI:C induced stress granules formation, we wondered whether a direct interaction of NS4B with PKR could explain our observations. Since NS4B is a protein which spans the ER membrane several times, we thought that the hypothetical region of interaction with PKR could be the cytoplasmic loop (C-loop) of NS4B. For this purpose, an *in-silico* analysis was done by docking the C-loop of NS4B with the PKR dimer. Interestingly, we observed that the C-loop fits nicely in the pocked formed by the PKR dimer (**Fig. 46**).

Next, three NS4B mutants were generated by engineering 3 deletions of four aminoacids in the C-loop as indicated in **Fig. 47**. The purpose of generating the mutants which will further be referred to as mutant1 (M1) shown in yellow, mutant2 (M2) shown in green and mutant3 (M3)

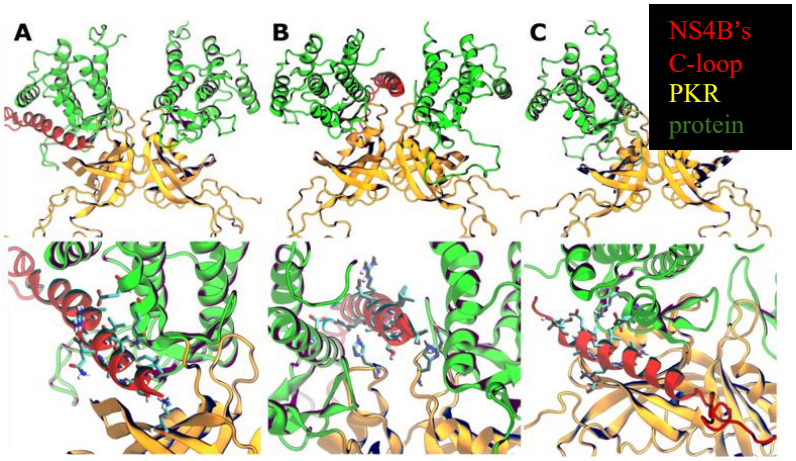

Figure 46 In silico analysis of NS4B and PKR

Docking analysis of PKR dimer (green and yellow) with NS4B cytoplasmic loop (red).

in pink was to understand whether a rescue in the SGs formation would occur upon transfection with the mutants and treatment with PolyI:C to induce SGs formation. If this occurred, we could be getting closer to the NS4B domain involved in the inhibition of SGs formation.

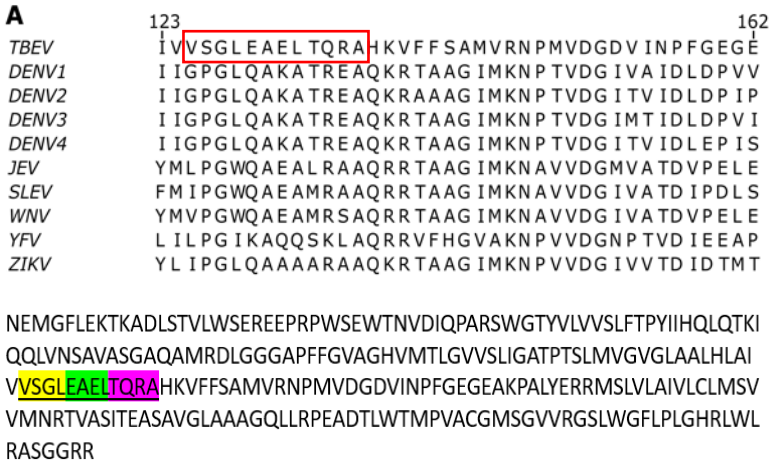

Figure 47 Alignment of NS4B cytoplasmic loop with other flaviviral cytoplasmic loops

The 5' of the NS4B cytoplasmic loop has important differences compared to the one of other flaviviruses. This region is indicated in red. Three mutants were inserted in the NS4B cytoplasmic loop as indicated below. The mutants are deletions of 4 amminoacids each.

Results part 2 – NS4B

NS4B C-loop mutants rescue stress granules formation

Since we observed that expression of NS4B strongly inhibits PolyI:C induced stress granules, three deletion mutants were generates as described before in the region of which showed the highest affinity to PKR in our *in-silico* analysis. Every NS4B mutant, referred to as Mutant1, Mutant2 and Mutant3, consists of four aminoacidic deletions. We overexpressed the 3 mutated NS4B and WT proteins in U2OS cells, induced stress granules formation by transfection of PolyI:C and quantified the stress granules in the different conditions. We observed that while in a normal condition PolyI:C induces stress granules in approximately 45% of cells, presence of NS4B_WT strongly inhibited formation of stress granules to an extent of less than 10% of cells. On the other hand, every one of the three mutants was more permissive to the formation of stress granules. Representative images are shown in **Fig. 48**. Quantification of the images is displayed then in **Fig. 49**.

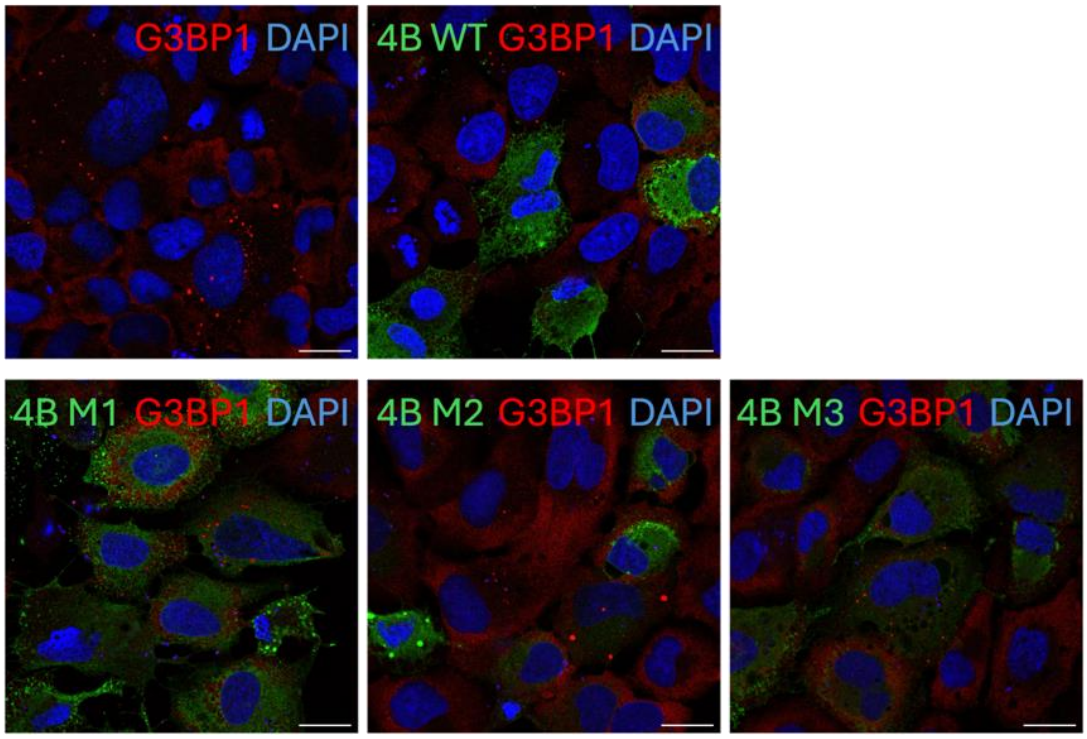

Figure 48 Visual representation of NS4B and its mutant induction of stress granules in U2OS_WT cells

U2OS cells were plated on coverslips, transfected with Lipofectamine LTX with the plasmids of interest for 20h. 16h post transfection PolyI:C was transfected and incubated for 4h to induce stress granules. Cells were fixed with PFA 3.7%, permeabilized with Triton 0.1% and stained with the antibodies of interest: an anti-FLAG to detect transfection of NS4B and its mutants and an anti-G3BP1 to detect stress granules positive cells, followed by an incubation with a secondary tagged with a 488nm fluorophore to stain FLAG-tag proteins and a 549nm fluorophore to stain G3BP1. Nuclei were stained with DAPI. Acquisition was done at the Zeiss Ayriscan with a 63X magnification. 20nm scalebar is set.

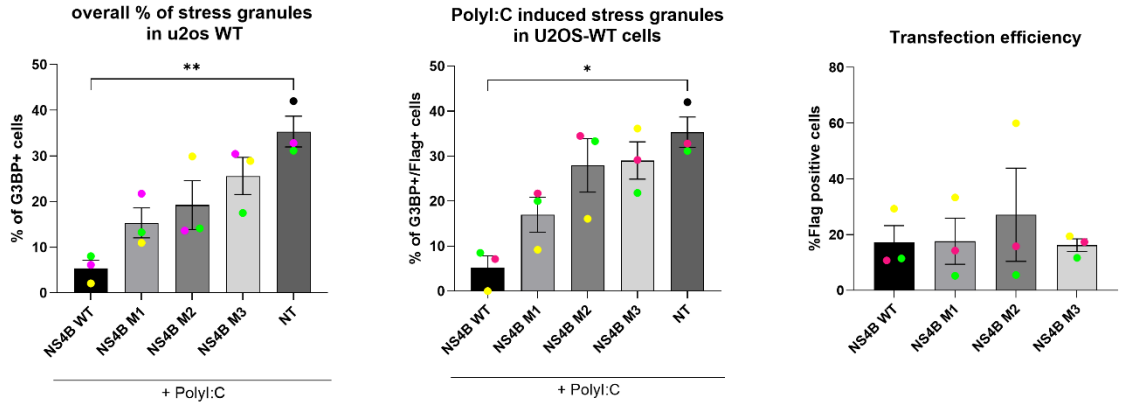

Figure 49 Quantification of data represented in Figure 49

Quantification of immunofluorescence data is displayed. Cells with stress granules were counted and normalized on the total cell number. For each condition ≥200 cells were counted. Experiment was performed in ≥3 independent biological replicates. Statistical significance was determined using the Kruskal–Wallis test with Dunn's multiple comparisons test. *, $P < 0.05$; **, $P < 0.01$; **, *$P < 0.001$*. Comparison was done against the PolyI:C treated sample (NT).

To dig more into the mechanism exploited by NS4B to inhibit the formation of stress granules we checked the phosphorylation status of proteins of our interest by western blot analysis displayed in **Fig. 50**.: PKR and its downstream effector eIF2α. As expected, upon PolyI:C treatment all cells present, at different level, the phosphorylated form of PKR which was not observable in the negative control. If we compare the samples where NS4B_WT was transfected we can observe a drastic reduction in P-PKR, suggesting that NS4B can actively interfere with the phosphorylation, i.e. activation, of PKR. On the other hand, transfection of all three mutants partially restored the phosphorylation levels of PKR, thus indicating a lower inhibition of PKR activation. The increase given by M1 was minimal, while the one of M2 and M3 was higher. Quantification of the western blot data is shown as well. This data confirms that the mutations inserted in NS4B c-loop affect the interaction with PKR, strengthening the hypothesis that TBEV uses NS4B as a main player in avoiding the activation of the cellular stress response. Surprisingly, we didn't see the same pattern of inhibition of phosphorylation of the downstream protein of PKR, P-eIF2α. The factor looks phosphorylated in all the

conditions suggesting that other kinases of the ISR might be involved at this time, such as PERK which also converges on the phosphorylation of eIF2α.

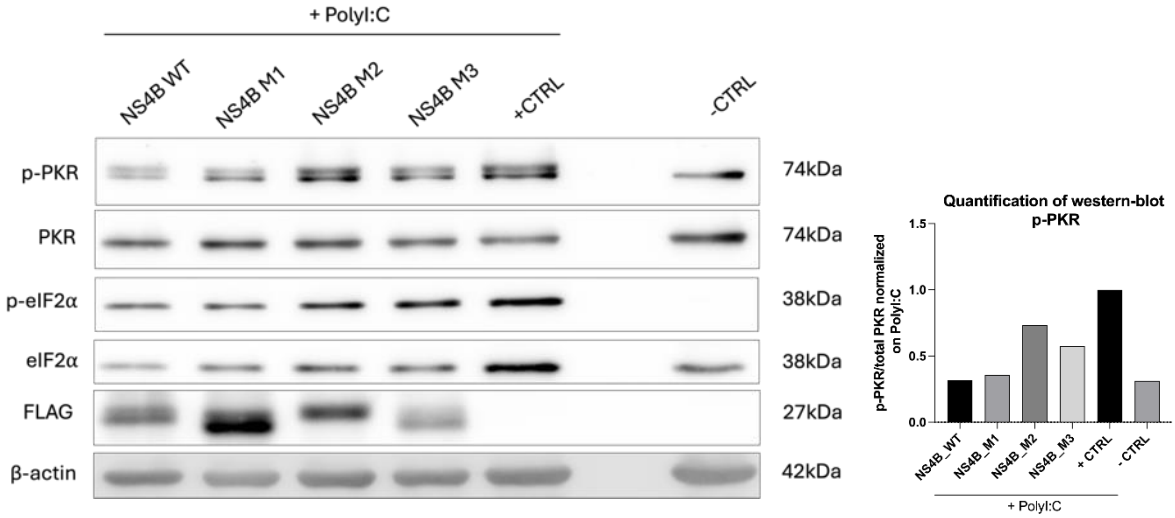

Figure 50 Western blot analysis of PKR and eIF2a protein levels upon NS4B and mutants transfection

U2OS_WT cells were transfected with Lipofectamine LTX with the plasmids of interest for 20h, 16h after transfection PolyI:C was added for 4h to induce stress granules. Proteins were collected in RIPA buffer for western-blot analysis. Proteins were run on a 12% SDS-PAGE, then transferred on a nitrocellulose membrane and incubated with the primary antibodies for 1h at RT or over-night at 4 degrees against the proteins of interest, further incubated for 1h at RT with the appropriate secondary antibodies HRP tagged as seen in a). Actin was used as loading control. Millipore or Super-ECL reagent were used for the detection of the proteins. In b) the quantification of the blot is shown displayed as the ratio between the intensity of the phosphorylated protein and its total.

PKR overexpression rescues SGs formation inhibited by NS4B

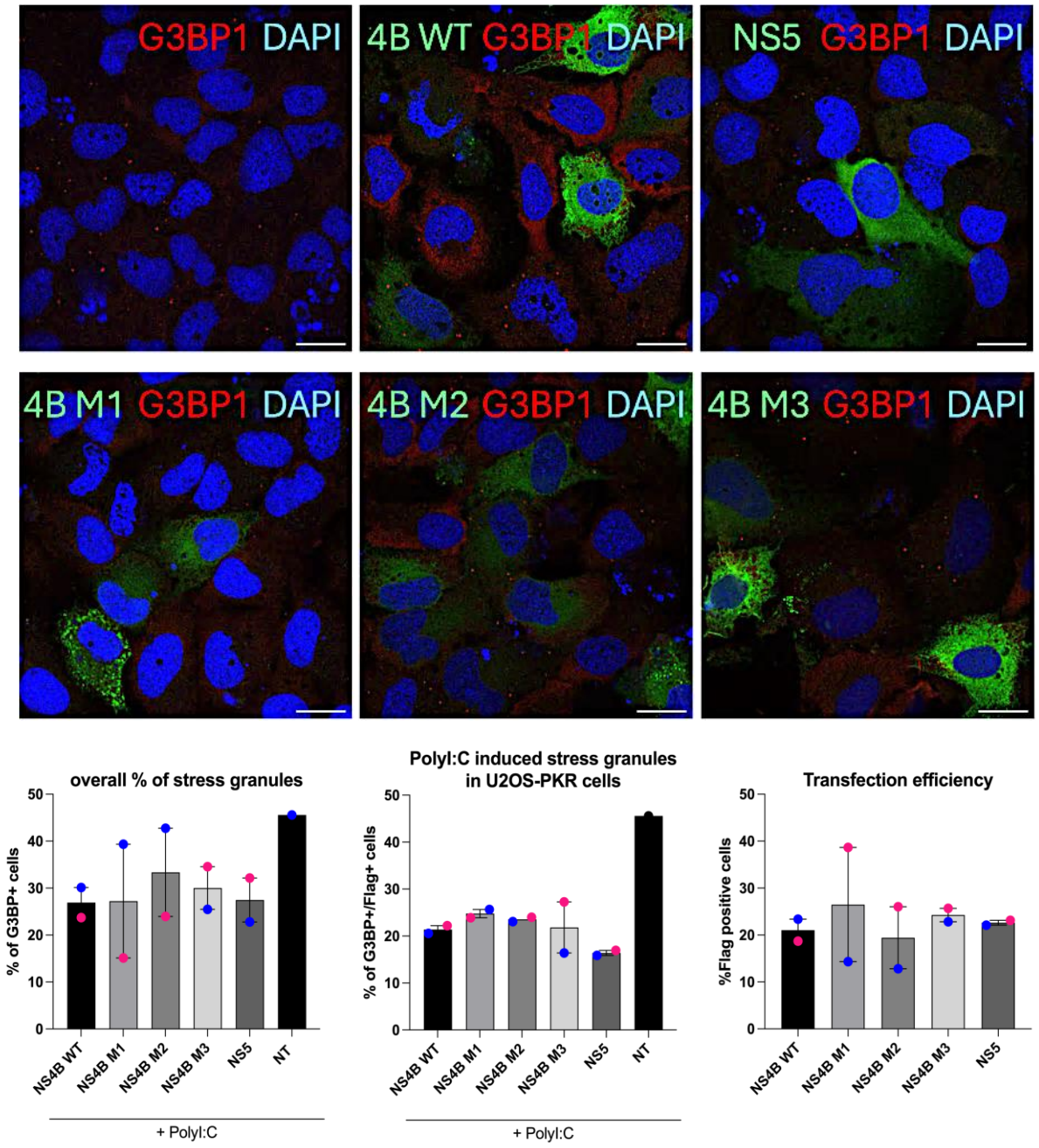

Figure 51 Visual representation of NS4B and its mutant induction of stress granules in U2OS_PKR cells and quantification of images

U2OS-PKR cells were plated on coverslips, transfected with Lipofectamine LTX with the plasmids of interest for 20h, 16h after transfection PolyI:C was added for 4h to induce stress granules. Cells were fixed with PFA 3.7%, permeabilized with Triton 0.1% and stained with the antibodies of interest: an anti-FLAG to detect transfection of NS4B and NS5 and its mutants and an anti-eIF4b to detect stress granules positive cells, followed by an incubation with a secondary tagged with a 488nm fluorophore to stain FLAG-tag proteins and a 549nm fluorophore to stain eIF4b. Nuclei were stained with DAPI. Acquisition was done at the Zeiss Airyscan 880 with a 63X magnification.

NS4B and NS5 were transfected in cells constitutively overexpressing PKR (U2OS_PKR) and stress granules formation was addressed to see if in a condition of overexpression of PKR induction of stress granules with PolyI:C would still be inhibited by NS4B. We added to the experiment NS5 transfection as well because, as previously seen in the preliminary data of this part of the results, NS5 was having, together with NS4B, the strongest effect in the inhibition of stress granules formation among all the TBEV proteins screened. Interestingly, we noticed that NS4B lost the capability to inhibit the PolyI:C induced stress granules formation when PKR was present in higher amount in cells (**Fig. 51**). This is in line with our idea that the NS4B given inhibition of stress granules formation occurs by blocking PKR activation since cells expressing more abundantly PKR, but transfected with the same concentration of NS4B, managed to induce more SGs. Same can be said for NS5 (this result needs to be compared to the % of cells with SG shown in **Fig. 45**, left).

In **Fig. 52** the comparison of SGs formation in U2OS_WT cells and U2OS_PKR cells visually demonstrates that:

A) There is an overall increase in the formation of stress granules in the PKR overexpressing cells

B) The effect of PKR overexpression is mostly striking in the NS4B_WT presence where we can observe that the inhibition given by NS4B is strongly decreased in presence of PKR.

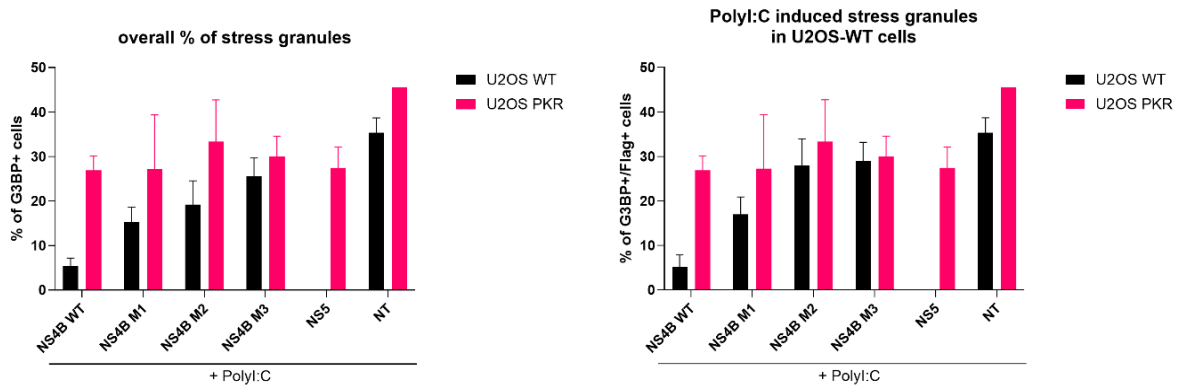

Figure 52 Comparison of stress granules formation in U2OS_WT cells and U2OS_PKR cells upon PolyI:C treatment

Comparison of stress granules formation in U2OS_WT cells (black bar) and U2OS_PKR cells (pink bar) in the overall cellular population (left), or by focusing only on the transfected cells (right).

The cell line used in this experiment was generated in the laboratory by a lentiviral transduction experiment to constantly overexpress PKR, transduced cells were selected with puromycin (**Fig. 53**).

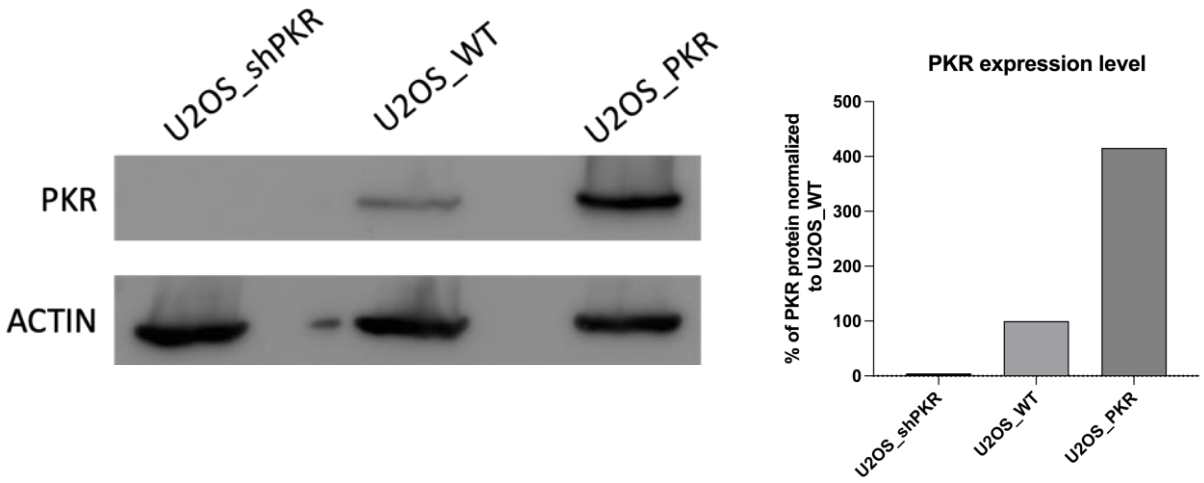

Figure 53 Western blot analysis indicating an increase in the total PKR levels in the U2OS_PKR cells

U2OS_shPKR, U2OS_WT and U2OS_PKR cells were seeded, and proteins were collected in RIPA buffer for western-blot analysis. Proteins were run on a 12% SDS-page gel, then transferred on a nitrocellulose membrane and incubated with the primary antibodies for 1h at RT or over-night at 4 degrees against the protien of interest, further incubated for 1h at RT with the appropriate secondary antibodies HRP tagged. Actin was used as loading control. Millipore or Super-ECL reagent were used for the detection of the proteins. In a) a visual rapresentation of PKR levels. In b) quantification of the blot in a) is shown. The band corresponding to PKR in each sample was normalized on its actin. The U2OS_WT PKR level was considered as 100% level of PKR and the other two were compared to U2OS_WT levels.

NS4B interacts with PKR

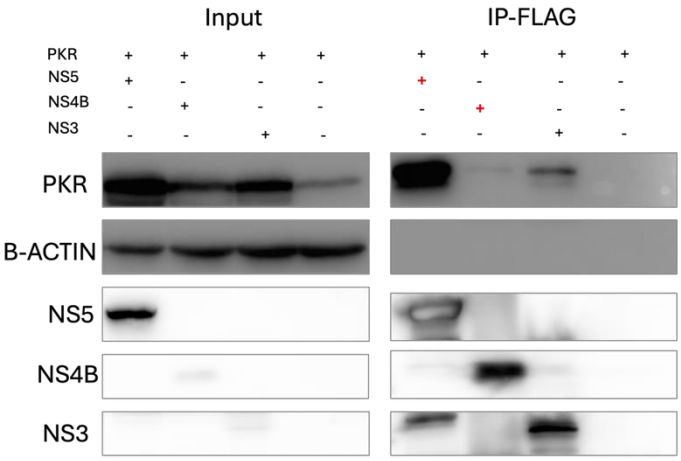

Figure 54 NS4B and NS5 are pulled down with PKR

U2OS_PKR cells were transfected with NS5_FLAG, NS4B_FLAG and NS3_FLAG with Lipofectamine LTX for 24h. Proteins were collected with a mild buffer suitable for IP experiments. Anti-FLAG beads were used for immunoprecipitation. Immunoprecipitated proteins were then loaded on a 12% SDS-page gel and transferred on a nitrocellulose membrane. Proteins of interest were detected with appropriate primary antibodies for 1h at RT ot over-night at 4 degrees, secondary antibodies HRP tagged were then used for 1h at RT. Immunoblotting was done with the usage of Millipore substrate or SuperECL.

To dig in the detail, we needed a proof that NS4B interacts with PKR to block its activation and downstream effect. We therefore set up a co-immunoprecipitation experiment in which

U2OS_PKR cells were transfected with NS4B_FLAG to address whether we were able to see the two proteins pulled down. Since we noticed that NS5 was also having a negative impact on stress granules formation, we included this protein in the experiment as well.
Interestingly, as visible in **Fig. 54**, pull-down of FLAG-tag proteins showed that PKR interacts both with NS4B and with NS5. This data showing the difference in the intensity of PKR's pull-down is not surprising, since NS5 is a bigger and soluble protein (approximately 100kDa), which localizes completely in the cytoplasm thus easier to immunoprecipitate in an IP assay, compared to NS4B (25kDa) which is a multi-spanning ER protein technically more complex to pull down since it requires a strong solubilization of the membranes otherwise there is the possibility to lose it during the sample preparation. Taken all this into consideration I believe the pull-down of a bigger protein (PKR 70kDa) with a smaller, transmembrane one (NS4B 25kDa) is more demanding compared to the pull-down of PKR with a bigger completely cytoplasmatic protein – NS5. Altogether this data demonstrates that NS4B interacts with PKR, which is in line with our previous data. Of note that there is also a strong effect given by NS5, which will be studied separately in future. An interaction with NS3 was observed as well, even though NS3 did not inhibit the PolyI:C induced SGs formation as seen in **Fig. 45, left**.

Generation of mutated TBEV in the NS4B region

We next wondered which effect would those mutations of NS4B have if inserted in the real replicative TBEV. We therefore exploited the Infectious Subgenomic Amplicon (ISA) reverse genetic method for TBEV developed by Haviernik et al. (Haviernik et al., 2021), to insert the mutations of interest in the replicative virus. The system consists of three fragments which together encode for the entire TBEV-Hypr genome carrying a gene encoding the mCherry fluorescent protein at 5' of the Fragment1. We obtained also from the laboratory of Prof. Ruzek an additional Fragment1 tagged with turbo-GFP instead of mCherry, as recently published by their laboratory (Berankova et al., 2025). As visible in the left part of **Fig. 55** provided by Berankova, the three fragments cover for the entire genome of TBEV, with fragment1 (F1) consistent of a 5'UTR up to NS1, then fragment2 (F2) encoding an F1 overlapping region of NS1 until the NS4A region, and lastly fragment3 (F3) consistent of the F2 overlapping region until the 3'UTR. Additionally, as visible at the right part of the figure, we can see that the fluorescent proteins are inserted in at the 5' of the sequence belonging to the capsid protein, and flanked by two ribosome skipping sequences referred to as P2A and T2A, which, upon recognition by the ribosome, expel the Turbo GFP (respectively mCherry) sequence in the cellular cytoplasm, thus normally proceeding the translation of the polyprotein.

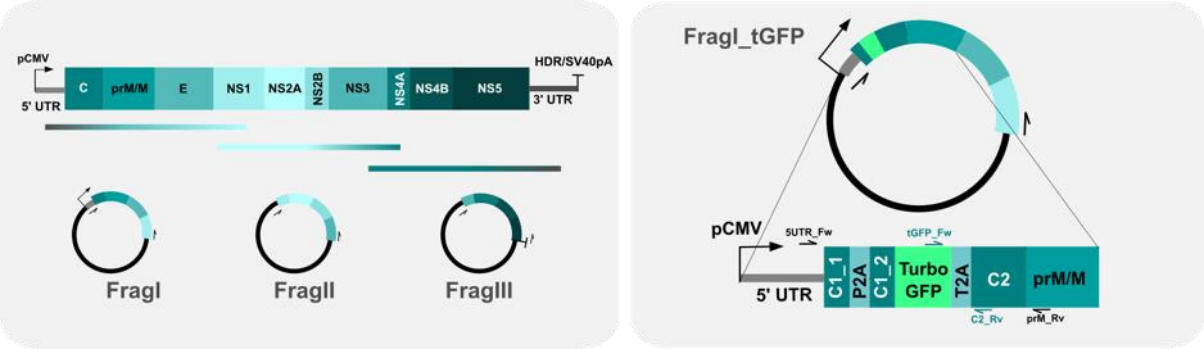

Figure 55 Schematic representation of TBEV reverse genetic

TBEV-tGFP scheme kindly provided by Prof. Daniel Ruzek and published in (Berankova et al., 2025). On the left part the scheme indicating the composition of the three fragments and the regions they cover, while on the right part the detail of the insertion of the fluorescent protein in the capsid sequence.

To obtain NS4B mutant viruses we needed to insert the desired mutations in Fragment2 of the system where the NS4B sequence is located. Since the three fragments of the reverse genetic are used in their linear form, we designed a forward (FW_M1) and a reverse (RV_M1) primer containing the deletions of interest. The FW_M1 mutated primer was used together with the F2 RV primer to obtain a PCR product referred to as A (700bps). The RV mutated primer was

used together with the F2 FW primer to obtain a PCR product referred as B (4kB) as shown

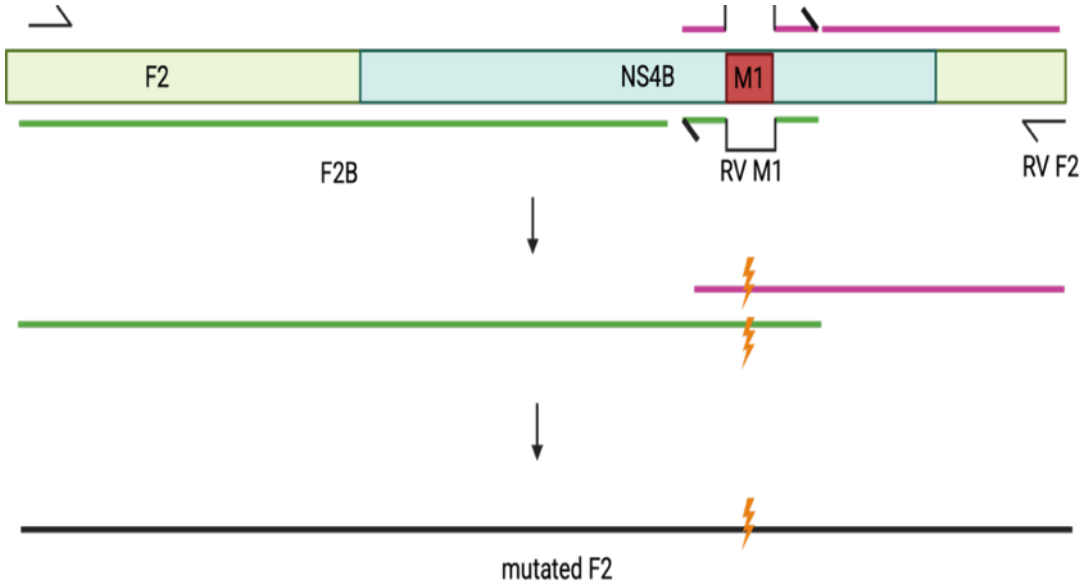

Figure 56 Schematic representation of the mutagenesis strategy

schematically on **Fig. 56**. The products were then run on an agarose gel, gel purified and sent for sequencing (**Fig. 57**).

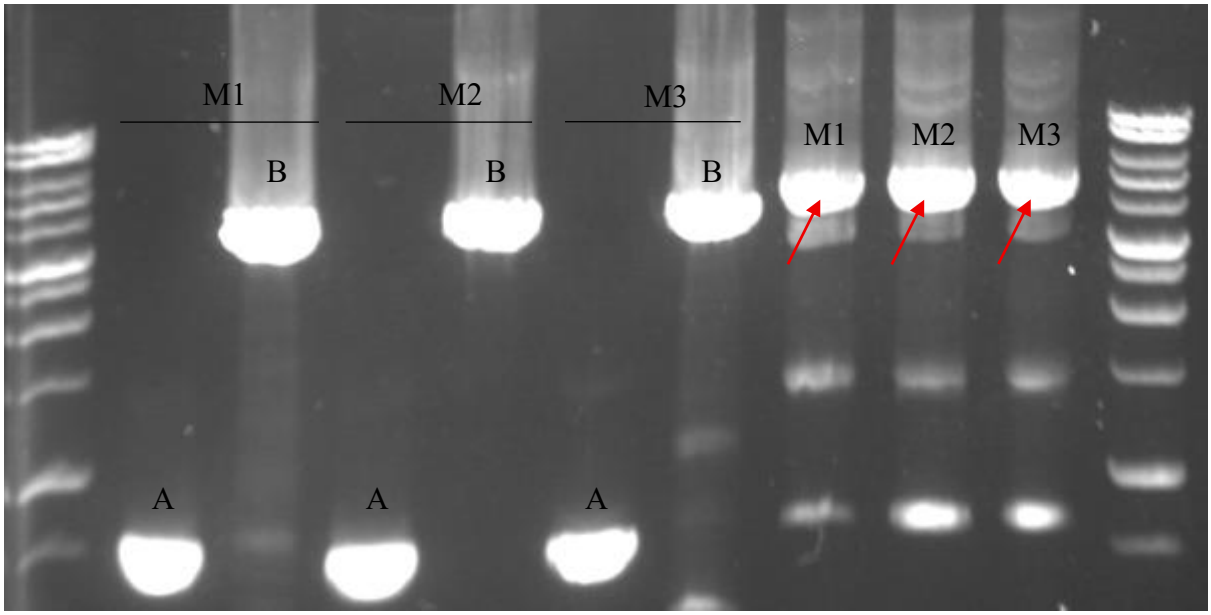

Figure 57 PCR products of Fragment2 prior and post ligation

PCR product was run on an agarose gel. First 6 wells indicate the PCR products of the insertion of the mutations. Last three wells indicate the ligation product. Ladder is 1kB.

After confirming the mutation is correctly inserted in the region of interest by sequencing the domain of interest where the mutation is inserted, another PCR is necessary to ligate the fragments A and B and obtain a fully mutated F2. This is done by using the two fragments (A and B) as templates and primers FW_F2 and RV_F2 to reconstruct by amplification the fragment 2. We can see in the last three wells of the gel that the 'ligation' (we name ligation

the PCR amplification used to obtain again the full-length Fragment 2 starting from F2A and F2B) of the two fragments proceeded correctly and we gel purified those fragments (indicated with the red arrows). Again, we needed to sequence the mutated F2 to confirm the deletions were present. Once confirmed that the mutated F2 fragments are correctly produced we could proceed by generating the mutated viruses.

To obtain full length replicative viruses the 3 fragments were transfected with the XtremeGene HP Transfection reagent on BHK21 cells and incubated for approximately 5 days or until a strong cytopathic effect was observed. Supernatant was collected to determine viral titre of the P0 viruses. Western-blot analysis was performed as well to check for the expression of GFP, mCherry and TBEV-E protein, and RNA was collected for sequencing.

Sanger sequencing on the amplified NS4B domain where deletions were inserted showed that in all the viruses, M1, M2 and M3 both mCherry and GFP, the 4 aa were correctly deleted **Fig. 58**. The whole viral genome was sequenced in the lab by a colleague using amplicon-based sequencing method for Oxford Nanopore MinION technology **Fig. 59**. The whole genome sequencing confirmed the correct deletion on NS4B of the mutants.

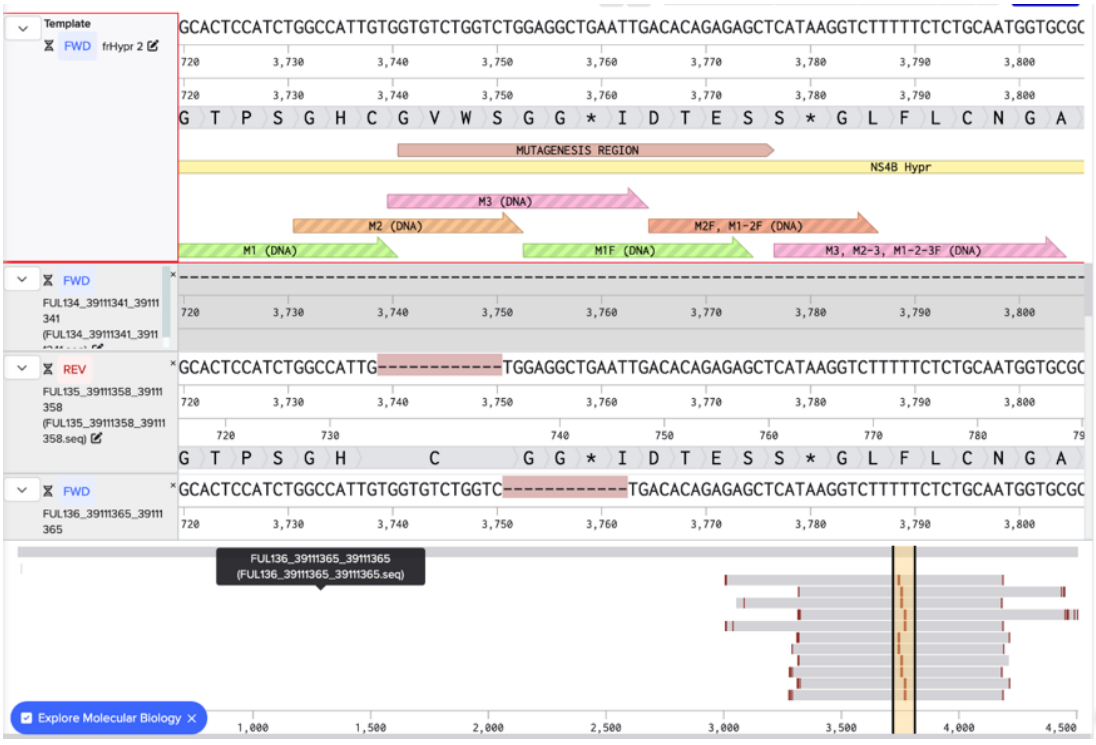

Figure 58 Sanger sequencing of NS4B mutated region in Fragment2

Alignment of the Sanger sequencing results of P0 showing that of the 12 samples (3 mutations, each sequenced with a FW and with a RV=6 and each condition in a GFP and mCherry version) each one contains the correct deletion.

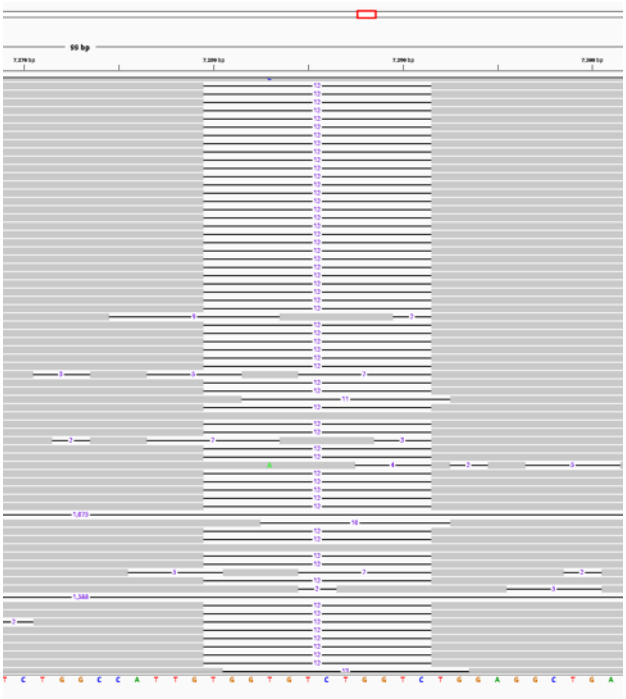

Figure 59 Whole genome sequencing of TBEV mutant viruses

Alignment of one of the 12 samples sequenced with ONT showing the 12 nt deletion () in the reads generated in the sample of interest.

From the western-blot analysis in **Fig. 60** we could see that the signal for TBEV E protein was strongly present in both TBEV WT viruses, however in the mutants, despite being faintly visible, was much less abundant compared to the WT version. The GFP was detectable as well, however we see a GFP signal in the mCherry viruses as well which might be given by some shared structural domains of the two proteins. Plus (+) indicates a positive control (U2OS cells infected with TBEV), while minus (–) is the negative control.

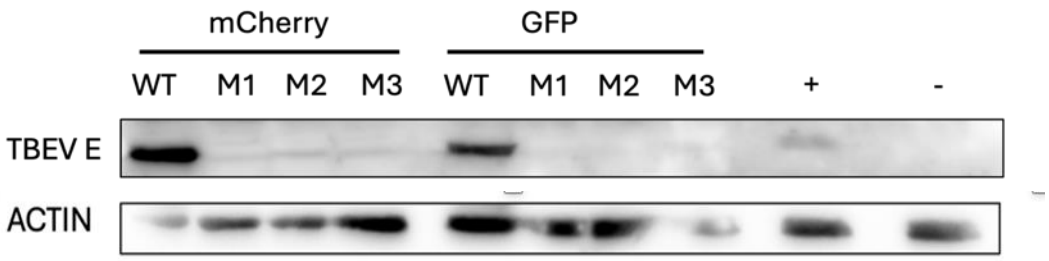

Figure 60 Western blot showing TBEV E protein signal upon infection with WT and mutant viruses

BHK21 cells were lysed and collected in LB directly after viruses were collected post-transfection. Proteins were run on a 12% SDS PAGE, then transferred on a nitrocellulose membrane and incubated with the primary antibodies for 1h at RT or over-night at 4 degrees against the proteins of interest, further incubated for 1h at RT with the appropriate secondary antibodies HRP tagged as seen in a). Actin was used as loading control. Millipore or Super-ECL reagent were used for the detection of the proteins.

The plaque assay of the P0 was not successful, no plaques were observed. Viruses were passaged on BHK21 cells for other 5 days. Again, the viruses needed to be sequenced, and this

time we got an overgrowth of the WT virus in the turbo-GFP M3 virus, as well as in the mCherry M2 and M3 viruses. Because of this we decided to continue the experiments only with the turbo-GFP viruses WT, M1 and M2. By focus forming assay we managed to quantify the viral titres (**Table 3**) of the three viruses that we manage to produce.

	FFU/mL (P1)
WT	1.85*10^3
M1	2.05*10^2
M2	2.15*10^2

Table 3 Viral titres of TBEV WT and mutants

Viral titers of passage1 viruses are shown. Focus forming assay was performed and the FFU/mL of WT, M1 and M2 viruses is represented in the table.

We immediately noticed that the WT virus grew better compared to the two mutants. This allowed us to speculate that the mutants were less virulent compared to the wild-type virus, in line with what we previously observed that the mutants allowed for a better cell-stress response given by a higher percentage of cells permissive for stress granules formation.

I decided to do a pivotal experiment by infecting U2OS cells for immunofluorescence staining of stress granules. The cells were infected with an extremely low MOI of 0.001 having obtained a P1 with a very low viral titre (**Table 3**). To allow the little amount of virus to properly infect the cell population and induce a stress response infection was carried for 96h, a longer time compared to all experiments performed so far to study the stress response in infection. The results will be shown and discussed in the next paragraph.

TBEV mutants M1 and M2 induce more stress-granules formation and decrease of viral E antigen

Once obtained stocks of mutated viruses an infection experiment was performed to address the formation of stress. We observed that upon infection with the mutant viruses the amount of stress granules doubles approximately compared to infection with the WT virus (**Fig. 61**). We observed that M1 was able to rescue the phosphorylation of PKR and eIF2a, while M2 did not (**Fig. 62**). This is puzzling because M2 was able to strongly induce SGs. This experiment needs to be repeated to confirm our observations.

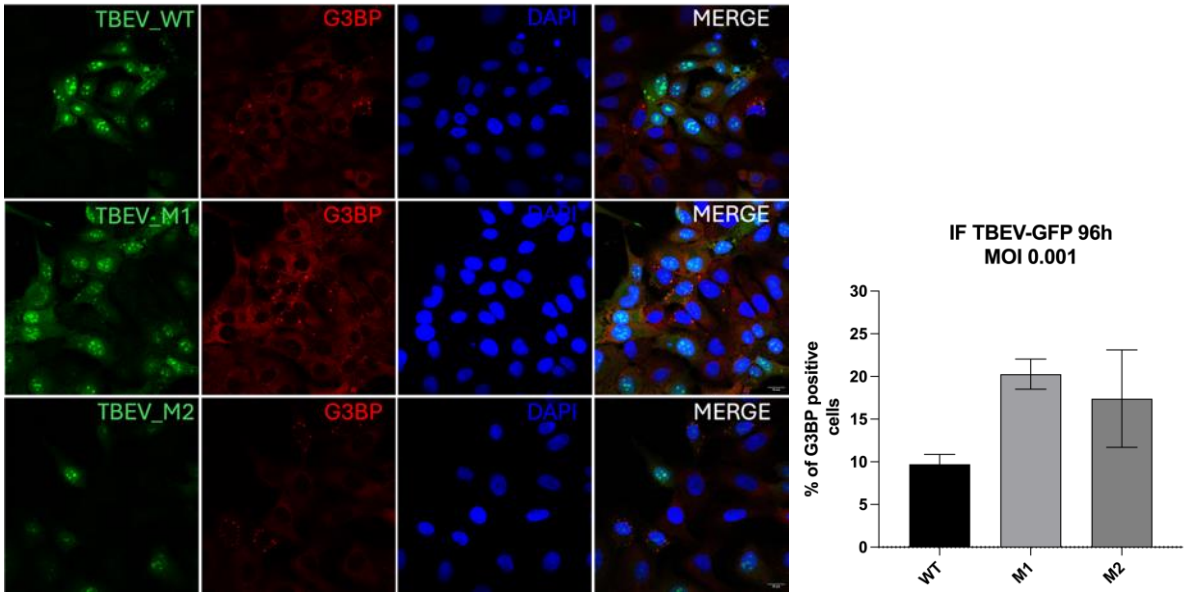

Figure 61 TBEV M1 and M2 induce more SGs

U2OS cells were plated on coverslips, infected with t-GFP viruses for 96h at an MOI 0.001. Cells were fixed with PFA 3.7%, permeabilized with Triton 0.1% and stained with the antibodies of interest: an anti-TBEV E protein to detect infected cells, followed by an incubation with a secondary tagged with a 549nm fluorophore. Nuclei were stained with TO-PRO3. Acquisition was done at the Zeiss Airyscan 880 with a 63X magnification. 20nm scalebar is set. b) % of GFP positive cells and % of E protein positive cells were counted from the same images. Experiment was performed in a single biological replicate.

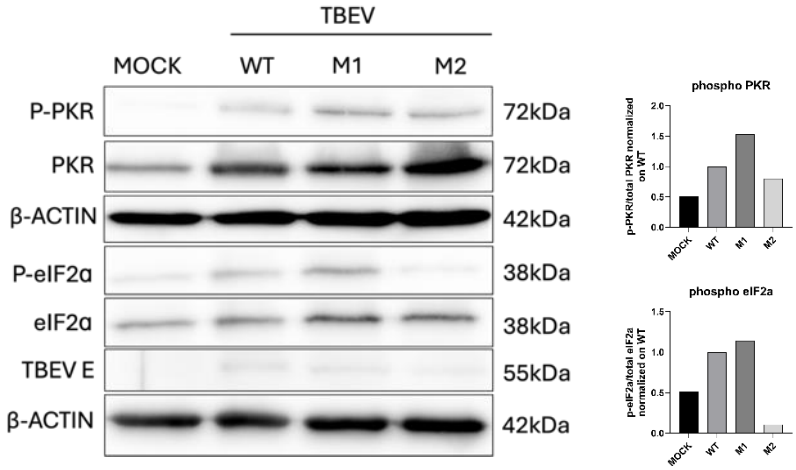

Figure 62 Western blot analysis of TBEV WT, M1 and M2 induced PKR and eIF2a activation

U2OS_WT cells were infected with TBEV mutants for 96h. Proteins were collected in RIPA buffer for western-blot analysis. Proteins were run on a 12% SDS-page gel, then transferred on a nitrocellulose membrane and incubated with the primary antibodies for 1h at RT or over-night at 4 degrees against the protein of interest, further incubated for 1h at RT with the appropriate secondary antibodies HRP tagged as seen in a). Actin was used as loading control. Millipore or Super-ECL reagent were used for the detection of the proteins. In b) the quantification of the blot is shown displayed as the ratio between the intensity of the phosphorylated protein and its total.

Then we looked at the level of replication. Staining of TBEV E protein showed a marked decrease for both mutants compared to WT (**Fig. 63**). However, GFP signal showed the opposite. This could be explained by differential turnover of GFP protein compared to E during the 96 hours of the infection. Finally, we measured the level of infectious virus and viral RNA and observed no major differences (**Fig. 64**). Although the reverse-genetics system could provide very useful information, still we could not complete a set of replicates to confirm our hypothesis.

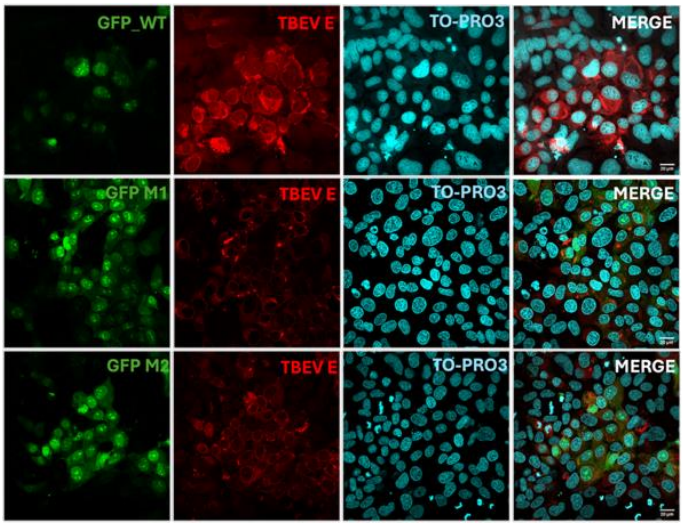

Figure 63 Comparison of t-GFP and TBEV E protein staining

U2OS cells were plated on coverslips, infected with t-GFP viruses for 96h at an MOI 0.001. Cells were fixed with PFA 3.7%, permeabilized with Triton 0.1% and stained with the antibodies of interest: an anti-TBEV E protein to detect infected cells, followed by an incubation with a secondary tagged with a 549nm fluorophore. Nuclei were stained with TO-PRO3. Acquisition was done at the Zeiss Airyscan 880 with a 63X magnification. 20nm scalebar is set. b) % of GFP positive cells and % of E protein positive cells were counted from the same images. Experiment was performed in a single biological replicate.

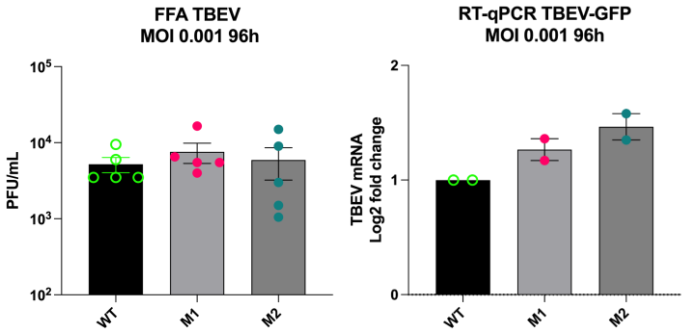

Figure 64 TBEV WT, M1 and M2 replicate equally

U2OS cells were plated, infected with t-GFP viruses for 96h at an MOI 0.001. a) Supernatant was collected for FFA and FFA/mL data are shown. b) cells were lyzed in Trizol, RNA was extracted, retrotranscribed to cDNA and used for RT-qPCR analysis. Experiment was performed in 3 biologically independent replicates.

DISCUSSION

Part 1 – TBEV NS2B is recognized by IKKε to induce ISGs

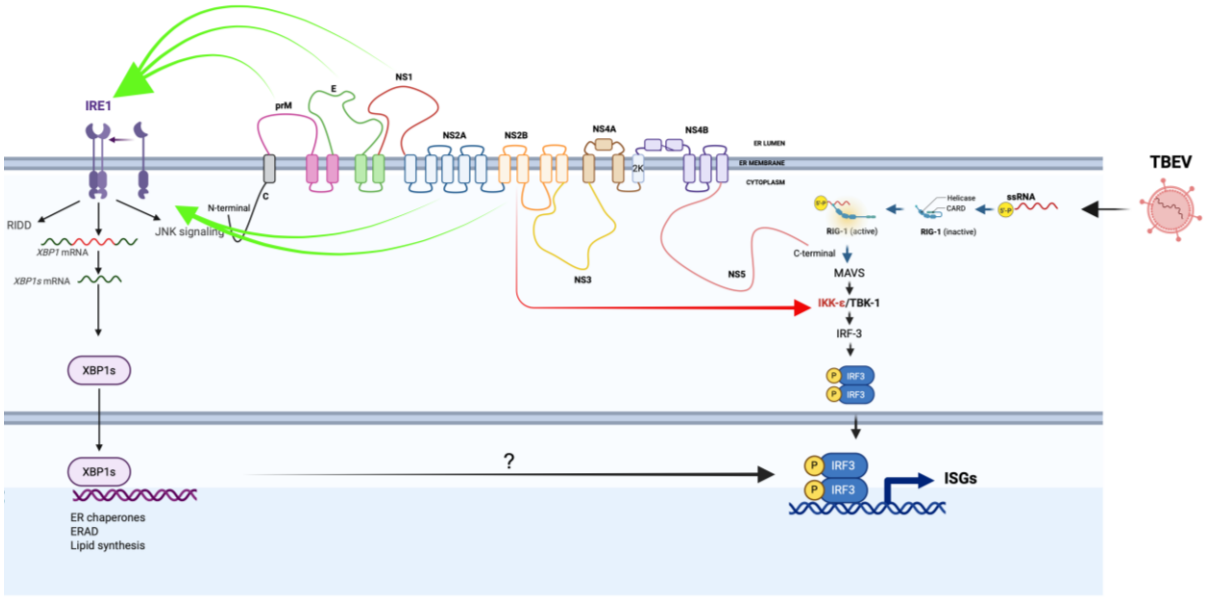

Figure 65 Graphical abstract illustrating our working hypothesis for NS2B mechanism in the innate immunity

TBEV, like the rest of the viruses belonging to the same family, is known to induce strong rearrangements of the endoplasmic reticulum by forming invaginations in which the virus replicates, as demonstrated by our laboratory in 2013 (Miorin et al., 2013). Those invaginations are not only the site where the virus replicates but are also a mean through which the virus is believed to escape the recognition by the antiviral cellular sensors (Mackenzie, 2005). In line with the hypothesis that TBEV hides replication intermediates in ER vesicles to escape cellular pattern recognition receptors (PRRs), the activation of the antiviral response has been shown to be delayed (Överby and Weber, 2011). For TBEV this was demonstrated by *Overby et al., 2010*, showing that upon TBEV infection the IFNβ induction is delayed, meaning that IFNβ is detected in cellular supernatant of TBEV positive cells only 24h after infection, giving the virus a replication advantage (Överby et al., 2010). They link this event to the sequestration of viral dsRNA in the vesicle packets (VPs) at the level of the endoplasmic reticulum, since the screen of all TBEV proteins didn't point out any viral protein acting as a direct inhibitor of the IFNβ induction. Next, from our laboratory, *Miorin et al., 2012* and *Miorin et al., 2013* demonstrated that, despite being delayed, the activation of IFNs upon TBEV infection relies on the activation of RIG-I, not MDA5, both known to be PRRs activated by viral RNAs. In addition, they showed that the induction of IFNβ by TBEV relies on the activation of the IRF3 protein (Miorin et al., 2013, 2012).

Since TBEV, like the rest of the *Orthoflaviviruses*, replicates at the level of the endoplasmic reticulum, an activation of the Unfolded Protein Response is to be expected. Indeed, several articles were published describing the virus-induced activation of the UPR, counting mainly on the IRE1 branch. This is true for Japanese encephalitis virus and dengue virus (Yu et al., 2006) as well as for West Nile virus (Medigeshi et al., 2007), and for Zika virus where IRE1 induced UPR activation is observed both *in vitro* and *in vivo* in neuronal cells (Tan et al., 2018). Interestingly, *Yu et al., 2013* showed an IRE1 dependent UPR activation upon TBEV infection, in line with our observations. However, they noticed that upon pharmacological inhibition of IRE1 by the usage of 3,5-Dibromosalicylaldehyde before viral infection, TBEV replication was impaired (Yu et al., 2013). Breitkopf and colleagues published in 2021 an article in which they also observed a strong IRE1 activation upon infection with three different Tick-borne flaviviruses: Neudoerfl, TBEV HB171 and LGTV, with Neudoerfl being the mostly neuroinvasive strain. They noticed that Neudoerfl was the one which best induced the IRE1 branch in several CNS-derived cell-lines giving more evidence about the importance of UPR in TBFV neuronal infection (Breitkopf et al., 2021). In addition, they observed that inhibition of IRE1 by blocking its kinase activity via KIRA6, endonuclease activity via STF083010 or both via GSK2850163 prior to viral infection reduced viral replication thus suggesting IRE1 has an important role in ensuring proper viral replication in CNS cells.

Carletti and Zakaria and colleagues from our laboratory published another paper in 2019 in which the importance of the UPR upon TBEV infection was further studied (Carletti et al., 2019). Briefly, a transcriptome analysis of TBEV infected cells indicated that early in infection there is an upregulation of UPR-related genes. Next, another RNAseq experiment in which cells were treated with tunicamycin (TM), a known activator of the UPR, prior TBEV infection, indicated that in the context of an active UPR the induction of ISGs occurs earlier in infection (8h.p.i.) given by the IRF3 nuclear translocation thus leading to an inhibition of viral replication. These observations were then linked to the IRE1 branch of UPR since its depletion allowed for a higher viral replication. In addition to this, depletion of IRF3 and RIG-I in the context of UPR priming prior TBEV infection allowed for a better viral replication as well. This confirmed once again the importance of IRF3 in the activation of the antiviral response upon TBEV infection and additionally proposed a link between UPR activation and the antiviral response. To sum up, *Carletti et al., 2019* propose that the UPR primes the IRF3/IFN pathway via IRE1 and that the RIG-I mediated PRR signalling given by the recognition of viral RNA synergizes with the UPR to mount a full antiviral response.

Starting from these observations, we wanted to dig more in the mechanistical part of those events: which was the viral component inducing UPR? How can UPR and RIG-I activation be linked? Are there other cellular components involved in the activation of the antiviral response? Those and other questions were at the basis of the work carried out in the past years.

Firstly, we identified 4 TBEV proteins capable of robust induction of XBP1 splicing when overexpressed alone: E, NS1, NS2A and NS2B (**Fig. 12**). Glycoproteins such as E and NS1 were somehow predicted to overload the ER and trigger the UPR, while NS2A and NS2B were totally unexpected. We can speculate that this activity may be related to their ability in inducing major rearrangements of the ER during infection. However, little is known on the mechanisms of membrane rearrangements of the ER and their relationship with the UPR, with only few publications in yeast (Ho et al., 2020; Promlek et al., 2011). We proceeded with further validation of the effect of the viral proteins on the expression levels of UPR-related genes, which were previously found to be upregulated upon TBEV infection (Carletti et al., 2019). The genes taken in consideration were EDEM, GADD34, DNAJC3, CHOP/DDIT3 and BiP, selected to describe the activation of each of the 3 branches of the UPR: EDEM and DNAJC3 are downstream of IRE1, CHOP and GADD34 are downstream of PERK and BiP is linked to both ATF6 and IRE1. We observed that, to some extent, each of the viral protein was inducing an up-regulation of the genes of interest (**Fig. 13**) indicating an activation of all UPR branches.

Next, we wanted to understand whether the UPR activation was IRE1a-dependent. We established an U2OS cell-line knocked-out for IRE1a and screened again for the induction of DNAJC3 (IRE1), BiP (ATF6; IRE1) and CHOP (PERK). Interestingly, in this case we observed that while the other viral proteins lost the capability of inducing UPR, NS2B still induced an upregulation of the targeted UPR-related genes (**Fig. 15**). Always in line with what described by *Carletti and Zakaria et al., 2019* in which a link between UPR activation and ISGs upregulation was observed (Carletti et al., 2019), we then wondered whether the TBEV viral proteins which induced UPR were also capable of activating the interferon response. We noticed that NS2B, and for some ISGs NS2A as well, managed to significantly up-regulate the tested ISGs (**Fig. 14**). Interestingly, we also observed that in the U2OS-IRE_KO cell-line, NS2B still managed to induce a higher expression of the tested ISGs compared to the control (**Fig. 16**). In addition to this, we observed that the activation of ISGs by NS2B is not related to the activation of UPR, at least not the IRE1 branch. This opened a new idea that NS2B might be recognized by a cellular component to induce the activation of the antiviral response. Indeed, we observed that priming cells with the viral proteins we previously selected reduce TBEV replication, with NS2B being the strongest inhibitor both at 8 h.p.i. (**Fig. 17A**) and 24 h.p.i.

(**Fig 17B**). We also observed that, while all the others lost their ability to reduce viral replication in the IRE1-KO cells, NS2B was still able to significantly reduce viral replication at 8 h.p.i. (**Fig. 17C**), an effect that was lost at the 24 h.p.i. (**Fig. 17D**). Those data might indicate that TBEV NS2B may induce UPR in an IRE1 independent manner. Therefore, while we confirmed that viral proteins such as E, NS1 and NS2A recapitulate UPR induction by TBEV infection observed previously, we also found a novel mechanism specific for NS2B.

Interestingly *Yu et al., 2006* observed in their DENV-2 screening that prM, E, NS1, NS2A, NS2B mostly induced XBP1 activation, and, of note, they added to their screening also the active protease NS2B3, which was, in their hand, the best activator of XBP1 (Yu et al., 2006). They additionally inserted mutations in the active NS2B3 protease to get a protease dead NS2B3 referred as S135A, as well as a helicase/NDPase dead NS2B3 referred as K199A. They observed that even the mutated versions of the proteins were still capable to induce XBP1 splicing. However, the same was not true for JEV's NS2B3 construct which did not induce XBP1 activation. Unluckily, at the time of our screening we couldn't include NS2B3 protease but we observed a significant induction of the pathway given by NS2B protein, and, since *Yu et al., 2006*, discuss that the induction observed by NS2B3 is not dependent on its enzymatic activity, we hypothesize that the whole NS2B3 is giving more stability to the protein resulting in a stronger induction, but the domain responsible for the activation of UPR is the luminal endoplasmic region of NS2B. We observed that the expression of the active NS2B3 protease induces a much higher expression level of ISGs, in some cases even higher than our positive control (PolyI:C treated cells). This aspect is very interesting and needs to be further explored, for the moment we can hypothesize that the NS2B3 complex gives to NS2B more stability which is more prone to get recognized by cellular factors, thus inducing ISGs upregulation (**Fig. 28**).

This is to our knowledge the first evidence that the presence of a viral protein alone induces ISGs in sterile conditions (not infected). In fact, nucleic acids are generally known to be the main Pathogen-Associated Molecular Pattern (PAMP) when it comes to viral infections, even though also some structural viral proteins have been described as PAMPs like envelope or capsid protein. On the other hand, in the context of fungal infection carbohydrates are considered main PAMPs, and in bacteria proteins and lipids have also been described. In contrast to what we are observing here, several viral proteins have been shown to antagonize the activation of ISGs by targeting different cellular components. For example, TBEV NS5 has been shown to impair Type I Interferon Signalling by suppressing IFNAR maturation and cell surface expression thus antagonizing the IFN-I JAK-STAT signalling pathway (Best, 2017).

Additionally, NS5 has been shown to inhibit also TYK2 a kinase essential to activate the JAK-STAT pathway resulting again in the inhibition of ISGs induction (Gracias et al., 2023).

Taking all these data together we decided to dig more in the mechanism standing behind the observation that NS2B drives the cell to an antiviral state. Since we know from the work previously published by *Miorin and colleagues* (Miorin et al., 2012) that the RIG-I pathway is the one active during TBEV infection we decided to do a dissection of the pathway with the aim to find a plausible target which recognized NS2B. A Dual luciferase assay was set up, with the Firefly Luciferase encoded under the control of the IFN-β promoter. We observed that NS2B always had a synergistic effect on the activation of the IFN-β promoter when co-expressed with components of the pathway, up to the level of co-transfection with IRF3-5D, when its effect was lost and comparable to that of the EGFP control (**Fig. 18**). Of note that IRF3-5D is the phosphomimetic form of IRF3 in which five serines are replaced by aspartates resulting in the generation of a constitutively active IRF3 (Lin et al., 1998). Together those data indicated that when NS2B is co-overexpressed with the components of the RIG-I pathway there is a synergistic effect observed until the level of IKKε, since already co-transfection with TBK-1 and downstream in the pathway IRF3-5D did not show any additive effect compared to the experimental control EGFP. This data indicates that the observed effect of NS2B on the induction of the IFN-β promoter might be depending on IKKε. Indeed, we dug more in this mechanism and wanted to understand whether NS2B was recognized by our two kinases. Indeed, we found that IKKε pulled down NS2B while TBK-1 did not (**Fig. 20**). In addition to this, immunofluorescence data showed that IKKε and NS2B colocalised more than TBK-1 and NS2B (**Fig. 21**). This reinforces our finding that TBEV NS2B protein is recognized by a cellular component - IKKε - capable of inducing IRF3 activation and further ISGs overexpression. So far IKKε has been described just as a factor responsible for the phosphorylation of IRF3 and IRF7 following activation of PRR pathways such as RIG-I/MDA5, cGAS-STING and TLRs, and has been described to be a target of several viral infections to block the antiviral response. It was never described as a protein directly recognizing a viral molecule to induce an antiviral response.

An interaction between IKKε and NS2B has already been described for DENV (Nie et al., 2023) but in that case the interaction was described as a pro-viral mechanism since the sequestration of several RIG-I components (they see an interaction occurring with MAVS/IPS1 as well) inhibits full activation of the pathway and reduces the transcription of several ISGs. Previously, *Angleró-Rodríguez et al., 2014* showed that in DENV NS2B3 complex, in both its

active and protease-deficient forms, could interact with IKKε (Angleró-Rodríguez et al., 2014). This finding is consistent with the observation that DENV, despite belonging to the same viral family as TBEV, has a different mechanism of action: IRF3 phosphorylation is inhibited at different levels of the pathway and ISGs induction is impaired by the activity of several NS proteins (Angleró-Rodríguez et al., 2014; Ashour et al., 2009; Dalrymple et al., 2015). In contrast during TBEV infection IRF3 phosphorylation is observed, and the immune response is active (Carletti et al., 2019; Miorin et al., 2012; Överby et al., 2010). To better characterize the activation of IRF3 we exploited the cell line U2OS-IRF3_GFP, a reporter system in which the cytoplasmic IRF3_GFP migrates to the nucleus upon activation of the pathway(Maistriau et al., 2017). In both our models (U2OS-IRF3_GFP and U2OS-wt) we observed that expression of NS2B protein could induce an increase in the IRF3 phosphorylation levels as well as its nuclear translocation (**Fig. 22** and **Fig. 24**). In addition to this, we analysed the protein levels of IFIT1, one of the ISGs upregulated by TBEV infection (**Fig. 23** and **Fig. 25**) and observed that in presence of NS2B its protein level is more abundant, in line with the previously observed increase at the mRNA level. This indicates that recognition of NS2B by IKKε, subsequent phosphorylation and nuclear translocation of IRF3 and upregulation of ISGs drives the cells into an antiviral state that creates a hostile environment for TBEV replication (**Fig. 22** to **Fig. 25**). A more detailed analysis demonstrated that levels of virus signal in cells which strongly overexpressed NS2B were much lower compared to the NS2B negative cells (**Fig. 31**), meaning that, a part for having an overall lower viral replication when NS2B is transfected, we show that indeed the cells that have high expression levels of NS2B get infected much less indicating these have an active mechanism ongoing to fight infection. This data agrees with what published by *Yuan et al., 2024*, where they describe a phenomenon of superinfection inhibition occurring on cells previously infected with Japanese encephalitis virus and later infected by Zika virus (Yuan et al., 2024). The authors entered more in the detail of this observation by overexpressing each JEV protein separately, followed by ZIKV infection, and they observed that NS2B presence was the responsible for the reduction of ZIKV replication. They attributed this effect to the cytoplasmic loop of NS2B (aa 46-103) since this construct was sufficient to inhibit ZIKV replication. Next, they validated this observation also by transfecting JEV NS2B and infecting with VSV, a negative-strand RNA virus where they could again see a reduction in viral replication. The same was not observed by co-infecting with PRV, a DNA virus. The authors did not further explore in the mechanism standing behind JEV NS2B inhibition of ZIKV; however, we could hypothesize that JEV NS2B acts in a way like the one

we are describing here for TBEV, i.e. recognized by a cellular factor such as IKKε leading the cells to an antiviral state, in which ZIKV replication is restricted. Interestingly, we observed that transfection of NS2B3 viral protease prior infection results in an even stronger inhibition of viral replication but understanding the reason of this will require further studies (**Fig. 29, right**). For now, we might hypothesize, as previously mentioned, that the NS2B3 complex gives more stability to NS2B resulting in a more efficient recognition by IKKε and induction of ISGs. However, when transfecting the protease deficient S135A NS2B3 prior to infection resulted in a similar inhibition as described for NS2B alone (**Fig. 29A, left** and **Fig. 29B, left**). Most probably, the presence of the full protease prematurely initiates the cleavage of the polyprotein affecting the correct assembly of replication complexes and further virus formation.

In conclusion, we describe here for the first time the role of a TBEV non-structural protein – NS2B as a putative PAMP capable of getting recognized by the cellular kinase IKKε which upon activation causes IRF3 nuclear translocation, induction of ISGs and leads the cells to an antiviral state. IKKε is generally described as a signal transducer active upon detection of PAMPs/DAMPs by PRR such as RIG-I, however, we are here proposing a more prominent role of IKKε which acts directly as a PRR thus recognizing NS2B as a PAMP to further induce a response given by IRF3 activation.

Part 2 TBEV NS4B inhibits virus-induced stress granules formation by blocking PKR activation

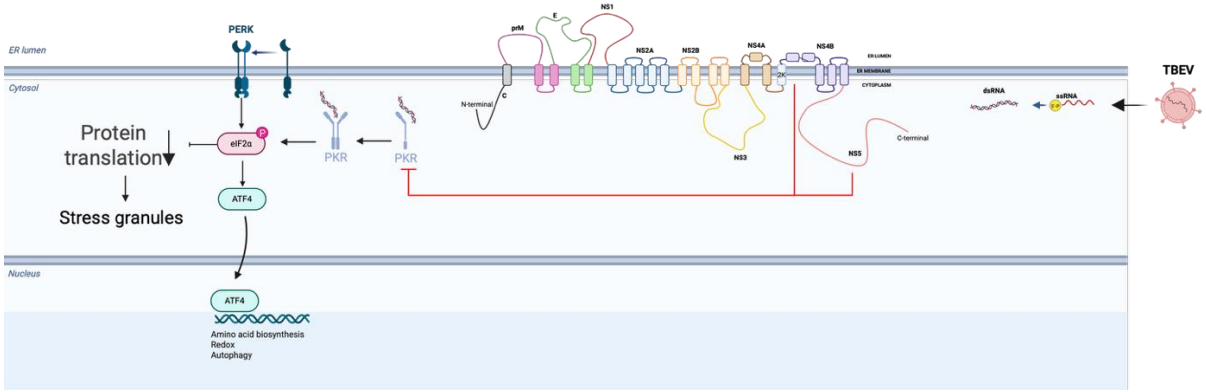

Figure 66 Graphical abstract illustration our working hypothesis of NS4B mechanism in SGs inhibition

Stress granules are membrane-less organelles formed upon sensing of diverse cellular stresses, resulting in the block of translation aiming to restore homeostasis. They are formed following activation of a cellular mechanism defined as Integrated Stress Response (ISR), characterized by four main groups of stress-inducing agents: heat-shock, aminoacid starvation, accumulation of unfolded proteins and viral infection, which activate Heme-Regulated Inhibitor (HRI), general control nonderepressible 2 (GCN2), Protein kinase R-like endoplasmic reticulum kinase (PERK) and protein kinase R (PKR), respectively. Activation of these kinases triggers their phosphorylation, which in turn converges to the phosphorylation of Eukaryotic Translation Initiation Factor 2 Alpha Subunit (eIF2α). eIF2α is one of the components of the eukaryotic initiation factor 2 (eIF2) complex critical for the initiation of protein translation. Indeed, the eIF2 complex formed by the α, β and γ subunits is responsible for the formation of the ternary complex when coupled with GTP and Met-tRNAi. Together, this complex delivers the Met-tRNAi to the small ribosomal subunit leading to the initiation of protein translation. When phosphorylated at serine 51, eIF2α, does not allow the efficient exchange of GDP to GTP resulting in the reduction of global protein translation and SG formation (McCormick and Khaperskyy, 2017). However, some genes, such as ATF4, are preferentially expressed when stress granules are formed and the translation is stalled. This occurs because normally eIF2α blocks ATF4 mRNA translation since it has two uORF (upstream open reading frame) before the mORF (main open reading frame) and in a context of abundance of eIF2-GTP the two uORFs get translated, but not the main one. This changes when eIF2α is phosphorylated since less eIF2-GTP is available, thus the ribosome is not loaded with a new Met-tRNAi to start a new cycle of translation, in the meantime, the ribosome slides on the mRNA and once reached the mORF of ATF4 it has loaded the ribosome with the Met-tRNAi to start translating ATF4

to protein. (Vattem and Wek, 2004). Another gene behaving the same way is GADD34 which is preferentially induced during stress mimicking the mechanism described for ATF4 (Lee et al., 2009).

The effect of Tick-borne encephalitis virus infection on the formation of stress granules has not been deeply investigated so far, even though several Flaviviruses were shown to inhibit or hijack the ISR and block SGs formation (Eiermann et al., 2020). From our laboratory, a work about TBEV and stress granules was published in 2014 in which, in line with what observed by Emara and Brinton 2007 (Emara and Brinton, 2007), who claim that TIAR is recruited by viral RNA thus blocks formation of SGs, the SGs components TIA-1 and TIAR were found to be colocalizing with dsRNA. However, Albornoz and colleagues described that TIA1 and TIAR bind the +RNA genome in the replication organelles. Interestingly, the depletion of TIA1 showed a higher viral replication titre, while the same was not observed by depleting TIAR presumably because TIAR reduction induces an upregulation of TIA1 (Albornoz et al., 2014). Carletti and colleagues from our laboratory demonstrated that TBEV infection led to the recruitment at the level of SGs of components of the innate immunity response, such as RIG-I, to induce a stronger antiviral response when SGs are formed following detection of dsRNA, which can then be exploited to activate RIG-I as well (Carletti et al., 2017). Indeed, this is in line with our observation not shown in the thesis that SGs are visible in TBEV infection starting at 16 h.p.i., same timing in which we previously observed the induction of the innate immune response (Carletti, unpublished observations), meaning the two antiviral mechanisms might be interconnected. We observed that upon TBEV infection, at 24 h.p.i. only less than 10% of cells show stress granules formation (**Fig. 42**) suggesting that also TBEV might be using a mechanism to inhibit the formation of SGs. To better understand this mechanism, we firstly defined that TBEV induced SGs are PKR dependent (**Fig. 44**), which was in line with some previous observations for ZIKV and WNV infections leading to PKR dependent activation of ISR (Courtney et al., 2012; Hou et al., 2017) . At this point we hypothesized that, as previously described for other Flaviviruses (Amorim et al., 2017; Arakawa et al., 2022; Hou et al., 2017; Wu et al., 2024), TBEV might also be exploiting its own proteins to block SGs formation possibly by acting at the PKR level. We went on by screening all TBEV proteins upon treatment with PolyI:C in their capability to induce SGs. We identified NS4B and NS5 as the main actors inhibiting PolyI:C induced SGs by immunofluorescence (**Fig. 45**), with NS4B being the strongest inhibitor of SGs formation. The inhibition was confirmed as well at the protein levels where we could see lower phosphorylation status of PKR when NS4B was present prior to induction of SGs by PolyI:C (**Fig. 45**). We thus decided to firstly study the role

of NS4B, later NS5 will also be addressed. There is a previous study proving that PKR is inhibited as a proviral strategy by directly interacting with JEV NS2A protein (Tu et al., 2012). In addition, there is another article in which JEV and DENV NS4B proteins have been shown to inhibit SGs formation by recruiting the valosin-containing protein- NPL4 complex to induce the disassembly of SGs and allow for an efficient viral replication (Arakawa et al., 2022). A similar strategy might be used by TBEV NS4B as well to block the formation of stress granules. NS4B is predominantly transmembrane, therefore defined as a highly hydrophobic protein (40% hydrophobic residues), as it is expected for a transmembrane protein. Structurally, it is composed by several transmembrane helicases and a long cytoplasmic loop. Functionally, the protein is important for the formation of the replication complex but has also been shown to act as an antagonist of the antiviral signalling, by inhibiting type I IFNs, as well as blocking SGs formation (Wang et al., 2022). Our *In-silico* analysis demonstrated that this cytoplasmic domain fits well in the PKR dimer (**Fig. 46**). The interaction between PKR and NS4B was further proven by an immunoprecipitation assay. We noticed that by pulling down NS4B we were able to detect PKR (**Fig. 54**). These data suggest that NS4B inhibits PKR activation by directly binding the protein. Taking advantage of the *in-silico* analyses we designed 3 NS4B mutants, each containing 4 aa deletions in the cytoplasmic loop as shown in **Fig. 47**. Interestingly, all NS4B mutants partially recovered the capability of PolyI:C to induce SGs (**Fig. 48** and **Fig. 49**). This information tells us that when the C-loop is mutated the inhibition on PKR is decreased, thus allowing for a better activation of eIF2α and more stress granules formation as visible from the images and respective quantification in **Fig. 49** and western-blot analysis **Fig. 50**. We then observed that in cells overexpressing PKR, transfection of NS4B and the respective mutants followed by treatment with PolyI:C induced a higher percentage of SGs positive cells compared to WT cells (**Fig. 51** and **Fig. 52**). This tells us that in a condition where PKR is overexpressed the sensing of PolyI:C is increased, thus the inhibition given by NS4B is reduced, confirming again the fundamental role of PKR in inducing SGs upon PolyI:C treatment and the involvement of NS4B in the inhibition of this process. We wanted to dig more deeply into this mechanism, so we decided to insert the mutations in fully replicative TBEV virus by a reverse-genetic approach (Haviernik et al., 2021). We could observe that, while the WT virus managed to induce less than 10% of cells with SGs, the NS4B mutated versions of TBEV induced more cells with SGs reaching approximately 20% in the M1 virus (**Fig. 61**). Accordingly, levels of phosphorylated PKR were increased in the mutated viruses (**Fig. 62**). However, even though more stress granules were produced with the C-loop mutated

viruses we thus hypothesized a stronger antiviral response would be occurring and virus would replicate less, this was observed only with the E antigen in immunofluorescence (**Fig. 63**), while we did not see any difference at the viral titre level (**Fig. 64, left**), as well as at the viral mRNA levels (**Fig. 64, right**). Before making any conclusion, it is important to complete independent replica to confirm the phenotype.

To summarize, we identified a mechanism used by TBEV to counteract the integrated stress response by inhibiting PKR activation followed by stress granules formation. TBEV NS4B C-loop actively interacts with PKR and inhibits the phosphorylation of eIF2α. Interestingly, we also observed that, upon mutation of the viral C-loop, more stress granules are formed, and more E protein signal is detectable indicating, however an increase in the viral titre and mRNA level was not detectable in this first set of experiment which needs to be repeated to bring final conclusions. A further step could include testing the JNJ-A07 drug, shown to be very efficient against DENV infection targeting the NS4B C-loop, thus disrupting the proper formation of the replication complex, but based on our data could also block NS4B given PKR inhibition, and allow for a better antiviral response by the formation of stress granules.

LIST OF ABBREVIATIONS

+ssRNA – positive single stranded RNA

Aa – aminoacid

ATF4 – Activating Transcription Factor 4

ATF5 – Activating Transcription Factor 5

ATF6 – Activating Transcription Factor 6

BBB – blood brain barrier

BiP – Binding Immunoglobulin Protein

bZIP – basic leucine zipper

C- loop – cytoplasmic loop

Ca^{2+} - Calcium

CARD – Caspase recruitment domain

Cca – approximately

CDC – Center for Disease Control and Prevention

CHOP – C/EBP homologous protein

CNS – central nervous system

CReP – constitutive repressor of eIF2a phosphorylation

CTD – C-terminal domain

DAMP – Damage-Associated Molecular Patterns

DC – dendritic cells

DENV – Dengue virus

DNA – deoxyribonucleic acid

dsRNA – double stranded RNA

eIF2 – Eukaryotic Initiation Factor 2

eIF4F – Eukaryotic initiation factor 4F

ER – Endoplasmic Reticulum

ERAD – Endoplasmic-reticulum-associated protein

GADD34 – Growth Arrest and DNA Damage-Inducible Protein 34

GCN2 - general control nonderepressible 2

GTP – Guanosine Triphosphate

HCV – Hepatitis C virus

HIV-1 – Human Immunodeficiency Virus type 1

HRI – Heme-regulated inhibitor

HSP70 – Heat Shock Protein 70

HSP90 – Heat Shock Protein 90

IFN - Interferon

IgG – Immunoglobulin G

IgM – Immunoglobulin M

IKKε – Inhibitor of nuclear factor kappa-B kinase subunit epsilon

IPS1 – same as MAVS

IRE1α – Inositol-requiring enzyme 1α

IRF3 - Interferon regulatory factor 3

ISGs – Interferon Stimulated Genes

ISR – Integrated stress response

JEV – Japanese Encephalitis Virus

Kb – kilobase

kDa – kilodalton

LGP2 – RIG-I-like receptor LGP2

MAVS - Mitochondrial antiviral-signaling protein

MDA5 – Melanoma differentiation-associated protein 5

mRNA – messenger RNA

NF-kB – Nuclear Factor kappa-light-chain-enhancer of activated B cell

NLR – NOD-like receptor

NPL4 – Nuclear protein localization protein 4

NS1 – Non-structural protein 1

NS2B – Non-structural protein 2B

NS2B3 – Non-structural protein 2/3

NS3 – Non-structural protein 3

NS4B – Non-structural protein 4B

Nt – nucleotide

ORF – Open Reading Frame

PAMP – Pathogen Associated Molecular Patterns

PERK – PKR-like ER kinase

PKR – Protein Kinase R

PolyI:C – Polynosinic:polycytidylic acid

PP1 – Protein Phosphatase 1

RBD – RNA binding domain

RIDD – Regulated IRE1a-dependent decay

RIG- I – Retinoic acid-inducible gene I

RLR – RIG-like receptor

RNA – ribonucleic acid

RNAse – ribonuclease

ROS – Reactive Oxygen Species

S1P – site 1 protease

S2P – site 2 protease

SG – stress granules

TBEV – Tick-borne encephalitis virus

TBEV-FE – TBEV Far Eastern

TBK1 – TANK-binding kinase 1

TIA1 – Tia1 cytotoxic granule-associated rna binding protein

TIAR

TIRF – TIR-domain-containing adapter-inducing interferon-β

TLR3 – Toll-like receptor 3

tRNA – transfer RNA

UPR – Unfolded Protein Response

USUV – Usutu Virus

UV – ultraviolet

VCP – Valosin-containing protein

WNV – West Nile Virus

XBP1 – X-box binding protein 1

ZIKV – Zika virus

PUBLISHED PAPERS

Martinez-Orellana, P., Manzati, M., Pozzi, D., Xiao, Y., Di Clemente, A., Mearelli, M., **Kalebić, C**., Perrera, V., Ferrarini, D., Carletti, T., Falcone, C., Giugliano, M., Marcello, A., 2025. SARS-CoV-2-induced damage to rat cortical neuronal networks ex vivo is mediated by the pro-inflammatory activation of the cGAS-STING pathway. J. Neurovirol. https://doi.org/10.1007/s13365-025-01283-6

BIBLIOGRAPHY

Aguirre, S., Luthra, P., Sanchez-Aparicio, M.T., Maestre, A.M., Patel, J., Lamothe, F., Fredericks, A.C., Tripathi, S., Zhu, T., Pintado-Silva, J., Webb, L.G., Bernal-Rubio, D., Solovyov, A., Greenbaum, B., Simon, V., Basler, C.F., Mulder, L.C.F., García-Sastre, A., Fernandez-Sesma, A., 2017. Dengue virus NS2B protein targets cGAS for degradation and prevents mitochondrial DNA sensing during infection. Nat. Microbiol. 2, 17037. https://doi.org/10.1038/nmicrobiol.2017.37

Albornoz, A., Carletti, T., Corazza, G., Marcello, A., 2014. The Stress Granule Component TIA-1 Binds Tick-Borne Encephalitis Virus RNA and Is Recruited to Perinuclear Sites of Viral Replication To Inhibit Viral Translation. J. Virol. 88, 6611–6622. https://doi.org/10.1128/JVI.03736-13

Alcon-LePoder, S., Drouet, M.-T., Roux, P., Frenkiel, M.-P., Arborio, M., Durand-Schneider, A.-M., Maurice, M., Le Blanc, I., Gruenberg, J., Flamand, M., 2005. The Secreted Form of Dengue Virus Nonstructural Protein NS1 Is Endocytosed by Hepatocytes and Accumulates in Late Endosomes: Implications for Viral Infectivity. J. Virol. 79, 11403–11411. https://doi.org/10.1128/JVI.79.17.11403-11411.2005

Amberg, S.M., Rice, C.M., 1999. Mutagenesis of the NS2B-NS3-Mediated Cleavage Site in the Flavivirus Capsid Protein Demonstrates a Requirement for Coordinated Processing. J. Virol. 73, 8083–8094. https://doi.org/10.1128/JVI.73.10.8083-8094.1999

Amorim, R., Temzi, A., Griffin, B.D., Mouland, A.J., 2017. Zika virus inhibits eIF2α-dependent stress granule assembly. PLoS Negl. Trop. Dis. 11, e0005775. https://doi.org/10.1371/journal.pntd.0005775

Angleró-Rodríguez, Y.I., Pantoja, P., Sariol, C.A., 2014. Dengue Virus Subverts the Interferon Induction Pathway via NS2B/3 Protease-IκB Kinase ε Interaction. Clin. Vaccine Immunol. 21, 29–38. https://doi.org/10.1128/CVI.00500-13

Arakawa, M., Tabata, K., Ishida, K., Kobayashi, M., Arai, A., Ishikawa, T., Suzuki, R., Takeuchi, H., Tripathi, L.P., Mizuguchi, K., Morita, E., 2022. Flavivirus recruits the valosin-containing protein–NPL4 complex to induce stress granule disassembly for efficient viral genome replication. J. Biol. Chem. 298, 101597. https://doi.org/10.1016/j.jbc.2022.101597

Ashour, J., Laurent-Rolle, M., Shi, P.-Y., García-Sastre, A., 2009. NS5 of Dengue Virus Mediates STAT2 Binding and Degradation. J. Virol. 83, 5408–5418. https://doi.org/10.1128/JVI.02188-08

Berankova, M., Leoni, S., Holoubek, J., Haviernik, J., Salat, J., Grandgirard, D., Leib, S.L., Ruzek, D., 2025. Three-dimensional mapping of tick-borne encephalitis virus distribution in the mouse brain using a newly engineered TurboGFP reporter virus. Emerg. Microbes Infect. 14, 2542246. https://doi.org/10.1080/22221751.2025.2542246

Best, S.M., 2017. The Many Faces of the Flavivirus NS5 Protein in Antagonism of Type I Interferon Signaling. J. Virol. 91, e01970-16. https://doi.org/10.1128/JVI.01970-16

Bhatt, S., Gething, P.W., Brady, O.J., Messina, J.P., Farlow, A.W., Moyes, C.L., Drake, J.M., Brownstein, J.S., Hoen, A.G., Sankoh, O., Myers, M.F., George, D.B., Jaenisch, T., Wint, G.R.W., Simmons, C.P., Scott, T.W., Farrar, J.J., Hay, S.I., 2013. The global distribution and burden of dengue. Nature 496, 504–507. https://doi.org/10.1038/nature12060

Bhattacharyya, S., 2014. Canâ€™t RIDD off viruses. Front. Microbiol. 5. https://doi.org/10.3389/fmicb.2014.00292

Biswal, M., Yao, W., Lu, J., Chen, J., Morrison, J., Hai, R., Song, J., 2024. A conformational selection mechanism of flavivirus NS5 for species-specific STAT2 inhibition. Commun. Biol. 7, 76. https://doi.org/10.1038/s42003-024-05768-8

Blom, K., Cuapio, A., Sandberg, J.T., Varnaite, R., Michaëlsson, J., Björkström, N.K., Sandberg, J.K., Klingström, J., Lindquist, L., Gredmark Russ, S., Ljunggren, H.-G., 2018. Cell-Mediated Immune Responses and Immunopathogenesis of Human Tick-Borne Encephalitis Virus-Infection. Front. Immunol. 9, 2174. https://doi.org/10.3389/fimmu.2018.02174

Bollati, M., Alvarez, K., Assenberg, R., Baronti, C., Canard, B., Cook, S., Coutard, B., Decroly, E., De Lamballerie, X., Gould, E.A., Grard, G., Grimes, J.M., Hilgenfeld, R., Jansson, A.M., Malet, H., Mancini, E.J., Mastrangelo, E., Mattevi, A., Milani, M., Moureau, G., Neyts, J., Owens, R.J., Ren, J., Selisko, B., Speroni, S., Steuber, H., Stuart, D.I., Unge, T., Bolognesi, M., 2010. Structure and functionality in flavivirus NS-proteins: Perspectives for drug design. Antiviral Res. 87, 125–148. https://doi.org/10.1016/j.antiviral.2009.11.009

Bonenfant, G., Williams, N., Netzband, R., Schwarz, M.C., Evans, M.J., Pager, C.T., 2019. Zika Virus Subverts Stress Granules To Promote and Restrict Viral Gene Expression. J. Virol. 93, e00520-19. https://doi.org/10.1128/JVI.00520-19

Branda, F., Nakase, T., Maruotti, A., Scarpa, F., Ciccozzi, A., Romano, C., Peletto, S., De Filippis, A.M.B., Alcantara, L.C.J., Marcello, A., Ciccozzi, M., Lourenço, J.,

Giovanetti, M., 2024. Dengue virus transmission in Italy: historical trends up to 2023 and a data repository into the future. Sci. Data 11, 1325. https://doi.org/10.1038/s41597-024-04162-7

Breitkopf, V.J.M., Dobler, G., Claus, P., Naim, H.Y., Steffen, I., 2021. IRE1-Mediated Unfolded Protein Response Promotes the Replication of Tick-Borne Flaviviruses in a Virus and Cell-Type Dependent Manner. Viruses 13, 2164. https://doi.org/10.3390/v13112164

Bressanelli, S., Stiasny, K., Allison, S.L., Stura, E.A., Duquerroy, S., Lescar, J., Heinz, F.X., Rey, F.A., 2004. Structure of a flavivirus envelope glycoprotein in its low-pH-induced membrane fusion conformation. EMBO J. 23, 728–738. https://doi.org/10.1038/sj.emboj.7600064

Caracciolo, I., Bassetti, M., Paladini, G., Luzzati, R., Santon, D., Merelli, M., Sabbata, G.D., Carletti, T., Marcello, A., D'Agaro, P., 2015. Persistent viremia and urine shedding of tick-borne encephalitis virus in an infected immunosuppressed patient from a new epidemic cluster in North-Eastern Italy. J. Clin. Virol. 69, 48–51. https://doi.org/10.1016/j.jcv.2015.05.019

Caracciolo, I., Mora-Cardenas, E., Aloise, C., Carletti, T., Segat, L., Burali, M.S., Chiarvesio, A., Totis, V., Avšič–Županc, T., Mastrangelo, E., Manfroni, G., D'Agaro, P., Marcello, A., 2020. Comprehensive response to Usutu virus following first isolation in blood donors in the Friuli Venezia Giulia region of Italy: Development of recombinant NS1-based serology and sensitivity to antiviral drugs. PLoS Negl. Trop. Dis. 14, e0008156. https://doi.org/10.1371/journal.pntd.0008156

Carletti, T., Zakaria, M.K., Faoro, V., Reale, L., Kazungu, Y., Licastro, D., Marcello, A., 2019. Viral priming of cell intrinsic innate antiviral signaling by the unfolded protein response. Nat. Commun. 10, 3889. https://doi.org/10.1038/s41467-019-11663-2

Carletti, T., Zakaria, M.K., Marcello, A., 2017. The host cell response to tick-borne encephalitis virus. Biochem. Biophys. Res. Commun. 492, 533–540. https://doi.org/10.1016/j.bbrc.2017.02.006

Chambers, T.J., Grakoui, A., Rice, C.M., 1991. Processing of the yellow fever virus nonstructural polyprotein: a catalytically active NS3 proteinase domain and NS2B are required for cleavages at dibasic sites. J. Virol. 65, 6042–6050. https://doi.org/10.1128/jvi.65.11.6042-6050.1991

Chambers, T.J., Weir, R.C., Grakoui, A., McCourt, D.W., Bazan, J.F., Fletterick, R.J., Rice, C.M., 1990. Evidence that the N-terminal domain of nonstructural protein NS3 from

yellow fever virus is a serine protease responsible for site-specific cleavages in the viral polyprotein. Proc. Natl. Acad. Sci. 87, 8898–8902. https://doi.org/10.1073/pnas.87.22.8898

Chazal, M., Beauclair, G., Gracias, S., Najburg, V., Simon-Lorière, E., Tangy, F., Komarova, A.V., Jouvenet, N., 2018. RIG-I Recognizes the 5′ Region of Dengue and Zika Virus Genomes. Cell Rep. 24, 320–328. https://doi.org/10.1016/j.celrep.2018.06.047

Chen, J.-J., 2007. Regulation of protein synthesis by the heme-regulated eIF2α kinase: relevance to anemias. Blood 109, 2693–2699. https://doi.org/10.1182/blood-2006-08-041830

Chen, X., Shi, C., He, M., Xiong, S., Xia, X., 2023. Endoplasmic reticulum stress: molecular mechanism and therapeutic targets. Signal Transduct. Target. Ther. 8, 352. https://doi.org/10.1038/s41392-023-01570-w

Chuansumrit, A., Chaiyaratana, W., Tangnararatchakit, K., Yoksan, S., Flamand, M., Sakuntabhai, A., 2011. Dengue nonstructural protein 1 antigen in the urine as a rapid and convenient diagnostic test during the febrile stage in patients with dengue infection. Diagn. Microbiol. Infect. Dis. 71, 467–469. https://doi.org/10.1016/j.diagmicrobio.2011.08.020

Constant, D.A., Mateo, R., Nagamine, C.M., Kirkegaard, K., 2018. Targeting intramolecular proteinase NS2B/3 cleavages for *trans* -dominant inhibition of dengue virus. Proc. Natl. Acad. Sci. 115, 10136–10141. https://doi.org/10.1073/pnas.1805195115

Courtney, S.C., Scherbik, S.V., Stockman, B.M., Brinton, M.A., 2012. West Nile Virus Infections Suppress Early Viral RNA Synthesis and Avoid Inducing the Cell Stress Granule Response. J. Virol. 86, 3647–3657. https://doi.org/10.1128/JVI.06549-11

Dalrymple, N.A., Cimica, V., Mackow, E.R., 2015. Dengue Virus NS Proteins Inhibit RIG-I/MAVS Signaling by Blocking TBK1/IRF3 Phosphorylation: Dengue Virus Serotype 1 NS4A Is a Unique Interferon-Regulating Virulence Determinant. mBio 6, e00553-15. https://doi.org/10.1128/mBio.00553-15

De Vries, L., Harding, A.T., 2023. Mechanisms of Neuroinvasion and Neuropathogenesis by Pathologic Flaviviruses. Viruses 15, 261. https://doi.org/10.3390/v15020261

Del Pino, J., Jiménez, J.L., Ventoso, I., Castelló, A., Muñoz-Fernández, Ma.Á., De Haro, C., Berlanga, J.J., 2012. GCN2 Has Inhibitory Effect on Human Immunodeficiency Virus-1 Protein Synthesis and Is Cleaved upon Viral Infection. PLoS ONE 7, e47272. https://doi.org/10.1371/journal.pone.0047272

Dong, J., Qiu, H., Garcia-Barrio, M., Anderson, J., Hinnebusch, A.G., 2000. Uncharged tRNA Activates GCN2 by Displacing the Protein Kinase Moiety from a Bipartite tRNA-Binding Domain. Mol. Cell 6, 269–279. https://doi.org/10.1016/S1097-2765(00)00028-9

Eiermann, N., Haneke, K., Sun, Z., Stoecklin, G., Ruggieri, A., 2020. Dance with the Devil: Stress Granules and Signaling in Antiviral Responses. Viruses 12, 984. https://doi.org/10.3390/v12090984

Emara, M.M., Brinton, M.A., 2007. Interaction of TIA-1/TIAR with West Nile and dengue virus products in infected cells interferes with stress granule formation and processing body assembly. Proc. Natl. Acad. Sci. 104, 9041–9046. https://doi.org/10.1073/pnas.0703348104

Feng, Z., Luo, N., Liu, Y., Hu, J., Ma, T., Yao, Y., 2021. ER stress and its PERK branch enhance TCR-induced activation in regulatory T cells. Biochem. Biophys. Res. Commun. 563, 8–14. https://doi.org/10.1016/j.bbrc.2021.05.061

Franchi, L., Warner, N., Viani, K., Nuñez, G., 2009. Function of Nod-like receptors in microbial recognition and host defense. Immunol. Rev. 227, 106–128. https://doi.org/10.1111/j.1600-065X.2008.00734.x

Gao, Z., Zhang, X., Zhang, L., Wu, S., Ma, J., Wang, F., Zhou, Y., Dai, X., Bullitt, E., Du, Y., Guo, J.-T., Chang, J., 2022. A yellow fever virus NS4B inhibitor not only suppresses viral replication, but also enhances the virus activation of RIG-I-like receptor-mediated innate immune response. PLOS Pathog. 18, e1010271. https://doi.org/10.1371/journal.ppat.1010271

Gilks, N., Kedersha, N., Ayodele, M., Shen, L., Stoecklin, G., Dember, L.M., Anderson, P., 2004. Stress Granule Assembly Is Mediated by Prion-like Aggregation of TIA-1□D. Mol. Biol. Cell 15.

Gracias, S., Chazal, M., Decombe, A., Unterfinger, Y., Sogues, A., Pruvost, L., Robert, V., Lacour, S.A., Lemasson, M., Sourisseau, M., Li, Z., Richardson, J., Pellegrini, S., Decroly, E., Caval, V., Jouvenet, N., 2023. Tick-borne flavivirus NS5 antagonizes interferon signaling by inhibiting the catalytic activity of TYK2. EMBO Rep. 24, e57424. https://doi.org/10.15252/embr.202357424

Harding, H.P., Novoa, I., Zhang, Y., Zeng, H., Wek, R., Schapira, M., Ron, D., 2000a. Regulated Translation Initiation Controls Stress-Induced Gene Expression in Mammalian Cells. Mol. Cell 6, 1099–1108. https://doi.org/10.1016/S1097-2765(00)00108-8

Harding, H.P., Zhang, Y., Bertolotti, A., Zeng, H., Ron, D., 2000b. Perk Is Essential for Translational Regulation and Cell Survival during the Unfolded Protein Response. Mol. Cell 5, 897–904. https://doi.org/10.1016/S1097-2765(00)80330-5

Harding, H.P., Zhang, Y., Ron, D., 1999. Protein translation and folding are coupled by an endoplasmic-reticulum- resident kinase 397.

Haviernik, J., Eyer, L., Yoshii, K., Kobayashi, S., Cerny, J., Nougairède, A., Driouich, J.-S., Volf, J., Palus, M., De Lamballerie, X., Gould, E.A., Ruzek, D., 2021. Development and characterization of recombinant tick-borne encephalitis virus expressing mCherry reporter protein: A new tool for high-throughput screening of antiviral compounds, and neutralizing antibody assays. Antiviral Res. 185, 104968. https://doi.org/10.1016/j.antiviral.2020.104968

Hetz, C., 2012. The unfolded protein response: controlling cell fate decisions under ER stress and beyond. Nat. Rev. Mol. Cell Biol. 13, 89–102. https://doi.org/10.1038/nrm3270

Hillary, R.F., FitzGerald, U., 2018. A lifetime of stress: ATF6 in development and homeostasis. J. Biomed. Sci. 25, 48. https://doi.org/10.1186/s12929-018-0453-1

Ho, N., Yap, W.S., Xu, J., Wu, H., Koh, J.H., Goh, W.W.B., George, B., Chong, S.C., Taubert, S., Thibault, G., 2020. Stress sensor Ire1 deploys a divergent transcriptional program in response to lipid bilayer stress. J. Cell Biol. 219, e201909165. https://doi.org/10.1083/jcb.201909165

Hou, S., Kumar, A., Xu, Z., Airo, A.M., Stryapunina, I., Wong, C.P., Branton, W., Tchesnokov, E., Götte, M., Power, C., Hobman, T.C., 2017. Zika Virus Hijacks Stress Granule Proteins and Modulates the Host Stress Response. J. Virol. 91, e00474-17. https://doi.org/10.1128/JVI.00474-17

Kato, H., Takeuchi, O., Sato, S., Yoneyama, M., Yamamoto, M., Matsui, K., Uematsu, S., Jung, A., Kawai, T., Ishii, K.J., Yamaguchi, O., Otsu, K., Tsujimura, T., Koh, C.-S., Reis E Sousa, C., Matsuura, Y., Fujita, T., Akira, S., 2006. Differential roles of MDA5 and RIG-I helicases in the recognition of RNA viruses. Nature 441, 101–105. https://doi.org/10.1038/nature04734

Kedersha, N., Panas, M.D., Achorn, C.A., Lyons, S., Tisdale, S., Hickman, T., Thomas, M., Lieberman, J., McInerney, G.M., Ivanov, P., Anderson, P., 2016. G3BP–Caprin1–USP10 complexes mediate stress granule condensation and associate with 40S subunits. J. Cell Biol. 212, e201508028. https://doi.org/10.1083/jcb.201508028

Kedersha, N.L., Gupta, M., Li, W., Miller, I., Anderson, P., 1999. RNA-binding Proteins TIA-1 and TIAR Link the Phosphorylation of eIF-2␣ to the Assembly of Mammalian Stress Granules. J. Cell Biol. 147.

Kesteleyn, B., Bonfanti, J.-F., Bardiot, D., Boeck, B.D., Goethals, O., Kaptein, S.J.F., Stoops, B., Coesemans, E., Muller, P., Doublet, F., Carlens, G., Koukni, M., Smets, W., Raboisson, P., Chaltin, P., Simmen, K., Van, M., Neyts, J., Marchand, A., Jonckers, T.H.M., n.d. Discovery of JNJ-1802, a first-in-class pan-serotype dengue virus NS4B inhibitor.

Kiemel, D., Kroell, A.-S.H., Denolly, S., Haselmann, U., Bonfanti, J.-F., Andres, J.I., Ghosh, B., Geluykens, P., Kaptein, S.J.F., Wilken, L., Scaturro, P., Neyts, J., Van Loock, M., Goethals, O., Bartenschlager, R., 2024. Pan-serotype dengue virus inhibitor JNJ-A07 targets NS4A-2K-NS4B interaction with NS2B/NS3 and blocks replication organelle formation. Nat. Commun. 15, 6080. https://doi.org/10.1038/s41467-024-50437-3

Klaitong, P., Smith, D.R., 2021. Roles of Non-Structural Protein 4A in Flavivirus Infection. Viruses 13, 2077. https://doi.org/10.3390/v13102077

Kofler, R.M., Heinz, F.X., Mandl, C.W., 2002. Capsid Protein C of Tick-Borne Encephalitis Virus Tolerates Large Internal Deletions and Is a Favorable Target for Attenuation of Virulence. J. Virol. 76, 3534–3543. https://doi.org/10.1128/JVI.76.7.3534-3543.2002

Komar, A.A., Merrick, W.C., 2020. A Retrospective on eIF2A—and Not the Alpha Subunit of eIF2. Int. J. Mol. Sci. 21, 2054. https://doi.org/10.3390/ijms21062054

Koyama, S., Ishii, K.J., Coban, C., Akira, S., 2008. Innate immune response to viral infection. Cytokine 43, 336–341. https://doi.org/10.1016/j.cyto.2008.07.009

Kubinski, M., Beicht, J., Gerlach, T., Volz, A., Sutter, G., Rimmelzwaan, G.F., 2020. Tick-Borne Encephalitis Virus: A Quest for Better Vaccines against a Virus on the Rise. Vaccines 8, 451. https://doi.org/10.3390/vaccines8030451

Labuda, M., Kozuch, O., Zuffová, E., Elecková, E., Hails, R.S., Nuttall, P.A., 1997. Tick-Borne Encephalitis Virus Transmission between Ticks Cofeeding on Specific Immune Natural Rodent Hosts. Virology 235, 138–143. https://doi.org/10.1006/viro.1997.8622

Lavoie, H., Li, J.J., Thevakumaran, N., Therrien, M., Sicheri, F., 2014. Dimerization-induced allostery in protein kinase regulation. Trends Biochem. Sci. 39, 475–486. https://doi.org/10.1016/j.tibs.2014.08.004

Lemaire, P.A., Anderson, E., Lary, J., Cole, J.L., 2008. Mechanism of PKR Activation by dsRNA. J. Mol. Biol. 381, 351–360. https://doi.org/10.1016/j.jmb.2008.05.056

Lencer, W.I., DeLuca, H., Grey, M.J., Cho, J.A., 2015. Innate immunity at mucosal surfaces: the IRE1-RIDD-RIG-I pathway. Trends Immunol. 36, 401–409. https://doi.org/10.1016/j.it.2015.05.006

Leung, J.Y., Pijlman, G.P., Kondratieva, N., Hyde, J., Mackenzie, J.M., Khromykh, A.A., 2008. Role of Nonstructural Protein NS2A in Flavivirus Assembly. J. Virol. 82, 4731–4741. https://doi.org/10.1128/JVI.00002-08

Ličková, M., Fumačová Havlíková, S., Sláviková, M., Klempa, B., 2021. Alimentary Infections by Tick-Borne Encephalitis Virus. Viruses 14, 56. https://doi.org/10.3390/v14010056

Lin, R., Heylbroeck, C., Pitha, P.M., Hiscott, J., 1998. Virus-Dependent Phosphorylation of the IRF-3 Transcription Factor Regulates Nuclear Translocation, Transactivation Potential, and Proteasome-Mediated Degradation. Mol. Cell. Biol. 18, 2986–2996. https://doi.org/10.1128/MCB.18.5.2986

Lindqvist, R., Upadhyay, A., Överby, A.K., 2018. Tick-Borne Flaviviruses and the Type I Interferon Response. Viruses 10, 340. https://doi.org/10.3390/v10070340

Lu, L., Han, A.-P., Chen, J.-J., n.d. Translation Initiation Control by Heme-Regulated Eukaryotic Initiation Factor 2 Kinase in Erythroid Cells under Cytoplasmic Stresses.

Mackenzie, J., 2005. Wrapping Things up about Virus RNA Replication. Traffic 6, 967–977. https://doi.org/10.1111/j.1600-0854.2005.00339.x

Maistriau, M., Carletti, T., Zakaria, M.K., Braga, L., Faoro, V., Vasileiadis, V., Marcello, A., 2017. A method for the detection of virus infectivity in single cells and real time: Towards an automated fluorescence neutralization test. Virus Res. 237, 1–6. https://doi.org/10.1016/j.virusres.2017.05.004

Marcelo, A., Koppenol, R., De Almeida, L.P., Matos, C.A., Nóbrega, C., 2021. Stress granules, RNA-binding proteins and polyglutamine diseases: too much aggregation? Cell Death Dis. 12, 592. https://doi.org/10.1038/s41419-021-03873-8

Medigeshi, G.R., Lancaster, A.M., Hirsch, A.J., Briese, T., Lipkin, W.I., DeFilippis, V., Früh, K., Mason, P.W., Nikolich-Zugich, J., Nelson, J.A., 2007. West Nile Virus Infection Activates the Unfolded Protein Response, Leading to CHOP Induction and Apoptosis. J. Virol. 81, 10849–10860. https://doi.org/10.1128/JVI.01151-07

Merrick, W.C., 1992. Mechanism and Regulation of Eukaryotic Protein Synthesis. MICROBIOL REV 56.

Michelitsch, A., Wernike, K., Klaus, C., Dobler, G., Beer, M., 2019. Exploring the Reservoir Hosts of Tick-Borne Encephalitis Virus. Viruses 11, 669. https://doi.org/10.3390/v11070669

Miorin, L., Albornoz, A., Baba, M.M., D'Agaro, P., Marcello, A., 2012. Formation of membrane-defined compartments by tick-borne encephalitis virus contributes to the early delay in interferon signaling. Virus Res. 163, 660–666. https://doi.org/10.1016/j.virusres.2011.11.020

Miorin, L., Romero-Brey, I., Maiuri, P., Hoppe, S., Krijnse-Locker, J., Bartenschlager, R., Marcello, A., 2013. Three-Dimensional Architecture of Tick-Borne Encephalitis Virus Replication Sites and Trafficking of the Replicated RNA. J. Virol. 87, 6469–6481. https://doi.org/10.1128/JVI.03456-12

Misra, J., Carlson, K.R., Spandau, D.F., Wek, R.C., 2024. Multiple mechanisms activate GCN2 eIF2 kinase in response to diverse stress conditions. Nucleic Acids Res. gkae006. https://doi.org/10.1093/nar/gkae006

Moncan, M., Mnich, K., Blomme, A., Almanza, A., Samali, A., Gorman, A.M., 2021. Regulation of lipid metabolism by the unfolded protein response. J. Cell. Mol. Med. 25, 1359–1370. https://doi.org/10.1111/jcmm.16255

Muller, D.A., Young, P.R., 2013. The flavivirus NS1 protein: Molecular and structural biology, immunology, role in pathogenesis and application as a diagnostic biomarker. Antiviral Res. 98, 192–208. https://doi.org/10.1016/j.antiviral.2013.03.008

Nanduri, S., Carpick, B.W., Yang, Y., Williams, B.R.G., Qin, J., n.d. Structure of the double-stranded RNA-binding domain of the protein kinase PKR reveals the molecular basis of its dsRNA-mediated activation.

Nie, Y., Deng, D., Mou, L., Long, Q., Chen, J., Wu, J., 2023. Dengue Virus 2 NS2B Targets MAVS and IKKε to Evade the Antiviral Innate Immune Response. J. Microbiol. Biotechnol. 33, 600–606. https://doi.org/10.4014/jmb.2210.10006

Oikawa, D., Tokuda, M., Hosoda, A., Iwawaki, T., 2010. Identification of a consensus element recognized and cleaved by IRE1α. Nucleic Acids Res. 38, 6265–6273. https://doi.org/10.1093/nar/gkq452

Onomoto, K., Jogi, M., Yoo, J.-S., Narita, R., Morimoto, S., Takemura, A., Sambhara, S., Kawaguchi, A., Osari, S., Nagata, K., Matsumiya, T., Namiki, H., Yoneyama, M., Fujita, T., 2012. Critical Role of an Antiviral Stress Granule Containing RIG-I and PKR in Viral Detection and Innate Immunity. PLoS ONE 7, e43031. https://doi.org/10.1371/journal.pone.0043031

Ortiz, D.I., Piche-Ovares, M., Romero-Vega, L.M., Wagman, J., Troyo, A., 2021. The Impact of Deforestation, Urbanization, and Changing Land Use Patterns on the Ecology of Mosquito and Tick-Borne Diseases in Central America. Insects 13, 20. https://doi.org/10.3390/insects13010020

Överby, A.K., Popov, V.L., Niedrig, M., Weber, F., 2010. Tick-Borne Encephalitis Virus Delays Interferon Induction and Hides Its Double-Stranded RNA in Intracellular Membrane Vesicles. J. Virol. 84, 8470–8483. https://doi.org/10.1128/JVI.00176-10

Överby, A.K., Weber, F., 2011. Hiding from intracellular pattern recognition receptors, a passive strategy of flavivirus immune evasion. Virulence 2, 238–240. https://doi.org/10.4161/viru.2.3.16162

Pakos-Zebrucka, K., Koryga, I., Mnich, K., Ljujic, M., Samali, A., Gorman, A.M., 2016. The integrated stress response. EMBO Rep. 17, 1374–1395. https://doi.org/10.15252/embr.201642195

Pierson, T.C., Diamond, M.S., 2020. The continued threat of emerging flaviviruses. Nat. Microbiol. 5, 796–812. https://doi.org/10.1038/s41564-020-0714-0

Postler, T.S., Beer, M., Blitvich, B.J., Bukh, J., De Lamballerie, X., Drexler, J.F., Imrie, A., Kapoor, A., Karganova, G.G., Lemey, P., Lohmann, V., Simmonds, P., Smith, D.B., Stapleton, J.T., Kuhn, J.H., 2023. Renaming of the genus Flavivirus to Orthoflavivirus and extension of binomial species names within the family Flaviviridae. Arch. Virol. 168, 224, s00705-023-05835–1. https://doi.org/10.1007/s00705-023-05835-1

Prasad, V., Greber, U.F., 2021. The endoplasmic reticulum unfolded protein response – homeostasis, cell death and evolution in virus infections. FEMS Microbiol. Rev. 45, fuab016. https://doi.org/10.1093/femsre/fuab016

Promlek, T., Ishiwata-Kimata, Y., Shido, M., Sakuramoto, M., Kohno, K., Kimata, Y., 2011. Membrane aberrancy and unfolded proteins activate the endoplasmic reticulum stress sensor Ire1 in different ways. Mol. Biol. Cell 22, 3520–3532. https://doi.org/10.1091/mbc.e11-04-0295

Pulkkinen, L.I.A., Barrass, S.V., Domanska, A., Överby, A.K., Anastasina, M., Butcher, S.J., 2022. Molecular Organisation of Tick-Borne Encephalitis Virus. Viruses 14, 792. https://doi.org/10.3390/v14040792

Pulkkinen, L.I.A., Barrass, S.V., Lindgren, M., Pace, H., Överby, A.K., Anastasina, M., Bally, M., Lundmark, R., Butcher, S.J., 2023. Simultaneous membrane and RNA binding by tick-borne encephalitis virus capsid protein. PLOS Pathog. 19, e1011125. https://doi.org/10.1371/journal.ppat.1011125

Pulkkinen, L.I.A., Butcher, S.J., Anastasina, M., 2018. Tick-Borne Encephalitis Virus: A Structural View. Viruses 10, 350. https://doi.org/10.3390/v10070350

Pustijanac, E., Buršić, M., Talapko, J., Škrlec, I., Meštrović, T., Lišnjić, D., 2023. Tick-Borne Encephalitis Virus: A Comprehensive Review of Transmission, Pathogenesis, Epidemiology, Clinical Manifestations, Diagnosis, and Prevention. Microorganisms 11, 1634. https://doi.org/10.3390/microorganisms11071634

Rehwinkel, J., Gack, M.U., 2020. RIG-I-like receptors: their regulation and roles in RNA sensing. Nat. Rev. Immunol. 20, 537–551. https://doi.org/10.1038/s41577-020-0288-3

Ricketts, M.D., Emptage, R.P., Blobel, G.A., Marmorstein, R., 2022. The heme-regulated inhibitor kinase requires dimerization for heme-sensing activity. J. Biol. Chem. 298, 102451. https://doi.org/10.1016/j.jbc.2022.102451

Robertson, S.J., Mitzel, D.N., Taylor, R.T., Best, S.M., Bloom, M.E., 2009. Tick-borne flaviviruses: dissecting host immune responses and virus countermeasures. Immunol. Res. 43, 172–186. https://doi.org/10.1007/s12026-008-8065-6

Ruggieri, A., Dazert, E., Metz, P., Hofmann, S., Bergeest, J.-P., Mazur, J., Bankhead, P., Hiet, M.-S., Kallis, S., Alvisi, G., Samuel, C.E., Lohmann, V., Kaderali, L., Rohr, K., Frese, M., Stoecklin, G., Bartenschlager, R., 2012. Dynamic Oscillation of Translation and Stress Granule Formation Mark the Cellular Response to Virus Infection. Cell Host Microbe 12, 71–85. https://doi.org/10.1016/j.chom.2012.05.013

Sarratea, M.B., Alberti, A.S., Redolfi, D.M., Truant, S.N., Iannantuono Lopez, L.V., Bivona, A.E., Mariuzza, R.A., Fernández, M.M., Malchiodi, E.L., 2023. Zika virus NS4B protein targets TANK-binding kinase 1 and inhibits type I interferon production. Biochim. Biophys. Acta BBA - Gen. Subj. 1867, 130483. https://doi.org/10.1016/j.bbagen.2023.130483

Scheuner, D., Song, B., McEwen, E., Liu, C., Laybutt, R., Gillespie, P., Saunders, T., Bonner-Weir, S., Kaufman, R.J., 2001. Translational Control Is Required for the Unfolded Protein Response and In Vivo Glucose Homeostasis. Mol. Cell 7, 1165–1176. https://doi.org/10.1016/S1097-2765(01)00265-9

Sharma, R., Quilty, F., Gilmer, J.F., Long, A., Byrne, A.-M., 2017. Unconjugated secondary bile acids activate the unfolded protein response and induce golgi fragmentation via a src-kinase-dependant mechanism. Oncotarget 8, 967–978. https://doi.org/10.18632/oncotarget.13514

Siwecka, N., Rozpędek-Kamińska, W., Wawrzynkiewicz, A., Pytel, D., Diehl, J.A., Majsterek, I., 2021. The Structure, Activation and Signaling of IRE1 and Its Role in Determining Cell Fate. Biomedicines 9, 156. https://doi.org/10.3390/biomedicines9020156

Tan, Z., Zhang, W., Sun, J., Fu, Z., Ke, X., Zheng, C., Zhang, Y., Li, P., Liu, Y., Hu, Q., Wang, H., Zheng, Z., 2018. ZIKV infection activates the IRE1-XBP1 and ATF6 pathways of unfolded protein response in neural cells. J. Neuroinflammation 15, 275. https://doi.org/10.1186/s12974-018-1311-5

Tang, D., Kang, R., Coyne, C.B., Zeh, H.J., Lotze, M.T., 2012. PAMP s and DAMP s: signal 0s that spur autophagy and immunity. Immunol. Rev. 249, 158–175. https://doi.org/10.1111/j.1600-065X.2012.01146.x

Thoresen, D., Wang, W., Galls, D., Guo, R., Xu, L., Pyle, A.M., 2021. The molecular mechanism of RIG-I activation and signaling. Immunol. Rev. 304, 154–168. https://doi.org/10.1111/imr.13022

Tu, Y.-C., Yu, C.-Y., Liang, J.-J., Lin, E., Liao, C.-L., Lin, Y.-L., 2012. Blocking Double-Stranded RNA-Activated Protein Kinase PKR by Japanese Encephalitis Virus Nonstructural Protein 2A. J. Virol. 86, 10347–10358. https://doi.org/10.1128/JVI.00525-12

Umareddy, I., Pluquet, O., Wang, Q.Y., Vasudevan, S.G., Chevet, E., Gu, F., 2007. Dengue virus serotype infection specifies the activation of the unfolded protein response. Virol. J. 4, 91. https://doi.org/10.1186/1743-422X-4-91

Wahaab, A., Liu, K., Hameed, M., Anwar, M.N., Kang, L., Li, C., Ma, X., Wajid, A., Yang, Y., Khan, U.H., Wei, J., Li, B., Shao, D., Qiu, Y., Ma, Z., 2021. Identification of Cleavage Sites Proteolytically Processed by NS2B-NS3 Protease in Polyprotein of Japanese Encephalitis Virus. Pathogens 10, 102. https://doi.org/10.3390/pathogens10020102

Wang, Y., Xie, X., Shi, P.-Y., 2022. Flavivirus NS4B protein: Structure, function, and antiviral discovery. Antiviral Res. 207, 105423. https://doi.org/10.1016/j.antiviral.2022.105423

White, J.P., Lloyd, R.E., 2012. Regulation of stress granules in virus systems. Trends Microbiol. 20, 175–183. https://doi.org/10.1016/j.tim.2012.02.001

Whitehorn, J., Yacoub, S., 2019. Global warming and arboviral infections. Clin. Med. 19, 149–152. https://doi.org/10.7861/clinmedicine.19-2-149

Wu, X., Zhang, L., Liu, C., Cheng, Q., Zhao, W., Chen, P., Qin, Y., Chen, M., 2024. The NS2B-PP1α-eIF2α axis: Inhibiting stress granule formation and Boosting Zika virus replication. PLOS Pathog. 20, e1012355. https://doi.org/10.1371/journal.ppat.1012355

Yoshida, H., Matsui, T., Yamamoto, A., Okada, T., Mori, K., 2001. XBP1 mRNA Is Induced by ATF6 and Spliced by IRE1 in Response to ER Stress to Produce a Highly Active Transcription Factor. Cell 107, 881–891. https://doi.org/10.1016/S0092-8674(01)00611-0

Yu, C., Achazi, K., Niedrig, M., 2013. Tick-borne encephalitis virus triggers inositol-requiring enzyme 1 (IRE1) and transcription factor 6 (ATF6) pathways of unfolded protein response. Virus Res. 178, 471–477. https://doi.org/10.1016/j.virusres.2013.10.012

Yu, C.-Y., Hsu, Y.-W., Liao, C.-L., Lin, Y.-L., 2006. Flavivirus Infection Activates the XBP1 Pathway of the Unfolded Protein Response To Cope with Endoplasmic Reticulum Stress. J. Virol. 80, 11868–11880. https://doi.org/10.1128/JVI.00879-06

Yuan, H., Rao, J., Zhang, J., Ye, J., Cao, S., Chen, H., Song, Y., 2024. Japanese encephalitis virus inhibits superinfection of Zika virus in cells by the NS2B protein. J. Virol. 98, e01859-23. https://doi.org/10.1128/jvi.01859-23

Zeng, Q., Liu, J., Li, Z., Zhang, Y., Zu, S., Ding, X., Zhang, H., 2023. Japanese encephalitis virus NS4B inhibits interferon beta production by targeting TLR3 and TRIF. Vet. Microbiol. 284, 109849. https://doi.org/10.1016/j.vetmic.2023.109849